Studies in Nonlinear and Stochastic Phenomena and Quality Factor Enhancement in a Nanomechanical Resonator

A THESIS
SUBMITTED TO THE FACULTY OF THE GRADUATE SCHOOL
OF THE UNIVERSITY OF MINNESOTA DULUTH
BY

Md Raf E Ul Shougat

IN PARTIAL FULFILLMENT OF THE REQUIREMENTS
FOR THE DEGREE OF
MASTER OF SCIENCE

Advisor: Dr. Subramanian Ramakrishnan M.Sc., MSE, Ph.D.

July, 2019

Acknowledgements

It has been a dream from the early years of my undergraduate journey to pursue my Master of Science degree in a topic which would be closely related to mathematics as well as mechanical engineering. I am highly thankful to my advisor Dr. Subramanian Ramakrishnan for taking me in his group and giving me an opportunity to work on such a problem. When I started the journey of my master's thesis, I was not confident enough whether I can complete the thesis. My very first thanks for the completion of this thesis goes to Dr. Ramakrishnan for his organized and focused guidance from learning the very basic to advanced knowledge needed for the thesis. He always threw challenging and interesting questions and steered me in the right direction. He greatly helped me with his insightful thoughts about the progress I was making to attack the problems. Our efforts did not go in vain. We have been able to write three conference papers and one journal paper from this masters thesis. I am also grateful for his super guidance and support in my Ph.D. application which helped me a great deal to earn a Ph.D. fellowship with a position of 'Research Assistant' in the field of nonlinear dynamics; related to the work of my master's thesis.

I can't thank enough my parents who have gone through much struggles from my early childhood for my education and for inspiring me to go for higher education. I thank them for supporting me even at this stage of my life being 8000 miles away. I am thankful to my siblings for their love and support when I was struggling with my problems. Truth to be told, the completion of this thesis would not have been possible without the immense love and support I received from my family members.

It is my pleasure to show my sincere gratitude to Dr. Michael Greminger and Dr. Andrea Schokker for being kind enough to be in my thesis committee. I want to thank them for giving me constructive reviews and right direction to complete the thesis. I

want to thank Dr. Greminger for his time and playing a crucial role in my Ph.D. application as well. I would also like to thank Dr. Michael Pluimer for helping me greatly in my Ph.D. application process and for being so nice and friendly to me from the very beginning.

I would like to thank Connor Edlund, one of our research group members, currently pursuing Ph.D. at the University of Minnesota, who has immense contribution in building up my code for the numerical simulation from the very beginning of the master's journey. He never got disturbed even with my silly questions. His prior experience of working in nonlinear dynamics with Dr. Ramakrishnan made my life easier and helped me be in the right track from the early stage.

I am thankful for the support I got from all of my friends here at Duluth. Maksud, Pasha, Rakib, Maqsood, Touhid, Samsul, Sudipta, Bipasha, Nitol, Nafis, Irfan, Gills, Heather are some of the names that immediately come to my mind. I can never forget the support and love of Razon, Sumona and Omi who have always inspired me to go forward staying back in my country.

I want to thank Kim and Tracy for their administrative assistance and I would also like to thank the Swenson College of Science and Engineering for the funding and support.

It is my great pleasure to show my sincere gratitude to my all time favorite teacher and personality - Professor Ashraful Islam, who has an immense contribution to the journey of my life both academically and philosophically.

Finally, I am highly thankful to the Almighty for blessing me with the strength of passing through this path, facing all the obstacles with confidence and courage.

Dedication

To my father - Kebez Uddin Ahmed & mother- Suriya Begum.

Abstract

Nonlinear damping has recently been experimentally observed in carbon nanotube and graphene-based nanoelectromechanical (NEMS) resonators and shown to be an effective means to achieve higher quality (Q) factors. Moreover, it has been shown that white noise excitation can be exploited to shrink the resonance width of the frequency response characteristics of the resonator as a pathway to higher Q factors. Motivated thus, this thesis is a study of certain fundamental characteristics of the nonlinear dynamics of a nanoelectromechanical resonator in both the deterministic and stochastic regimes with a focus on the influence of those characteristics on the Q factor. Using a Duffing oscillator based model, this thesis: (1) derives an analytical expression between oscillation amplitude and frequency of a NEMS resonator using the harmonic balance method to study the frequency response characteristics and validates the results using numerical simulation, (2) studies the deterministic dynamics of a NEMS resonator deriving an analytical relationship between the phase angle and maximum oscillation of the resonator response, (3) derives an analytical expression between the resonance frequency and resonance amplitude, (4) studies the hysteresis characteristics both in the stochastic and deterministic regimes elucidating the effects of nonlinear damping and external excitation on the hysteresis region, (5) finds that stochastic excitation with increasing intensity can shrink the hysteresis width, (6) shows that increasing the magnitude of the linear damping coefficient results in the decrease of Q-factors, (7) shows that in the combined presence of both parametric and external excitation, increasing the ratio of pump frequency to external forcing frequency results in lower resonant frequency and lower resonance width, (8) observes that in the parametrically driven nanomechanical resonator, higher parametric oscillation amplitude increases the resonance amplitude with a small impact on the resonance frequency, (9) solves the stochastic model using the Euler-Maruyama method and generates frequency response curves where it is found that higher noise intensity of Lévy stable stochastic process can increase the Q factor, (10) finds that the Q factor is increased by decreasing the nonlinear damping and external harmonic driving amplitude. In summary, this thesis presents a set of novel results

on the nonlinear, stochastic dynamics of a NEMS resonator and discusses the implications of the results for achieving enhanced Q factors. The results are of interest both from a theoretical viewpoint as well as in sensing applications using a nanoresonator.

Contents

List of Tables

List of Figures

Chapter 1

Introduction

1.1 Definitions

Electromechanical systems are characterized by the coexistence of both mechanical and electrical degrees of freedom and interactions between them. Indeed, conversion of electrical energy into mechanical energy and vice versa occurs in these systems and they find widespread applications in many aspects of our day to day life. Some common examples that immediately come to our mind are electrical motors which take electrical energy and convert it into mechanical movement, and generators which generate electricity by transforming mechanical energy. Miniaturized versions of these electromechanical devices are known as micro electromechanical systems (MEMS). MEMS can be typically characterized based on the dimensions of the devices starting from a few millimeters in the upper end all the way down to 1 micron in the lower end. Unparalleled advancement of fabrication technology in the last couple of decades has taken these dimensions to even smaller scales, down to a few nano metres [1, 2, 3]. The devices which find their applications and functionality in the nano scale are commonly known as Nanoelectromechanical system (NEMS). NEMS bridges a relation between nanoelectronic circuits and mechanical actuators or motors. In general, MEMS and NEMS can be distinguished by dimensions in such a way that the MEMS devices operate in the microscale and NEMS devices are able to operate in the nanoscale. Another important distinguishing parameter is the surface area to volume ratio. NEMS devices possess a very high surface area to volume ratio compared to the MEMS devices [4] which has made NEMS

extraordinarily popular in sensing applications. A nanoelectromechanical resonator is an excellent example of a NEMS device which is used widely in sensory applications. It is basically a nano scale beam which can oscillate at a specific frequency and depending on the geometry and actuating mechanism it can exhibit resonance. The unique dynamical characteristics of a nanomechanical resonator makes it remarkably useful in sensing physical quantities.

1.2 Manufacturing of NEMS

One of the most remarkable technological advancements the world has seen in the last few decades is the development of MEMS and its extended branch-NEMS showing their potential applications in many fields starting from the basic science to engineering. These advancements were achieved due to the noteworthy progress in materials and manufacturing technology. A brief description of the materials and manufacturing technologies in NEMS (or MEMS) is discussed in this section.

1.2.1 Materials for MEMS/NEMS

Silicon (Si) has been used as a material for microfabrication from the mid of twentieth century after it was discovered that Silicon has piezoresistive property. More importantly, it was found that Si possessed higher piezoresistive coefficients than the other materials used for regular strain gauges which marked the beginning of the development of Si based strain gauge devices [4]. After that with the discovery of germanium (Ge) showing the similar piezoresistive effect Si shows, piezoresistive sensors were made [5] using Si and Ge which played a pioneering role in the development of the MEMS and NEMS technology that we have now. Single-crystal silicon (Si), Silicon dioxide (SiO_2), Silicon carbide (SiC), Polycrystalline silicon-germanium (poly SiGe), Polycrystalline germanium(polyGe) are the forms of Si and Ge based material used in MEMS. The striking properties that make Si applicable in manufacturing microelectromechanical devices are: [6, 4]:

- Silicon is extremely light having a density of around 2.3 g/cm^3

- It is dimensionally stable due to its very high melting point that is around 1400 degree celsius.

- Mechanical hysteresis is hardly seen in Silicon which makes it attractive for sensor fabrication.

- Single-crystal Si exhibits very high modulus of elasticity (about 190 GPa) which facilitates its use for building resonant beams.

- Si is comparatively easier to micromachine even in a bulk amount.

- It is a semi-conductive material having an energy gap of 1.14 eV and it is also abundant in earth's crust.

On the other hand, NEMS devices are generally fabricated from two popular 2-D materials namely carbon nanotube (CNT) and graphene. Between them, graphene has gained significant attention due to its multifaceted characteristics (electronic, optical, magnetic, thermal, mechanical and so on) which makes it suitable in nanoelectronics industry [7]. Graphene got its attention after Geim *et al.* mechanically exfoliated a single layer of graphene from graphite [8], a great achievement in the history of science and technology. The crystallographic structure of graphene is two-dimensional having a thickness of one atomic layer of carbon and a lateral dimension of 1 to 10 micro meter [9]. The properties that make graphene notably effective in NEMS devices are as follows [9, 10, 11, 12, 13]:

- Graphene has a Youngs modulus of 1000 GPa which is higher than that of CNT and 10 times higher than that of Silicon. This property makes it the strongest and thinnest material discovered so far.

- It possesses significantly high carrier mobility which is important in device physics.

-Graphene shows remarkable impermeability because sheets of graphene are attached together so closely that other materials can not pass through graphene net. It is impermeable to almost all regular gases.

- It also shows piezoresistive effect like Silicon.

- If not doped or patterned, intrinsic graphene has no band gap.

- It has very high heat and electrical conductivity.

- Graphene has extremely high breaking strength.

- Because the structure is very thin, defects are not common in graphene sheets unlike other bulky materials.

In summary, the extremely light and thin structure with unique mechanical and electrical attributes made graphene the strongest candidate to build nanoelectromechanical devices like nanoresonators or sensors with an improved performance.

1.2.2 Methods of NEMS/MEMS fabrication

Since this thesis is related to the study of graphene based NEMS resonator, we are limiting our discussion to graphene NEMS devices. Graphene based NEMS devices can be fabricated in two ways:

- Top down method.

- Bottom up method.

There are two main steps in the fabrication process: production of graphene itself and then releasing of the suspended graphene structure. Since it is known that graphite is a multilayered graphene material where several layers of graphene stack on top of each other by Van der Waals bonds [12], graphene can be produced from graphite by mechanical exfoliation also known as 'Scotch tape method' [9]. In this process, a scotch tape is used to lower the thickness of the graphite through peeling the layers over and again. Then the thin layers of graphite are rubbed against a solid surface (SiO_2) which results in the production of monolayered graphene. Though this is the most popular method so far practiced in the synthesis of graphene, the process has the disadvantages that it is not scalable and that the mechanical exfoliation is a difficult procedure. This mechanical exfoliation based procedure is known as 'Top-down method'.

There is another process available for graphene synthesis known as the CVD (Chemical Vapor Deposition) technique. Copper or Nickel are used in this method with

graphene on their surfaces. CVD based on Cu gained more attention due the fact that using Cu 95% single layered graphene was produced. Ni based CVD technique yields multilayered graphene. A major disadvantage of this method is that it results in lower mechanical strength at the grain boundaries. This procedure is known as 'Bottom-up method'.

Since the synthesis of graphene has been so widespread, it has become easier to produce nanodevices like arrays of field effect transistors[14] or nanoresonators [15]. A nanoresonator can be fabricated in a similar fashion discussed above. [15] shows graphene nanoresonator fabrication using CVD method where it is grown on Silicon carbide (SiC). Then through etching process, the nanoresonator is separated from the surface of SiC.

1.3 Historical Background

Though there is a long history of investigations in electromechanical systems going back to the eighteenth century (for instance a device was invented by Coulomb to measure electrical charge in 1785), research related to miniaturized electromechanical systems is still relatively young and did not gather momentum until the middle of the twentieth century. The technological innovation during World War II, specifically radar stimulated research in semiconducting material synthesis (i.e. Silicon) laid the foundation of this field. To this date this material group has been the basis for fabricating nano/micro devices. The research in MEMS was first inspired by the seminal talk of Richard Feynman in 1959 American Physical Society meeting There's Plenty of Room at the Bottom [1] where he discussed about the future prospects of microsystem research. He remarked:"Why cannot we write the entire 24 volumes of the Encyclopaedia Brittanica on the head of a pin?" " It is a staggeringly small world that is below. In the year 2000, when they look back at this age, they will wonder why it was not until the year 1960 that anybody began seriously to move in this direction."

This visionary scientist also announced that he would give $1000 to the person who can build a motor '1/64 of an inch'. William McLellan was the person who won the prize after substantial effort by building it by hand. The process was very painstaking and not recommended for batch fabrication. Industrially acceptable process for MEMS

fabrication came after few years. A brief overview of the historical development in MEMS/NEMS is given as follows [9, 16, 17] where the idea of reproduction of the table and updating are based on [16] :

Table 1.1: Historical overview in MEMS/NEMS

1940s (World War II)	Radar inspired research in silicon synthesis.
1959	Richard Feynman's lecture in 1959 APS meeting (There is Plenty of Room at the Bottom).
1960	Invention of planar batch manufacturing process.
1964	First batch manufactured MEMS device - resonant gate transistor was produced by Nathanson and his group.
1970	Invention of microprocessor.
1979	Development of accelerometer in micromachining process.
1981	The first journal research paper published on molecular nanotechnology: "Protein design as a pathway to molecular manufacturing" by K. Eric Drexler [18].
1982	Invention of scanning tunneling microscope.
1984	Invention of polysilicon surface micromachining process leading to the combined MEMS and IC fabrication for the first time.
1985	Discovery of Buckminsterfullerene (C_{60}).
1986	Invention of AFM.
1991	Invention of CNT.
1996	New process discovered to produce CNT with higher accuracy marking the most significant progress in the field of MEMS to this time.
2000s	Fabrication and application of MEMS device increased at a high rate.
2004	Separation of single layer graphene from graphite by Geim and Novoselov.

2007	Isolation of graphene nanomembrane.
2007	Cornell researchers became successful in actuation and detection of motion of a graphene nanoelectromechanical resonator.

1.4 Applications of a Nanoelectromechanical Resonator

The last couple of decades witnessed unprecedented advancement in nano system specifically after the discovery of graphene leading to the development of nano scale devices. Mostly these devices have applications in sensing nano scale physical quantities (i.e. mass, motion, charge etc.). Among the nanoscale devices built so far, the nanomechanical resonator has earned the greatest attention because it can achieve extremely high frequency (up to 10^9 Hz) [19]. The high frequency characteristics are obtained due to its extremely small dimensions. The resonant frequency (f_n) of the resonator has an inversely proportional relationship with the square of the resonator's length ($f_n \propto L^{-2}$) [20]. It implies that if a resonator's length is lowered by half, resonant frequency can be four times higher. The reason we are concerned about resonant frequency is that it is intimately related to the sensing accuracy of the resonator.

1.4.1 Mass Detection

One of the most incredible applications of the NEMS resonator is the ability of nano scale mass sensing. Mass sensing depends on the resonant frequency and resonant frequency shift and is governed by the following simplified relation: [19, 21]:

$$\frac{\Delta f_n}{f_n} = -\frac{1}{2}\frac{\Delta m}{m} \tag{1.1}$$

where Δf_n and f_n represent the frequency shift and the resonant frequency respectively, m and Δm represent the initial mass of the resonator and the accumulated mass respectively. The equation clearly indicates that the higher the frequency the smaller the mass that can be detected. In other words, the higher the quality factor (Q-factor $\propto \Delta f_n$), the better is the detection sensitivity. Since the nanomechanical resonator is capable of reaching ultra high frequency regime, this device is well suited for ultra

sensitive mass detection. Ekinci *et al.* [19] experimentally showed attogram scale mass detection using NEMS resonator. In this process, they used a 32.8 MHz nanoresonator in vacuum and a stream of atoms dissolved on the surface of this resonator. Later, they found the amount of added molecules (responsivity of 2.53 $\times 10^{-18}$ g) measuring the resonant frequency shift Δf_n. Besides this, they also predicted the possibility of sensing a single molecule using a nanoresonator. Jensen *et al.* [22] using a double-walled carbon nanotube based nanoresonator recorded a mass sensitivity of 1.3 $\times 10^{-25}$g. Other important research efforts with a concentration on the nano scale mass sensing using nanomechanical resonators may be found in [23, 24, 25]

Nonlinear Oscillation and Mechanical Tension in Mass Detection

The earlier method of mass sensing shown in the previous discussion is based on the assumption that no nonlinearity is coming into play in the sensing scheme and the oscillations are strictly harmonic. However, this is not the reality. There is a rich literature discussing the fact that the dynamics of a nanoresonator is reliably determined by nonlinearity and hence the oscillation is mostly in nonlinear regime [3, 26]. Dai *et al.* [27] considered nonlinear oscillation based on continuum elastic model to detect nano scale mass using carbon nano tube resonator. They observed that with a small electrostatic force showed nonlinear oscillation yields to a specific resonant frequency shift which is not found in harmonic oscillation regime. They also observed that resonant frequency increased when the electrostatic force is large enough to carry the dynamics in the nonlinear oscillation regime. They derived the following equation modifying Duffing equation to describe the dynamics of a nanomechanical resonator taking the absorbed mass into account:

$$[\alpha + \beta\, T]\, z(t) + \gamma\, [z(t)]^3 + \eta\, \ddot{z}(t) = p_0\, cos(\Omega\, t) \tag{1.2}$$

where, $\alpha = \frac{16\pi^4\, E\, I}{3L^2}$
$\beta = \frac{4\,\pi^2}{3\,L}$
$\gamma = \frac{8\,\pi^4\, E\, A}{9\,L^3}$
$\eta = \frac{2}{3}\,\rho_{CNT}\, AL + \Delta M$

E,I,A and L are Youngs modulus, cross sectional moment of inertia, cross sectional

are and length of the resonator respectively. Their numerical study suggests that if the excitation is large enough to turn the oscillation in the nonlinear regime, resonant frequency gets higher caused by added mass. Additionally, they observed that in the case of a longer nanoresonator, detection sensitivity increases since it results in higher resonant frequency with larger resonant shift as well. In summary, nonlinearity can significantly increase the accuracy of the mass detection scheme.

Besides this they also studied the effects of mechanical tension on the mass detection sensitivity. They showed that mechanical tension can decrease the resonant frequency. Using the continuum elastic model they report the following relation:

$$\omega_0 \approx \tilde{\omega}_0 \sqrt{1+\tilde{\tilde{T}}} \tag{1.3}$$

where, $\tilde{\omega}_0$ is the initial resonant frequency when no mechanical tension is considered and $\tilde{T}$ is the mechanical tension which can be written as $\tilde{T} = \frac{TL^2}{EI}$ This relation yields the following relation between resonant frequency shift and the added mass under the effect of mechanical tension:

$$\frac{\Delta\omega}{\Delta\tilde{\omega}_0} = -\frac{1}{2}\frac{\Delta m}{m_{CNT}}\sqrt{1+\tilde{\tilde{T}}} \tag{1.4}$$

As a result, in one way the detection sensitivity increases for considering mechanical tension while this tension results in the decrease of resonant frequency. In other words, mechanical tension may not help in nonlinear oscillation based mass detection scheme due to the two opposite effects on the sensitivity.

1.4.2 Actuation and Motion Sensing

With the scaling down of the resonator, the oscillatory response regime gets smaller and actuation becomes important as well as the sensing of nano scale deflection. Techniques used for MEMS devices are not useful here anymore due to speed, coupling and compatibility issues. Actuation and motion detection of NEMS resonator are discussed in this section.

Actuation of Motion

There are two widely known methods of actuation of motion [28, 29]: Magnetomotive and capacitive actuation. In the magnetomotive actuation, the nanoresonator is set inside a strong magnetic field made. Besides this magnetic field, ac current is driven through the nanoresonator. As a result Lorentz force is generated [29]. The oscillatory motion of the resonator can be described using the following relation:

$$X(\omega) = \frac{l\,B\,I(\omega)}{m_{eff}\,\omega_0^2 - \omega^2 + \frac{i\,\omega\,\omega_0}{Q}} \tag{1.5}$$

where I(ω) denotes the ac current magnitude,l is the resonator length and B is the magnetic field strength. The only difficulty with this method is that it requires a very strong magnetic field.

More information relating magnetomotive scheme of NEMS beam actuation can be found here [30].

In the capacitive method of actuation, a scheme similar to the one applied in MEMS domain is followed for NEMS resonator as well. Firstly, the capacitor is charged and then attractive force generates between the capacitor plates. Specific voltage is applied between the resonator and the gate electrode. Major drawback with this method is that the actuation efficiency is lower at higher frequency. Sekaric *et al.* experimentally showed this actuation method worked at a resonant frequency of 640 MHz [31]. There are some other methods for actuation and among them thermal actuation offers a possible effective way which is yet to be fully explored.

Detection of Motion

Similar to the the actuation technique, a magnetic field can be used in motion detection scheme [29, 32, 33]. Here an amplifier is connected to the magnetomotive transducer with an assumption of the amplifier being the dominant noise source. The generated emf in the magnetic circuit is given by the following equation:

$$v_0(t) = \xi\,l\,B\,\dot{x}(t) \tag{1.6}$$

where, B is the magnetic field strength, l is the resonator length and ξ is a geometric factor, x(t) is the displacement of beam. It is noted that the amplifier used in this has

to be a low noise amplifier since the beam displacement is very small. The kernel of this method is that depending on the movement of the nanoresonator, variable emf will be produced which can re recorded by the detection circuit. Differences in emf will give us the required measure of deflection.

Optomechanical coupling has also been used in the motion detection domain [28]. In this approach, Ekinci and his coworkers used an array of 63 cantilever nanomechanical beams. The lengths of these beams varied from 5m to 18.8 μm keeping the thickness (t) and widths (w) same for all : w= 500 nm and t= 230 nm. Using near-field optomechanical coupling technique they found a maximum deflection sensitivity of $0.024/\mu m$ for each cantilever in the array.

Akin to the actuation technique, the capacitive method is applicable in the displacement detection scheme. Here with the variation of the nanoresonator motion, the capacitance is varied in the circuit which alters the voltage across the capacitor based on the following relation:

$$dQ = VdC + CdV \tag{1.7}$$

where, dQ is the change of charge in the capacitor, dC is the change of capacitance and dV is the change in voltage. Though it is easier to implement this scheme in the MEMS device, miniaturization of the capacitive detection circuit faces much more difficulties.

Some other methods of motion/displacement detection include piezoresistive and piezoelectric detection [29], electron tunneling [29], using scanning electron microscope (SEM) [34], using a quantum point contact [35] and so on. More research on the detection of motion using NEMS beam can be found here [36, 37, 38]

1.4.3 Nanoresonator in Biological Detection

Nanomechanical resonators have many spectacular applications in biological science such as cell detection [39, 40, 41], virus detection [42, 43], protein detection [25, 44, 45], DNA detection [46, 47, 48], enzymatic activity detection [49, 50] and so on. Among them, cell detection has attracted the attention of the biological community the most due to the fact that early detection of many intimidating cells (i.e. cancer cell) are possible with the help of a nanoresonator. Craighead and his group [39] for the first time successfully utilized microcantilever in cell detection. Later, his group [51] used

arrays of nanomechanical beams to detect individual DNA molecule. They measured the shift of resonant frequency which occurred because of the accumulated mass on the nanomechanical resonator. In this process, each resonator was driven thermooptically and optical interference was used to detect their motion. By doing so, they were able to detect single DNA molecule attached on the nano beam. The frequency shift was found to be proportion to the number of bound DNA molecules in each device. The smallest of the cantilevers used gave the highest sensitivity which was 194 Hz/attogram.

In another investigation, Craighead *et al.* [52] used nanomechanical resonator arrays to detect prion proteins (PrP) which is a cause of neurodegenerative disease. Here they used antibodies as an additional mass labels which resulted in a sensitivity of 2 μg/mL and with nanoparticles mass labels they showed a sensitivity of 2 ng/mL.

Again, Craighead *et al.* [42] in another research effort, used an array of cantilever based nanomechanical resonating element to detect virus particles. A special kind of Baculovirus was used as a binding element. With the addition of virus particles, the resonant frequency changes which works as an identifying factor in virus detection. Additionally, the detector array was able to distinguish different concentration of virus solution varying from 10^5 to 10^7 pfu/mL.

In summary, we can say that NEMS have dramatically changed the sensing technology. However, NEMS are useful in the study of fundamental science as well. For example, it can be used in the study of a quantum phenomenon named as 'Casimir effect' [53] which can produce a force of hundreds of piconewtons to result motion in nanomechanical devices. Electron spin detection has been possible in MEMS device (magnetic resonance force microscopy) [54] and there has been many efforts to detect nuclear spin which is extremely challenging due to the fact that it generates forces of about $10^{-21}N$. This force is even smaller than 1/1000 of the force generated from single electron spins [53]. Schwab and his group [55] reported an experimental investigation of position detection approach determined by Heisenberg uncertainty principle using a nanomechanical resonator coupled to a single electron transistor. They were able to achieve a position resolution factor of 4.3 above the quantum limit. Some other applications of NEMS resonator include detection of quantum state [56],detection of quantum interference [57] and in building quantum computers [53].

Providing an overview of the applications of NEMS resonator both in engineering

and fundamental science, now we are turning our attention towards the nonlinear phenomenona in the dynamics of a nanomechanical resonator.

1.5 Nonlinear Behavior of a Nanomechanical Resonator

Nanomechanical resonators often show nonlinear characteristics due to their extremely small size. Some widely reported nonlinear phenomena are : hardening, softening, bistability, mixed hardening and softening behavior and nonlinear resonances in nanomechanical resonators. Husain and his co-workers [58] reported nonlinear phenomena studying doubly-clamped nanowire-based resonator which is '43 nm in diameter and 1.3 μm in length'. In the process of building this Platinum based nanoresonator, they took a mixed manufacturing approach. They combined both 'top-down' and 'bottom-up' methods of manufacturing which is known as 'Hybrid' method. Analysing the response characteristics, they showed that with the increase of driving force the response changes the nature from linear to nonlinear regime where hysteresis is remarkably noted. To give a broader picture of nonlinear response, their experimental result is given below:

The response also depicts a region of bistability which is not found in linear resonators. The resonance response is a resonance in the hardening regime. The hardening nature of the resonator increased with increasing driving force. They reported an increase of driving voltage from 40 μV to 400 μV with a step size of 40 μV to generate this figure. They also reported that the critical oscillation amplitude above which bistability occurs is associated to the geometry of the resonator. The relation they ended up is as follows:

$$x_c = \frac{d\sqrt{2}}{\sqrt{0.528\,Q\,(1\,-\,v^2\,)}} \tag{1.8}$$

where, x_c is the critical amplitude, d is the nanoresonator diameter, Q is the quality factor, and v is the Poissons ratio of the material used. These concepts are not found in a linear oscillator. In another investigation, Kacem *et al* [59] found four bifurcation points under different conditions where they observed all hardening,softening and mixed hardening-softening based resonance. Further, Kacem and his group [60] also explored doubly clamped nanomechanical resonators modeled using Euler-Bernoulli equation taking both mechanical and electrostatic nonlinearities into account. Here they again

reported their findings of hardening,softening and mixed hardening-softening based response of the nanoresonator.

Study of nonlinear phenomena is important for many engineering design considerations. For example, Roessig and his coworkers [61] working with a tuning fork oscillator showed that in the nonlinear regime, frequency stability breaks and coupling with noise mixing due to mechanical and electrostatic nonlinearities, the performance of the resonator degrades. The nonlinearities can also lead to motion instability causing a collapse in the system [60]. So, it can be said that nonlinear dynamics of a nanoresonator deserves significant attention which is going to be the central aspect of this thesis.

1.6 Motivation and Thesis Outline

Based upon the discussion up to this point, hopefully it is evident that the principal application of a nanomechanical resonator is in the sensing of physical quantities. In order to use it in nanoelectronic circuit efficiently, a complete understanding of the dynamics of a nanoresonator is a must. The nonlinear dynamic response is also affected by the stochastic excitation which in turn influences the sensing performance as well. So, the deterministic and stochastic dynamics of a nanoresonator are going to be the central attention of this thesis. Hence, these two aspects of nanoresonators deserve an in-depth review which is discussed in the following sections.

1.6.1 Precursory Works with Nonlinear Damping

One of the most promising works in the field on damping based nonlinearity is done by Eichler and his group [3]. Linear damping has been reported in plenty of works for a long time. Linear damping for vibrating systems in general is proportional to the velocity. But Eichler *et al.* in their work reported that they found the damping largely dependent on the amplitude of the motion which can be described by a nonlinear damping force (not proportional to only 'velocity' like the linear damping force). They did experiment with graphene and carbon nanotube resonators at a very low temperature (90 mK) in a vacuum chamber. Oscillating voltage is applied to perform electrostatic actuation and the displacement of the resonator was detected using frequency modulation technique [62]. To support their ideas of nonlinear damping based nanoresonator, they performed

experiments in three different conditions using CNT/graphene resonators:

- Nanotube resonator under the effect of tensile stress.
- Graphene resonator under the effect of tensile stress.
- Nanotube resonator with slack.

Measuring the response in all three cases they found that resonant frequency increases and resonance width broadens with an increase in driving voltage. Additionally, they observed hysteresis phenomena under certain conditions. They later on explained these phenomena with the help of a nonlinear damping framework. Besides their study, Bunch *et al.* [63] in their experimental study of nanoresonators from graphene sheets also predicted that nonlinear damping might play a vital role on the performance of the resonator affecting the quality factor. This gives the motivation of analytical and numerical study of how the nonlinear damping is affecting the resonator dynamics and performance.

1.6.2 Precursory Works with Stochastic Dynamics

Noise has footprint in all physical systems. Depending on the intensity of the noise, it can either destroy or enhance the system characteristics. In the previously mentioned works of Eichler *et al.* [3] and Bunch *et al.* [63], stochastic effect was not taken into account. However, in a nano system, noise can drastically change the dynamics. Some examples of noise affected nano system are here [64, 65, 66, 67, 68]. Ros and his co-workers [66] studied graphene based nanomechanical resonator model considering the stochastic effects. Applying white Gaussian noise as external noise and thermomechanical noise as internal noise, they concluded that such types of noise with an increased intensity can increase the quality factor. They also mentioned that, without considering the stochastic effect, calculation of nonlinear damping coefficient done by Eichler *et al.* [3] would not give the correct result since they did not consider noise intensity as a factor to govern resonance width.

In another work, Badzey and his co-worker [64] observed resonance governed by stochastic excitation in bistable nanomechanical oscillators. They also reported an

amplification of signal strength in the presence of white noise. They predicted that stochastic resonance might play role in signal processing as well.

Nakada and his co-workers [69] performed numerical study applying the Euler-Maruyama method on the stochastic magnetization dynamics of two spin torque nano oscillator (STNO) pair coupled with each other. Through the injection of noisy current in the bistable regime they observed that the STNO pair can induce the stochastic state transition from the out-of-phase synchronization state to the in-phase synchronization state. The research mentioned above strongly suggests that stochastic excitation can change the dynamics and efficacy of a system which gives us the motivation to study how stochastic dynamics can affect the dynamics and performance of a nanomechanical resonator.

1.6.3 Thesis Outline

Motivated by the aforementioned research efforts, the objective of the thesis is to investigate the resonator dynamics in nanoscale. In order to accomplish that, graphene or carbon nanotube resonator is chosen due to their advantages in sensing applications. The purpose of this thesis is to study the dynamics of nanomechanical resonator both in deterministic and stochastic regimes. Specifically, our efforts will be to gain both analytical and numerical understanding of the deterministic dynamics of the resonator. Once that is done, stochastic analysis based on the Lévy flight excitation will be performed to get an understanding of the dynamics in the stochastic regime. The linear and nonlinear damping and external drive can have influence on the performance of the resonator. So, both analytical and numerical aspects are chosen to see their effect on the dynamics and eventually on the quality factor of the resonator. Later on, we seek to enhance the effectiveness of nanoresonator in sensory applications exploiting the unavoidable stochastic excitation at this nanoscale. We also investigate the dynamics of a nanoresonator under the effect of parametric excitation and see if the parametric excitation can improve the quality factor of a nanoresonator to be used in sensing scheme.

The structure of the thesis goes as follows:

- Chapter 1 discusses about the basics of nanomechanical resonators, introduces the

objectives of the thesis and briefly discusses the related literature and motivation of the thesis.

- Chapter 2 presents the modeling of the nanomechanical resonators, briefly discusses the analytical and numerical methods used in the later sections.
- In Chapter 3, the deterministic dynamics of a nanomechanical resonator is studied based on analytical and numerical methods discussed in Chapter 2.
- Chapter 4 describes the stochastic dynamics of a nanomechanical resonator based on Lévy noise. It also discusses the Q-factor enhancement based on both stochastic and deterministic model.
- Chapter 5 presents a final discussion of the analyses presented in the thesis.

Chapter 2

Modeling and Methodology

2.1 Introduction

It was previously mentioned in Chapter 1 (Sec. 1.6) that the purpose of this thesis is to perform numerical and analytical studies of the nonlinear characteristics of a nanoresonator. However, the dynamics of a nonlinear oscillator can often be approximated by the dynamics of a linear oscillator under certain assumptions. Keeping that in mind, firstly some concepts and mathematical ideas of a linear oscillator model are briefly presented in this section and then nonlinear modeling is introduced. Finally, methods of studying and analyzing the model are discussed.

- In sec. 2.2 linear oscillator model is discussed using two examples: spring-mass system and simple pendulum.
- Sec 2.3 presents modeling of nonlinear resonator related to Duffing oscillatory model. Characteristics of Duffing oscillator are also discussed briefly here in this section. Extending the discussion from Duffing oscillator, modeling of a nanomechanical resonator is introduced.
- Sec 2.4 talks about the Harmonic Balance Method as an analytical tool to study the model of a nanomechanical resonator.
- Sec 2.5 discusses the numerical method of studying the dynamics of a nanomechanical resonator in both deterministic and stochastic regime.

2.2 Linear System

Linear systems are used to model a wide range of engineering systems [70, 71, 72, 73, 74, 75]. Dynamical systems are well treated with the help of differential equations. Hence, the theory of linear and nonlinear oscillation (which are basically dynamical systems) depends largely on the mathematical analysis of differential equations. Spring-mass system or simple pendulum are the classic examples of linear oscillator model (simple harmonic oscillator model).

Let us consider a spring (linear) on a frictionless surface in a relaxed condition where one end is fixed while the other end is attached to a mass and free. Then some force (push or pull) is applied and then retracted along the axis of the spring. The spring starts oscillating along the axis under the restoring force. Mathematical analysis can tell us that the oscillation is harmonic. If the spring force follows Hooke's law, the system will turn out to be a simple harmonic oscillator.

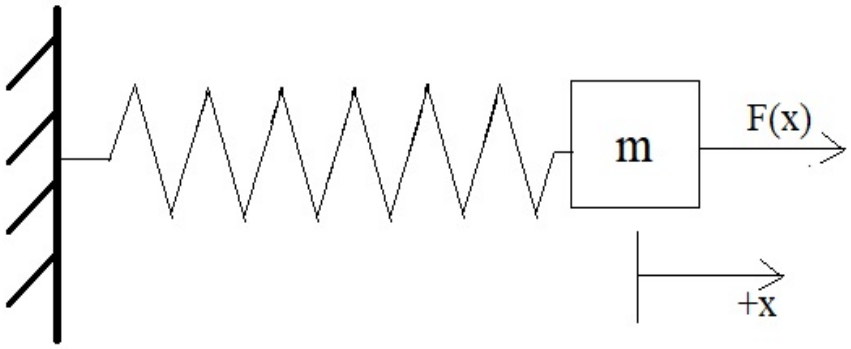

Figure 2.1: Simple Harmonic Oscillator

Spring force is be represented as follows:

$$F(x) = kx \tag{2.1}$$

where, k is the linear spring constant.

Applying Newtonian mechanics, the oscillatory motion can be written in terms of second order ordinary differential equation using the spring force as follows:

$$-kx = m\ddot{x} \tag{2.2}$$

With some rearrangement:

$$m\ddot{x} + \omega^2 x = 0$$

where, $\omega^2 = \frac{k}{m}$
The general solution of the Eqn.2.2 can be written as

$$x = A\,cos\,(\omega\,t) + B\,sin\,(\omega\,t)$$

If the spring force is modeled by higher order polynomial (not by Hooke's law), the oscillator will be turned to a nonlinear oscillator.

Again, if the resonator motion is modeled using a dashpot, under the effect of harmonic driving force, the previous second order differential equation (Eqn. 2.2) turns into the following way:

$$m\,\ddot{x} + \gamma\,\dot{x} + k\,x = F cos\,(\Omega\,t) \tag{2.3}$$

where, x is the mass displacement of mass m, k is the spring coefficient ($\omega^2 = \frac{k}{m}$), γ is the damping coefficient, F is the amplitude of the sinusoidal driving force.
Solution of the Eqn.2.3 for amplitude of the motion can written as follows:

$$|X| = \frac{F}{\sqrt{(m\,\Omega^2 - k\,)^2 + (\gamma\,\Omega)^2}} \tag{2.4}$$

From Eqn. 2.4, it is clear that the oscillation amplitude is directly proportional to the driving force amplitude. So, this is basically a linear system. Looking at the the governing equation (differential equation 2.3), we can also see that it is a linear differential equation.

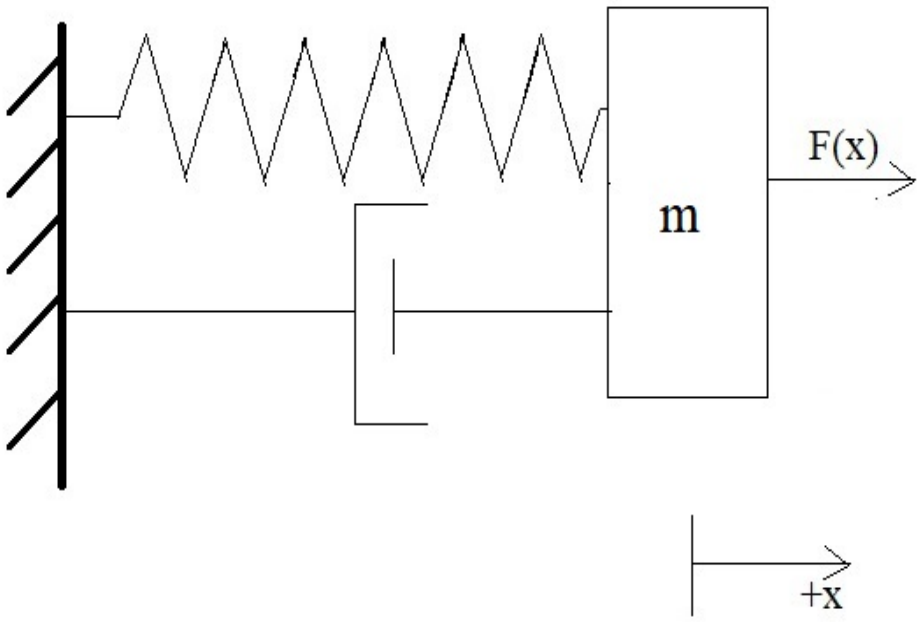

Figure 2.2: Damped harmonic oscillator

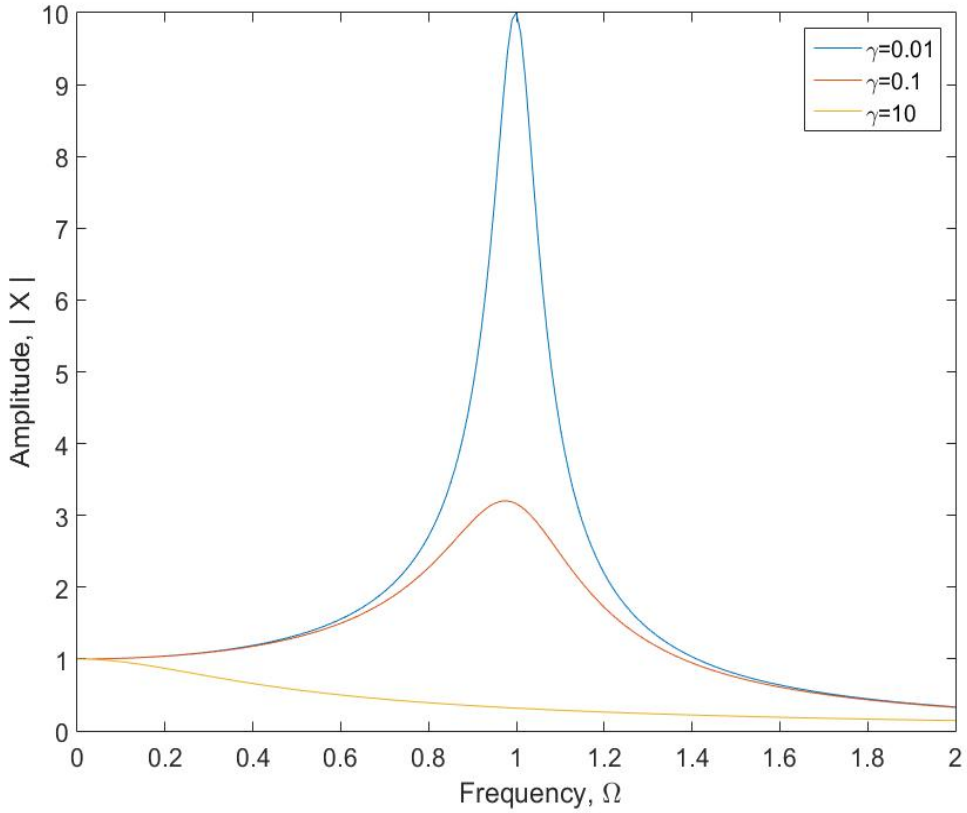

Figure 2.3: Frequency response curve of a damped harmonic oscillator

Fig.2.3 is the frequency response plot of a damped harmonic oscillator which shows underdamped and overdamped response. From the solution of Eqn.2.4, it can be shown that under the effect of constant force meaning without the presence of harmonic nature of the driving force, the response will be as follows:

$$X = F/k \tag{2.5}$$

which makes total sense since the frequency is zero and the spring will be stretched at a fixed amount. Here the question will shrink down to how much the spring will be stretched under the effect of constant forcing rather than a harmonic force. On the other hand, if the frequency is very high considering the damping force is small enough, $m\Omega^2$ term will be large enough to dominate in the denominator of Eqn. 2.6 and the solution can be written as:

$$\lim_{\Omega \to \infty} |X| = \frac{F}{m\,\Omega^2} \tag{2.6}$$

where, $\Omega \to \infty$ turns this expression $\sqrt{(m\,\Omega^2 - k\,)^2 + (\gamma\,\Omega)^2}$ into $m\,\Omega^2$. This means that if the system is driven by very high frequencies, the damping will be hardly felt rather the inertia due to the mass attached will be felt and the applied force will keep accelerating the system.

It is also noted that the denominator $[\sqrt{(m\,\Omega^2 - k\,)^2 + (\gamma\,\Omega)^2}]$ is always positive. When $m\,\Omega^2 = k\,$, the response,X will be large which will move towards a very large response if damping is low. In that case, this very large response will be the resonance of the system. In the case of resonance, the external harmonic forcing frequency will be the same as natural frequency (ω) of the oscillator (since, $k = m\,\omega^2$).

$$\begin{aligned} m\,\Omega^2 &= k \\ m\,\Omega^2 &= m\,\omega^2 \\ \Omega^2 &= \omega^2 \\ \Omega &= \omega \end{aligned} \tag{2.7}$$

Fig.2.3 shows the frequency response plot where the peak amplitude refers to the resonance condition. From the characteristics of the frequency response plot, it is clear

that for a linear oscillator, there will be no hysteresis region and resonance will occur exactly when the harmonic driving frequency matches the natural frequency. With the increase of damping (γ), the response amplitude decreases and hence, the resonance amplitude decreases as well. In the overdamped condition ($\gamma = 10$), the response starts decreasing from the very beginning with the increasing frequency and for the underdamped conditions ($\gamma = 0.01$ and 0.1), the response is larger closer to resonance frequency. The plotting is done considering, $m = 1$,$k = 1$ and that is why the natural frequency or the resonance frequency will be at $\Omega = \omega = 1$.

Here, we also note that, the restoring force in the spring for linear oscillator is $F = -kx$ and the potential energy would be $V = \frac{1}{2}kx^2$. Fig.1.6.3 shows the potential curve with k=1;

Another classic example of a linear oscillator is the simple pendulum. Let us assume a simple pendulum as shown in Fig. 2.5. A very small mass (point mass),m is suspended from an inextensible light spring of length, L. The bob can swing back and forth in the vertical plane (x-y plane). The equilibrium position is the point when there is no vertical deviation of the bob. Let us assume that the bob is displaced by a small angle (θ) with the downward vertical.

The moment of inertia, I can be written as $I = mL^2$. If the torque acting on the system is τ, the equation of motion of the pendulum turns out to be:

$$I\ddot{\theta} = \tau \tag{2.8}$$

The two forces acting on the bob (m) are the tension T, along the string and the downward gravitational force (mg). The tension has no effect on the torque since the line of action of the torque passes through the pivot. So, the only force that contributes to torque is the component of the gravitational force ($mgsin\theta$). Hence the expression of the torque can be written as:

$$\tau = -m\,g\,L\sin\,\theta \tag{2.9}$$

Now, combining Eqn. 2.8 and 2.9, Eqn. 2.10 can be written as:

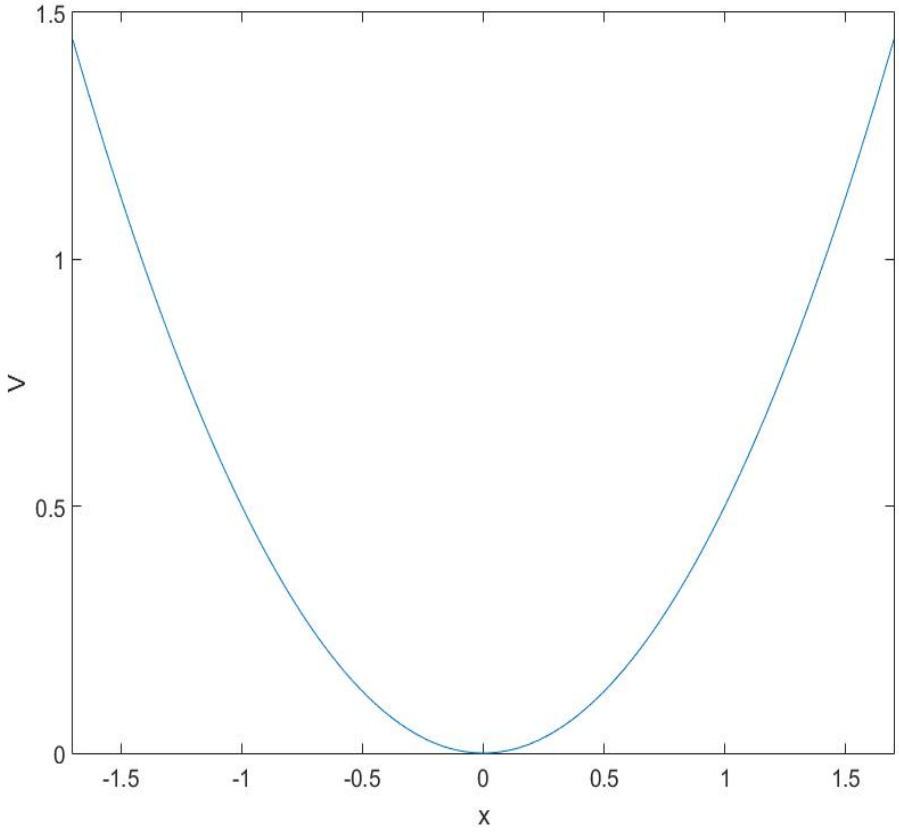

Figure 2.4: Potential energy for linear spring

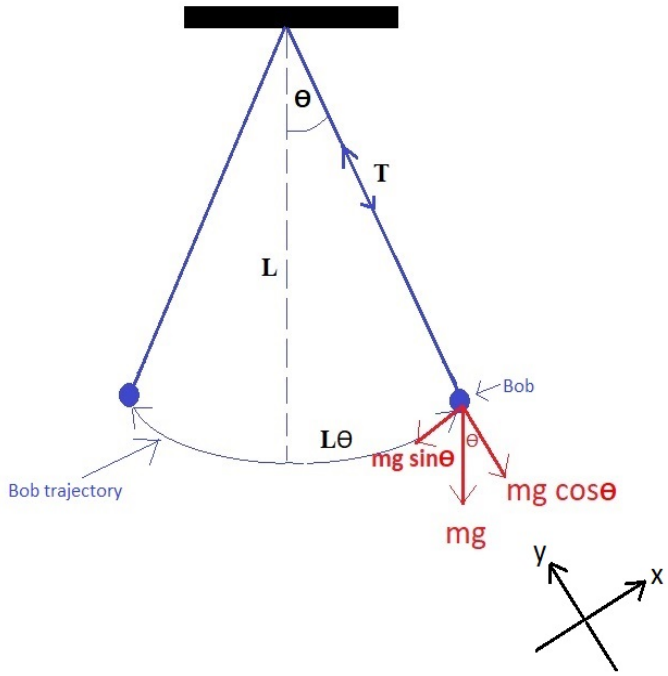

Figure 2.5: Simple pendulum

$$\begin{aligned} mL^2\ddot{\theta} &= -m\,g\,L\sin\,\theta \\ L\ddot{\theta} &= -g\,\sin\,\theta \end{aligned} \tag{2.10}$$

If the angle of deviation from the equilibrium, θ is restricted to be small, from trigonometry,

$$\sin\theta = \theta$$

Under this restriction, the equation of motion (Eqn. 2.10) can be written as:

$$L\ddot{\theta} + g\,\theta = 0 \tag{2.11}$$

$$\ddot{\theta} + \omega^2\,\theta = 0 \tag{2.12}$$

where $\omega = \sqrt{g/L}$

It is noted that Eqn.2.12 is the similar second order differential equation found earlier in the spring-mass system. Now, if we consider that the pendulum is driven by harmonic forcing under the effect of damping, it will be turned out to be an equation of simple harmonic oscillator.

$$\ddot{\theta} + \omega^2\,\theta + \gamma\,\dot{\theta} = F\,cos(\Omega\,t) \tag{2.13}$$

where, γ is the linear damping coefficient and Ω is the frequency of the harmonic driving force.

In summary, the simple harmonic oscillator provides a fundamental framework to describe linear systems. This equation will play a key role in modeling the dynamics of a nanomechanical resonator which is discussed in the next sections.

2.3 Nonlinear Oscillator

Like linear oscillators, nonlinear oscillators are also used to model a variety of physical systems or processes [76, 77, 78, 79, 80, 81, 82]. Duffing oscillator and Van der Pole

oscillator are two well known examples of nonlinear oscillators. Between them, Duffing oscillator plays an important role to model a nanomechanical resonator. Hence, modeling and characteristics of the Duffing oscillator will be our point of interest in this section.

Duffing oscillator is basically a modified version of driven harmonic oscillator as discussed in the previous section (section 2.2). It was named after Georg Duffing (1861 1944). The Duffing oscillator is defined by the following second order nonlinear differential equation:

$$\ddot{x} + \delta\,\dot{x} + \beta\,x + \alpha\,x^3 = F\,cos\,(\,\omega\,t\,) \tag{2.14}$$

where, α is responsible for linear stiffness and β controls the nonlinearity of the system.

the model clearly tells us that the equation differs from the damped driven harmonic oscillator by a term αx^3 of cubic stiffness which is known as nonlinear Duffing term. The presence of this single term changes the dynamics remarkably. Some of the important facts of the Duffing equation are given below:

- Exact analytical solution is not available in terms of simple functions. Solutions in terms of Jacobi elliptic functions do exist but are difficult to deal with in practice.
- A linear combination of solutions will not yield the solution of the Duffing equation like it does for simple harmonic oscillator since the superposition principle can not be applicable due to the nonlinear term.
- The solution is strongly dependent on the initial values.
- Frequency response characteristics can show hardening or softening regime depending on the parameters.
- Limit cycles can exist.

The potential energy of the Duffing oscillator can be written as follows:

$$V(x) = \frac{1}{2}\beta x^2 + \frac{1}{4}\alpha x^4 \tag{2.15}$$

In the case of $\beta > 0$, the Duffing equation can be described in terms of a nonlinear spring with a restoring force of $F = -\alpha x^3 - \beta x$. In this case, system will be monostable. The spring is called a hardening spring if $\alpha > 0$ and spring will be a softening spring if $\alpha < 0$.

For $\beta < 0$, the Duffing oscillator represents the double well potential of a point mass. The dynamics of a harmonically deflected steel beam in between two magnets can be defined using this parameter setting [Fig. 2.6].

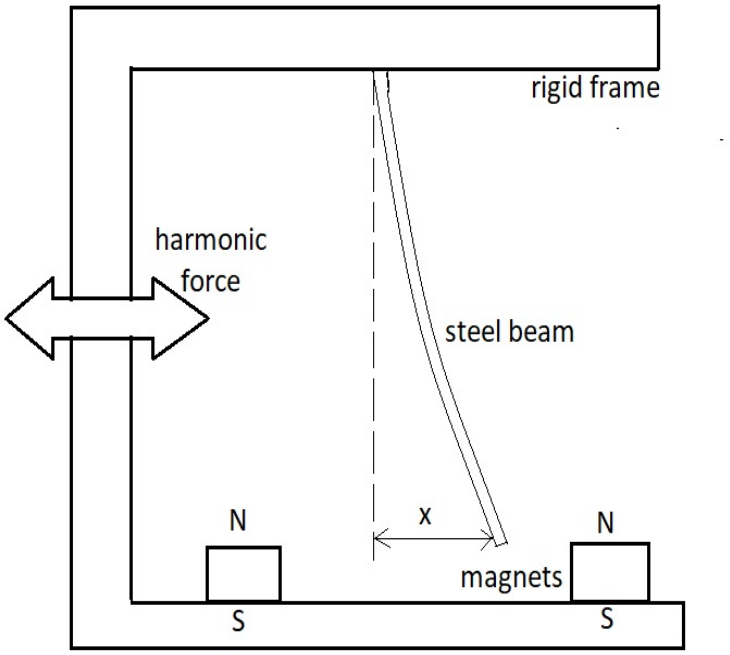

Figure 2.6: Deflected steel beam in between two magnets

Basically, depending on the sign of α and β, the potential and the characteristics of

the equilibrium points vary.

- If α and β have same sign with $\alpha > 0$ and $\beta > 0$, the spring will be in a hardening regime and the potential energy curve will exhibit monostability with one equilibrium point. Fig. 2.7 depicts this situation.

- If α and β have opposite signs with $\alpha > 0$ and $\beta < 0$, the spring will be in a hardening regime and the potential energy curve will exhibit bistability with 3 equilibrium point. Fig. 2.8 depicts this situation.

- If α and β have same sign with $\alpha < 0$ and $\beta < 0$, the spring will be in a softening regime and the potential energy curve will have one unstable equilibrium point. Fig. 2.9 depicts this circumstance.

- For α and β have opposite sign with $\alpha < 0$ and $\beta > 0$, the spring will be in a softening regime and the potential energy curve will have 3 equilibrium points with 1 stable point. Fig. 2.10 depicts this situation.

Relating to the potential energy curve of a linear spring (Fig.2.4), it can be said that in case of a Duffing oscillator, the potential energy due to the nonlinear spring could show bistability and more than one equilibrium point. Hence, the frequency response should also differ from the linear case. The frequency response curves for Duffing oscillator are plotted in Fig. 2.11 in 3 different cases. In each case $\beta = 1$, $\delta = 0.1$ and F=1 are considered.

- For $\alpha = 0$ the response will be the same as in the case of linear oscillator. There is no hysteresis region in the response and the resonance condition is also unchanged from the linear oscillator.

- For $\alpha < 0$ the response will differ from the case of linear oscillator since the curve will show response in softening regime. There will be hysteresis region in the response and the resonance frequency will be lower than the resonance frequency of linear oscillator.

- For $\alpha > 0$ the response will differ from the case of linear oscillator since the curve will show response in hardening regime. There will be hysteresis region in the

response and the resonance frequency will be higher than the resonance frequency of linear oscillator.

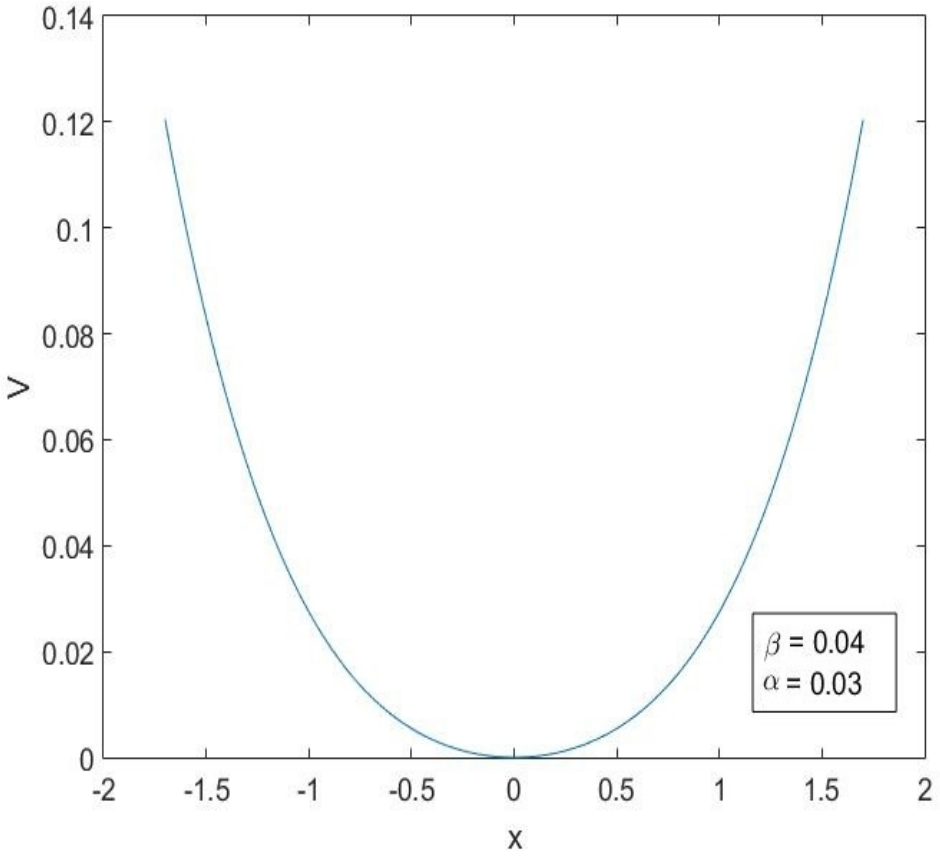

Figure 2.7: Single well potential (hardening regime)

The model of a nanoelectromechanical resonator has similarity with the Duffing oscillator. Looking at the models of simple harmonic oscillator and Duffing oscillator, it is clear that those do not consider nonlinear damping as an energy decaying factor. Resonators from meter scale to micro scale (in some case even in nano scale) can be modeled in terms of only linear damping. Eichler *et al.* [3] performed experiments with graphene and CNT based nanoresonators and explained the NEMS resonator dynamics with nonlinear damping based on the nonlinear damping theory provided in [26]. They explained graphene/CNT based nanoresonator dynamics modifying the Duffing

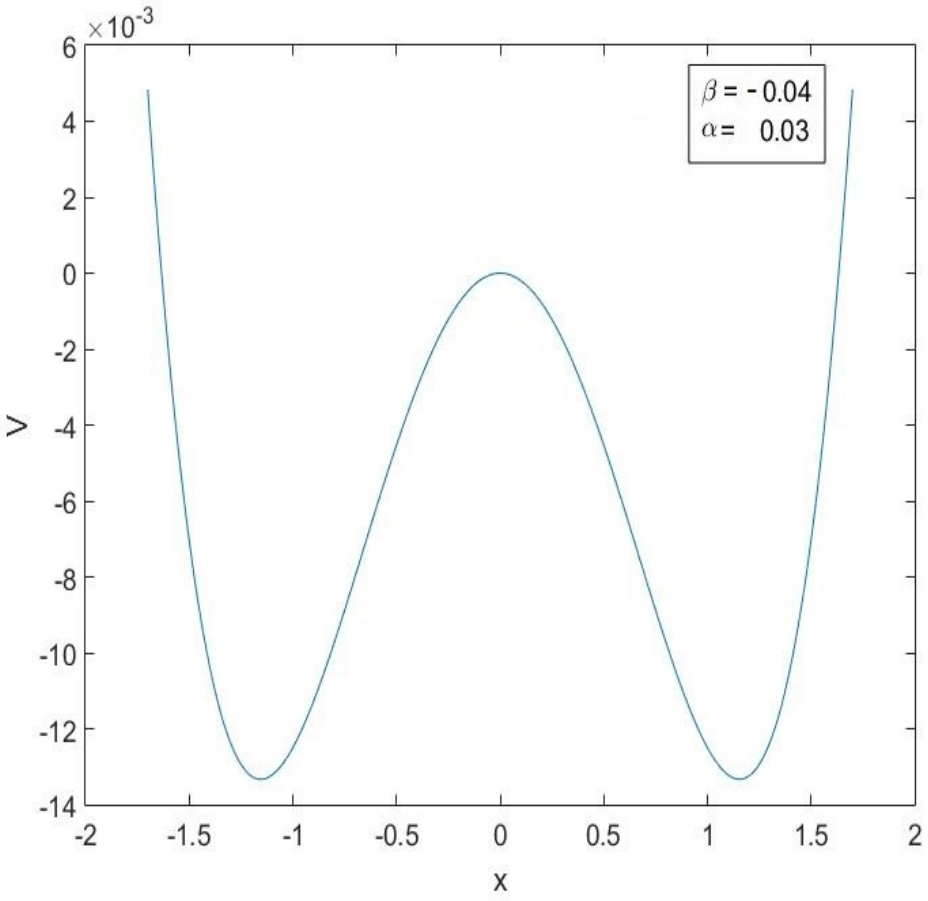

Figure 2.8: Double well potential (hardening regime)

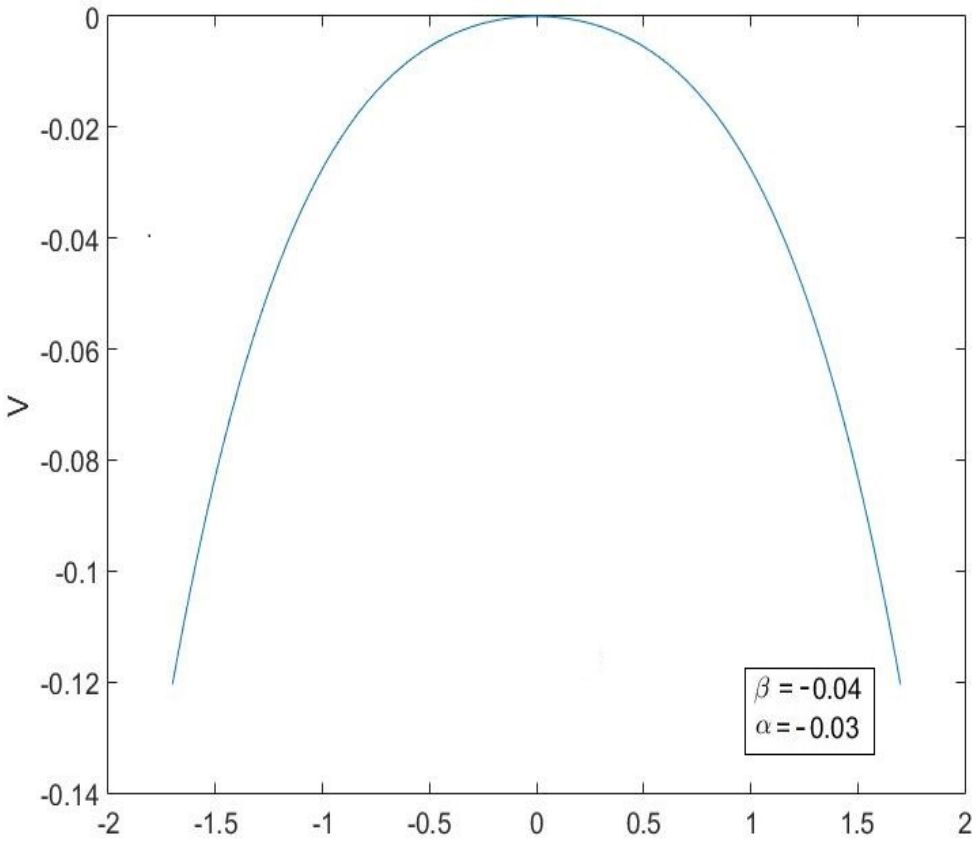

Figure 2.9: Single well potential(softening regime)

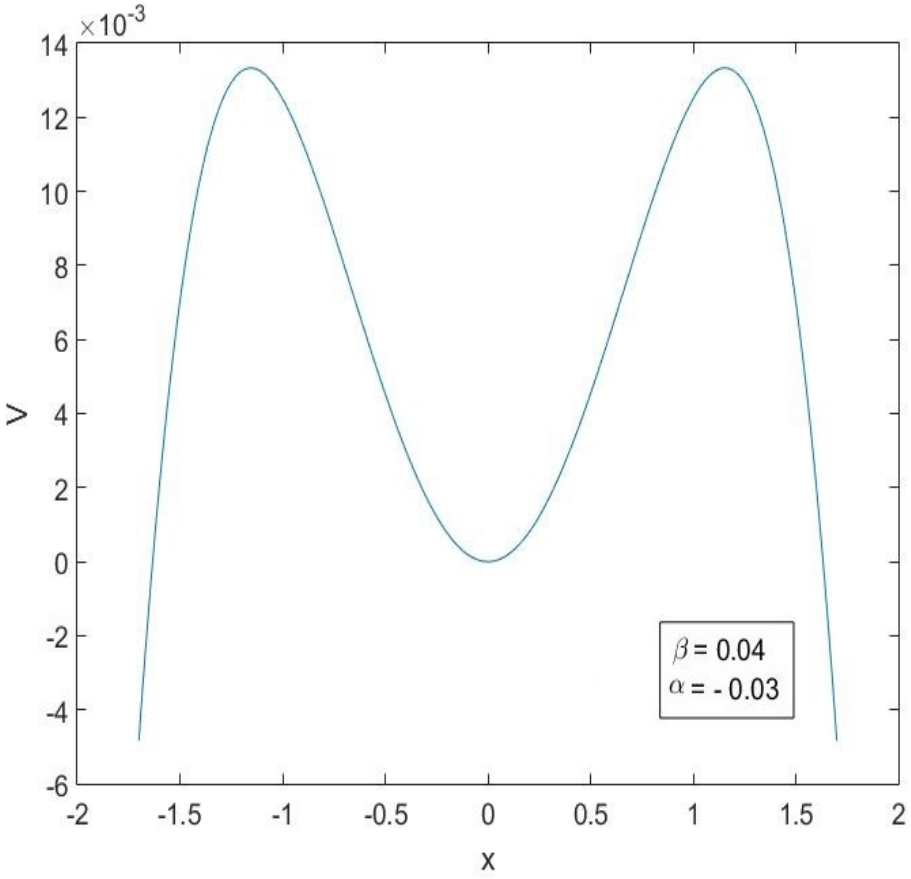

Figure 2.10: Double well potential(softening regime)

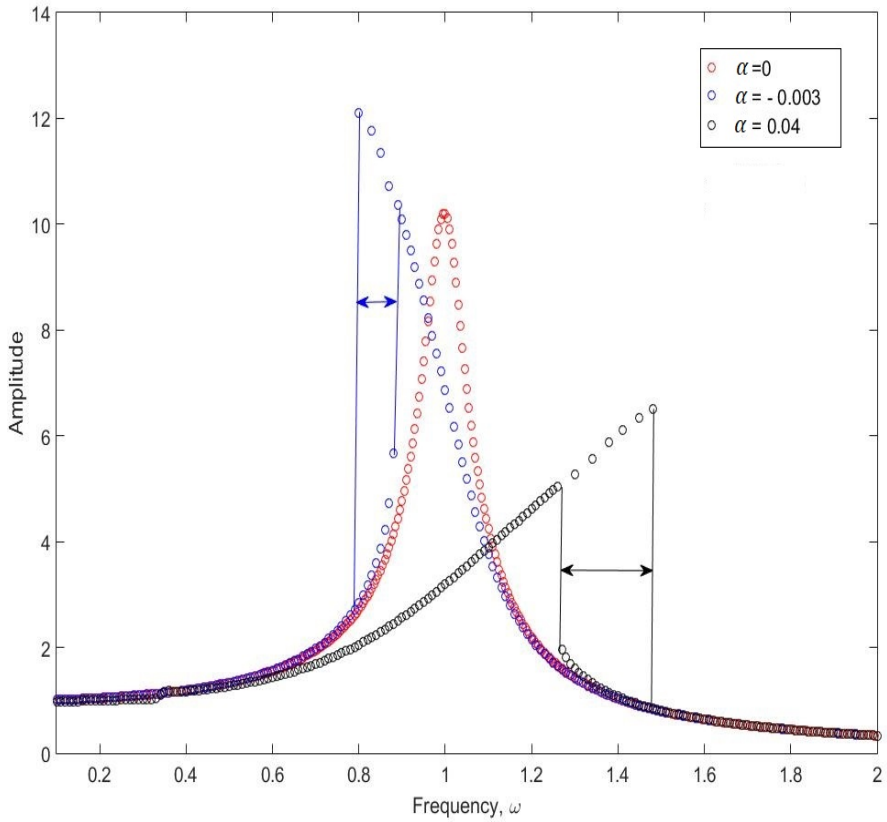

Figure 2.11: Frequency response of a Duffing oscillator

equation with an additional higher order nonlinear damping term, $\eta x^2 \dot{x}$. This nonlinear damping term differs with linear damping in such a way that, linear damping ($\delta \dot{x}$) is unchanged with the amplitude of the motion whereas nonlinear damping depends on the amplitude of the motion (nonlinear damping $\propto$ amplitude). Model equation of nanomechanical resonator including nonlinear damping term is given below [3, 26, 66]:

$$m\ddot{\tilde{x}} + k\tilde{x} + \alpha\tilde{x}^3 + \gamma\dot{\tilde{x}} + \tilde{\eta}\tilde{x}^2\dot{\tilde{x}} = F_{drive}\cos(2\pi f\tilde{t}) \tag{2.16}$$

Here, m represents the effective mass of the resonator, α is the coefficient of cubic stiffness, k is the linear stiffness coefficient (positive quantity), γ and η are the linear and nonlinear damping coefficients respectively. The linear stiffness coefficient, k is expressed as $k = m\omega_0^2$ (where $\omega_0 = 2\pi f$ is the natural frequency of fundamental mode) and F_{drive}, the amplitude of the external force. We reiterate that $\alpha > 0$ corresponds to the hardening stiffness regime (with a monostable quartic potential energy function) while $\alpha < 0$ corresponds to the softening stiffness regime (with a bistable quartic potential energy function).

Model Eqn. 2.16 will be our point of interest for the rest of this thesis. The analytical and computational scheme are based in the nondimesionalised form of this model. The derivation of the nondimensionalised model of Eqn. 2.16 is given in the next section.

2.3.1 Nondimensionalization

Nondimensionalization is considered to be the first step to deal with the analytical or numerical solution of a complex differential equation. The reasons behind nondimensionalization are as follows:

- It makes the equation comparatively simple reducing the number of variables.
- Dimensionless equations can be analyzed without any concern about the units of the physical parameters.
- In numerical simulation, the errors associated with the calculations due to the physical size of the parameters can be avoided.
- Since nondimensionalization process scales the parameters, it might take less numerical time and cost.

- Relative importance of the parameters/terms of the model equation is well understood.

Nondimensionalization of the Model Equation

Moving our attention back to Eqn. 2.16 it is clear that $\tilde{x}$, $\tilde{t}$ are the variables and m, k, γ, α, η, f, F_{drive} are the dimensional parameters. First step is to nondimensionalize the variables $\tilde{x}$ and $\tilde{t}$ into x and t respectively using the dimensional parameters. To do that let us assume:

$$\begin{aligned} x &= \frac{\tilde{x}}{x_s} \\ t &= \frac{\tilde{t}}{t_s} \\ k &= m w_0^2 \end{aligned} \tag{2.17}$$

where x_s and t_s are the scaling factors. These can be expresses as follows:

$$\begin{aligned} x_s &= \sqrt{\frac{m\, w_0^2}{\alpha}} \\ t_s &= \frac{1}{w_0} \end{aligned} \tag{2.18}$$

For convenience, let us rewrite the model equation (Eqn. 2.16) with some rearrangements and using '$\frac{d}{d\tilde{t}}$' as the notation of the derivative:

$$m\frac{d^2\tilde{x}}{d\tilde{t}^2} + m\, w_0^2\, \tilde{x} + \alpha\, \tilde{x}^3 + \gamma\, \frac{d\tilde{x}}{d\tilde{t}} + \tilde{\eta}\, \tilde{x}^2\, \frac{d\tilde{x}}{d\tilde{t}} \;=\; F_{drive}\, \cos\left(\, 2\, \pi\, f\, \tilde{t}\, \right) \tag{2.19}$$

Substituting $\tilde{x}$ and $\tilde{t}$ of Eqn.2.19 with the scaling factors of Eqn.2.17:

$$
\begin{aligned}
m\frac{d^2(x\,x_s)}{d(t_s\,t)^2} + m\,w_0^2\,(x\,x_s) + \alpha\,(x\,x_s)^3 + \gamma\,\frac{d(x\,x_s)}{d(t_s\,t)} + \\
\tilde{\eta}\,(x\,x_s)^2\,\frac{d(x\,x_s)}{d(t_s\,t)} \;=\; F_{drive}\,\cos\,(\,2\,\pi\,f\,t_s\,t\,) \\
\Rightarrow m\frac{d}{d\,(t_s\,t)}\Big[\frac{d(x\,x_s)}{d\,(t_s\,t)}\Big] + m\,w_0^2\,(x\,x_s) + \alpha\,(x\,x_s)^3 + \gamma\,\frac{d(x\,x_s)}{d(t_s\,t)} + \\
\tilde{\eta}\,(x\,x_s)^2\,\frac{d(x\,x_s)}{d(t_s\,t)} \;=\; F_{drive}\,\cos\,(\,2\,\pi\,f\,t_s\,t\,)
\end{aligned}
\tag{2.20}
$$

$$
\begin{aligned}
\Rightarrow m\frac{x_s}{t_s}\frac{d}{d\,(t_s\,t)}\Big[\frac{d\,x}{d\,t}\Big] + m\,w_0^2\,(x\,x_s) + \alpha\,(x\,x_s)^3 + \gamma\,\frac{x_s}{t_s}\frac{dx}{d\,t} + \\
\tilde{\eta}\,(x\,x_s)^2\,\frac{x_s}{t_s}\frac{dx}{d\,t} \;=\; F_{drive}\,\cos\,(\,2\,\pi\,f\,t_s\,t\,) \\
\Rightarrow m\frac{x_s}{t_s^2}\frac{d^2\,x}{d\,t^2} + m\,w_0^2\,(x\,x_s) + \alpha\,(x\,x_s)^3 + \gamma\,\frac{x_s}{t_s}\frac{dx}{d\,t} + \\
\tilde{\eta}\,(x\,x_s)^2\,\frac{x_s}{t_s}\frac{dx}{d\,t} \;=\; F_{drive}\,\cos\,(\,2\,\pi\,f\,t_s\,t\,)
\end{aligned}
\tag{2.21}
$$

Now, using the values of x_s and t_s used in Eqn. 2.18 into Eqn. 2.21:

$$\Rightarrow m\frac{\sqrt{\frac{m\,w_0^2}{\alpha}}}{(\frac{1}{w_0})^2}\frac{d^2\,x}{d\,t^2}+m\,w_0^2\left(x\sqrt{\frac{m\,w_0^2}{\alpha}}\right)+\alpha\left(x\sqrt{\frac{m\,w_0^2}{\alpha}}\right)^3+\gamma\frac{\sqrt{\frac{m\,w_0^2}{\alpha}}}{\frac{1}{w_0}}\frac{dx}{d\,t}+$$
$$\tilde{\eta}\left(x\sqrt{\frac{m\,w_0^2}{\alpha}}\right)^2\frac{x_s}{t_s}\frac{dx}{d\,t}\;=\;F_{drive}\,\cos\left(\,2\,\pi\,f\,\frac{1}{w_0}\,t\,\right)$$
$$\Rightarrow m\frac{\sqrt{\frac{m\,w_0^2}{\alpha}}}{(\frac{1}{w_0})^2}\frac{d^2\,x}{d\,t^2}++m\,w_0^2\left(x\sqrt{\frac{m\,w_0^2}{\alpha}}\right)+\alpha\left(x\sqrt{\frac{m\,w_0^2}{\alpha}}\right)^3+\gamma\frac{\sqrt{\frac{m\,w_0^2}{\alpha}}}{\frac{1}{w_0}}\frac{dx}{d\,t}+$$
$$\tilde{\eta}\left(x\sqrt{\frac{m\,w_0^2}{\alpha}}\right)^2\frac{\sqrt{\frac{m\,w_0^2}{\alpha}}}{\frac{1}{w_0}}\frac{dx}{d\,t}\;=\;F_{drive}\,\cos\left(\,2\,\pi\,f\,\frac{1}{w_0}\,t\,\right)$$
$$\Rightarrow w_0^3\sqrt{\frac{m^3}{\alpha}}\frac{d^2\,x}{d\,t^2}+w_0^3\sqrt{\frac{m^3}{\alpha}}\,x+\alpha\,x^3\,w_0^3\left(\sqrt{\frac{m}{\alpha}}\right)^3+\gamma w_0^2\sqrt{\frac{m}{\alpha}}\frac{d\,x}{d\,t}+$$
$$\tilde{\eta}\,x^2\left(\sqrt{\frac{m\,w_0^2}{\alpha}}\right)^3 w_0\,\frac{d\,x}{d\,t}\;=\;F_{drive}\,\cos\left(\frac{\tilde{w}}{w_0}\,t\,\right)$$
Here, we used $w=2\,\pi\,f$
$$\Rightarrow w_0^3\sqrt{\frac{m^3}{\alpha}}\frac{d^2\,x}{d\,t^2}+w_0^3\sqrt{\frac{m^3}{\alpha}}\,x+x^3\,w_0^3\sqrt{\frac{m^3}{\alpha}}+\gamma w_0^2\sqrt{\frac{m}{\alpha}}\frac{d\,x}{d\,t}+$$
$$\tilde{\eta}\,x^2\left(\sqrt{\frac{m\,w_0^2}{\alpha}}\right)^3 w_0\,\frac{d\,x}{d\,t}\;=\;F_{drive}\,\cos\left(\frac{\tilde{w}}{w_0}\,t\,\right)$$
(2.22)

Dividing the whole Eqn.2.22 with $w_0^3\sqrt{\frac{m^3}{\alpha}}$:

$$\frac{d^2\,x}{d\,t^2}+x+x^3+\frac{\gamma}{m\,w_0}\frac{d\,x}{d\,t}+\tilde{\eta}\,x^2\,\frac{w_0}{\alpha}\,\frac{d\,x}{d\,t}\;=\;\frac{F_{drive}}{w_0^3}\sqrt{\frac{\alpha}{m^3}}\,\cos\left(\frac{\tilde{w}}{w_0}\,t\,\right)$$
$$\Rightarrow\frac{d^2\,x}{d\,t^2}+x+x^3+\delta\,\frac{d\,x}{d\,t}+\eta\,x^2\,\frac{d\,x}{d\,t}=\;F_D\,\cos\left(\Omega\,t\,\right)$$
(2.23)

where,

$$\begin{aligned} \Omega &= \frac{\omega}{\omega_0} \\ \delta &= \frac{\gamma}{m\,\omega_0} \\ \eta &= \frac{\eta\,\tilde{\omega}_0}{\alpha} \\ F_D &= \frac{F_{drive}}{\omega_0^3}\sqrt{\frac{\alpha}{m^3}} \end{aligned} \tag{2.24}$$

which will be used for the rest of this thesis unless specified otherwise.
Finally we can write the final form of nondimensionalized model equation as follows:

$$\ddot{x} + x + x^3 + \delta\,\dot{x} + \eta\,x^2\,\dot{x} = F_D\,\cos\left(\Omega\,t\right) \tag{2.25}$$

which is the deterministic model equation of the dynamics of a nanoelectromechanical resonator. Study of this equation will be our core focus of this thesis.

2.3.2 Parametric Modeling of a Nanomechanical Resonator

Time dependent parameters are common in micro/nano systems. As a result, parametric excitation often occurs naturally in micro and nanoscale systems. It can be used to modulate the natural frequency of a resonator even without the presence of an external excitation. There has been many efforts to model the effect of parametric excitation on the dynamics of a nano/micro resonator. A popular approach is to model the dynamics in such a way that parametric excitation can modulate the effective spring constant of the nanoresonator [83, 84, 85]. Taking parametric excitation into account, using the same scaled form of a nanoresonator model (Eqn. 2.25, the dynamics of a nanoresonator can be modified by introducing a harmonic parametric excitation in the stiffness term [26, 86] as follows:

$$\ddot{x} + \delta\dot{x} + [1 + H\cos(\Omega_p t)]x + x^3 + \eta x^2\dot{x} = F_D\cos(\Omega_d t + \phi_g) \tag{2.26}$$

where H is the parametric excitation amplitude that regulates linear stiffness of the system, Ω_d represents the external forcing frequency and Ω_p denotes the pump frequency.

2.3.3 Stochastic Modeling of a Nanomechanical Resonator

One of the objectives of this thesis is to investigate the effect of external stochastic excitation on the dynamics of the nanoresonator since noise-induced effects are important to consider in the micro and nano scales. Lévy flight excitation is chosen as the stochastic process here since, in several situations, it provides a better representation of the noise process driving the dynamics than the typically considered white noise process (Brownian motion). Taking the noise into account, the deterministic model based on Ordinary Differential Equation (ODE) transforms into Stochastic Differential Equation Model (SDE). Additional external forcing as stochastic excitation is quite common in nano/micro scaled system which has been discussed in section 1.6.2 and this stochastic force is taken into account by introducing the term $\sigma\xi(t)$ into Eqn. 2.25:

$$\ddot{x} + x + x^3 + \delta\,\dot{x} + \eta\,x^2\,\dot{x} = F_D\,\cos(\Omega\,t) + \sigma\xi(t) \tag{2.27}$$

where, σ represents the noise intensity of the stochastic process $\xi(t)$. In case of white Gaussian noise process,$\xi(t)$ is a zero-mean, Dirac Delta function correlated process where the increments are drawn from a Gaussian distribution. On the other hand, the increments are taken from a Lévy distribution in the case Lévy stochastic process. Lévy flights are are known to possess extremely long jumps which implies that realizations can have values far from the mean. It is our interest to see the effect of this Lévy stochastic excitation on the hysteresis and the Q factor of the nanoresonator. Here, we note that the mathematical representation of Lévy distribution can be given [87, 88, 89] as follows:

$$L(s,\gamma,\mu) = \begin{cases} \sqrt{\frac{\gamma}{2\pi}}\,\frac{1}{(s-\mu)^{3/2}}\,e^{\left(-\frac{\gamma}{2(s-\mu)}\right)} & 0 < \mu < s < \infty \\ 0 & if \;\; s \leq 0 \end{cases} \tag{2.28}$$

where, $\gamma > 0$ is the width controlling parameter and μ holds for the location of the distribution peaks. Though the above mathematical representation is complex, Lévy distribution can simply be represented using a power law:

$$L(s) \sim |s|^{-1-\beta} \tag{2.29}$$

where, Lévy index, β affects the characteristics of tail regime of a Lévy distribution.

When β is smaller (closer to zero), longer step sizes are drawn in the distribution whereas for higher β values (closer to 2), smaller steps are observed in the distribution.

The Lévy distribution can also be represented by its Fourier transform as follows:

$$F(k) = exp(-\alpha|k|^{\beta}), 0 < \beta \leq 2 \tag{2.30}$$

where, α is the skewness factor, valued in between -1 and 1; $\alpha = 0$ indicates that distribution is symmetric. When $\beta = 2$, the Lévy distribution turns into the Gaussian distribution and for $\beta = 1$, the distribution turns into the Cauchy probability distribution. When β is small, the skewness of α becomes significant. As β increases, the dominance of α decreases.

Fig.2.12 shows the variation of probability distribution characteristics with β. With the decrease of β, the distribution peak goes higher and the long tailed characteristics become more dominant (See Fig.2.13). The tail is the shortest when β=2 and it becomes the normal probability distribution plot.

Fig.2.14 shows the skewness of the probability distribution plot.

- When $\alpha < 0$, long tail is on the left side making the distribution left skewed.
- When $\alpha > 0$, long tail is on the right side making the distribution right skewed.
- When $\alpha = 0$, tails on the both sides are equal making the distribution symmetric.

Fig.2.15 shows the variation of peaks in the probability distribution plot and Fig.2.16 depicts the variation of the width of the distribution curves. With increasing γ, the width becomes larger and the distribution peaks become smaller.

2.4 Analytical Method

Many of the real life problems we face are nonlinear in nature. In other words, many real life phenomena can be modeled using nonlinear differential equations. There have been several methods developed to study the dynamics of a nonlinear system. They are:

- Perturbation Method

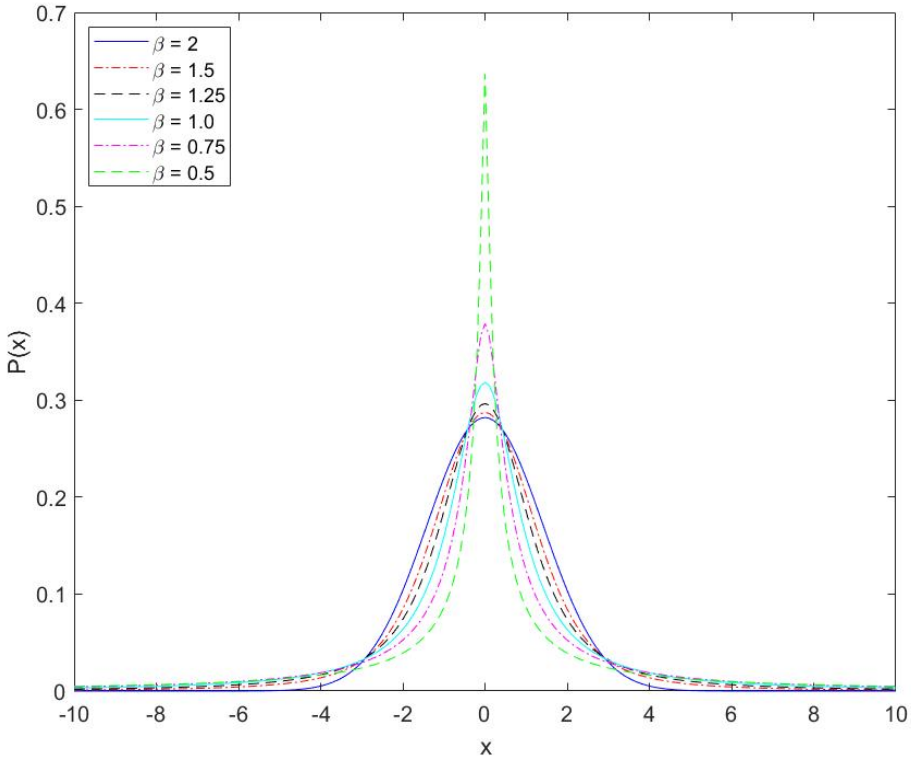

Figure 2.12: Comparison of β parameters in probability distribution plots. Here,$\alpha = 0, \gamma = 1, \mu = 0$.

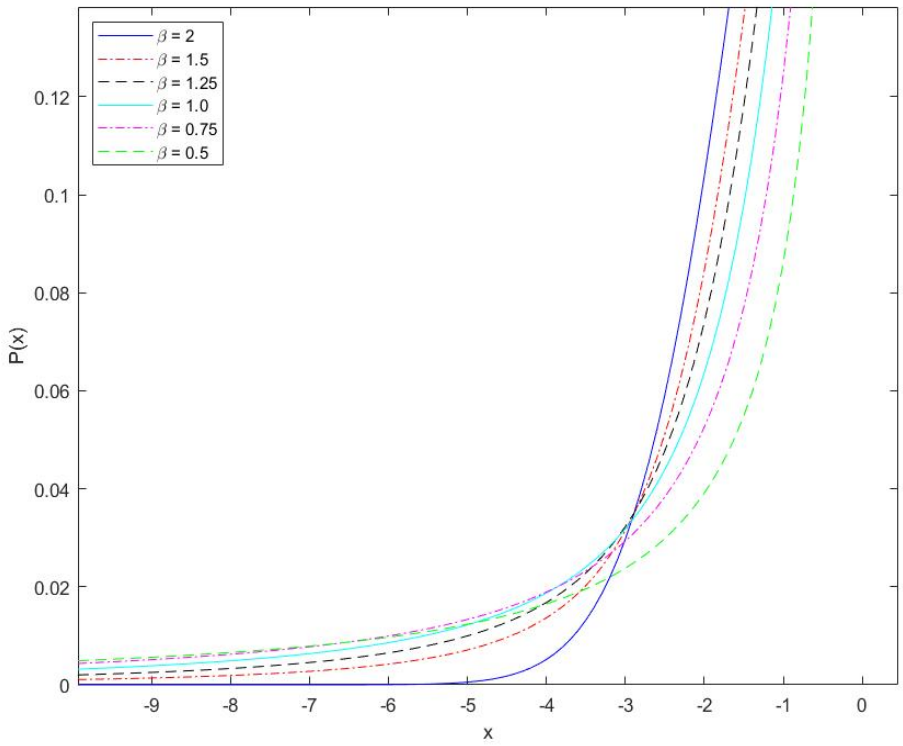

Figure 2.13: Comparison of β parameters in probability distribution plots (zoomed in). Long tail is observed. Here, $\alpha = 0, \gamma = 1, \mu = 0$.

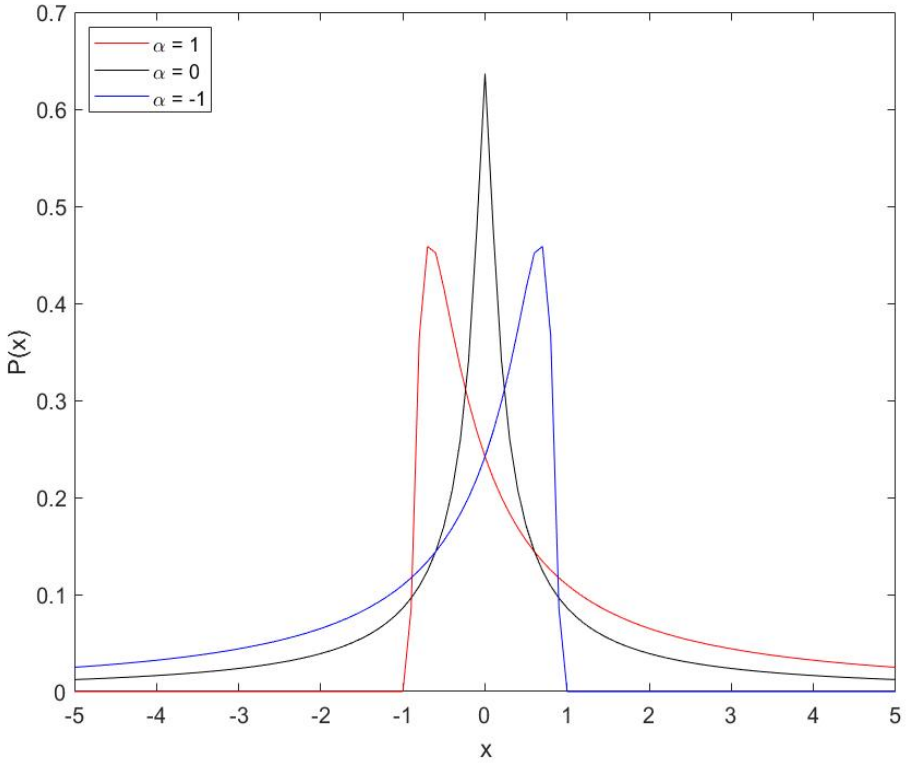

Figure 2.14: Comparison of α parameters in probability distribution plots. Here,$\beta = 0.5, \gamma = 1, \mu = 0$.

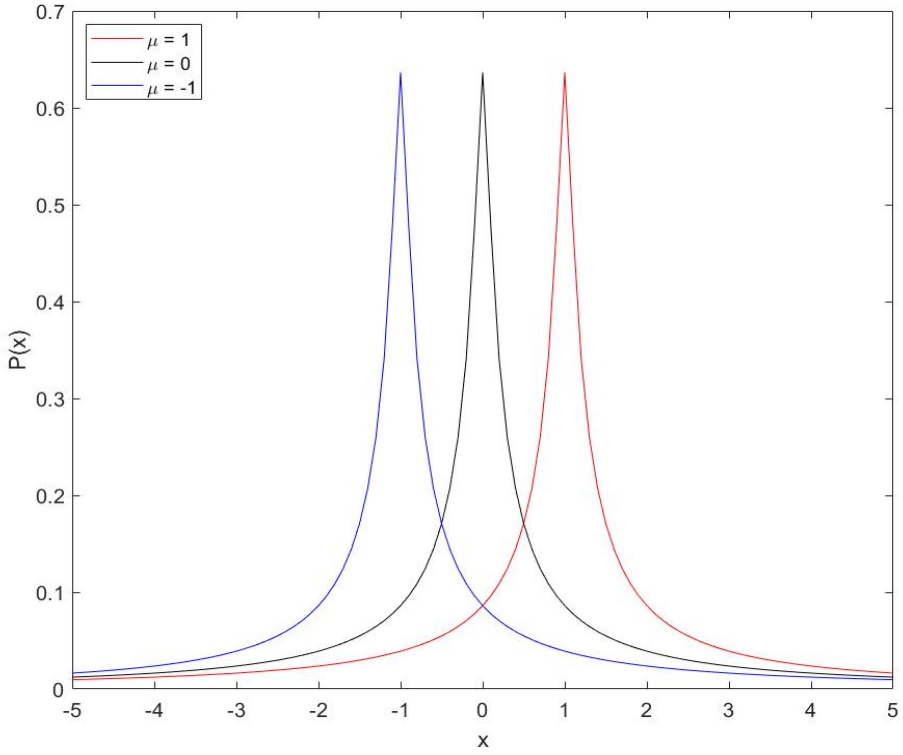

Figure 2.15: Comparison of μ parameters in probability distribution plots. Here, $\beta = 0.5 = 0, \gamma = 1, \alpha = 0$.

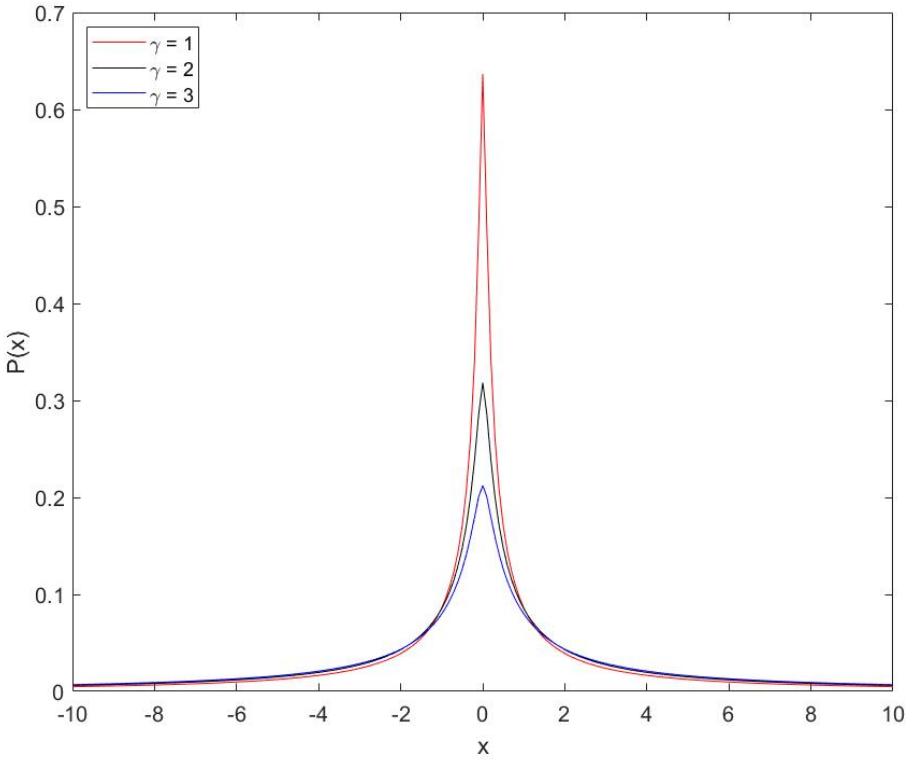

Figure 2.16: Comparison of γ parameters in probability distribution plots. Here, $\beta = 0.5 = 0, \mu = 1, \alpha = 0$.

- The Method of Harmonic Balance
- The Method of Krylov and Bogolyubov
- The Method of Multiple Scales
- The Optimal Homotopy Asymptotic Method
- The Optimal Homotopy Perturbation Method
- The Optimal Variational Iteration Method
- Optimal Parametric Iteration Method

Among them, 'The Method of Harmonic Balance (HBM)' is our focus in this thesis which is applied to solve nondimensionalized model equation of a nanomechanical resonator. If there exists a periodic solution to a differential equation, the solution can be sought using the terms of the Fourier Series. The steps which are followed to obtain solution using HBM are given below:

Step 1: Response should be like one of the following forms

$$x(t) = \sum_{m=0}^{M} A_m \cos(m\omega t + m\beta_0)$$

or

$$x(t) = \sum_{m=0}^{M} A_m \sin(m\omega t + m\beta_0)$$

or

$$x(t) = \sum_{m=0}^{M} \left[\hat{A_m} \cos(m\omega t) + \hat{B_m} \sin(m\omega t) \right] \tag{2.31}$$

Step 2: It needs to take only one term expansion of the Eqn. 2.31 Say,

$$x = A_1 \cos(\omega t + \beta\omega_0) = A_1 \cos(\phi) \tag{2.32}$$

Step 3: Substitute the one term expansion in the governing equation.

Step 4: Equate the coefficient of $\cos(\phi)$ to zero.

Step 5: A_1 is considered to be small and a relation between ω and A_1 is obtained.

Step 6: Solution has to be checked.

Step 7: If the solution is not correct, we have to go back to Step 3 where two terms need to be considered this time.

$$x = A_0 + A_1 \cos(\omega t + \beta\omega_0) = A_0 + A_1 \cos(\phi) \tag{2.33}$$

Step 8: Equate the coefficients of $\cos(\phi)$ and constant terms to zero.

Step 9: Follow steps 5 and 6.

Step 10: If solution is not correctly obtained, an extra term has to be added in Step 7. Say,

$$x = A_0 + A_1 \cos(\phi) + A_2 \cos(2\phi) \tag{2.34}$$

Step 11: Iterate the steps from Step 7 to Step 10 unless solution with good accuracy is obtained.

Harmonic balance method is popular in the study of nonlinear vibrations. But there are disadvantages with this method. Those are as follows:

- Before the formulation of the solution, it is important to know the type of solution, based upon which a decision can be taken about using HBM method.
- The harmonics which are neglected need to be checked thoroughly in case they are actually in the higher order or not.
- One has to know which harmonic terms need to be included in the solution.
- If higher number of terms needed in the assumed solution, the corresponding algebraic calculations can be very tedious.
- Stability analysis is not possible with this method.

Despite having these disadvantages, this method has been proven to be successful in obtaining solutions in the strongly nonlinear regime where perturbation techniques are not that much dependable. Further information about this aspect of the harmonic balance method is available in [90, 91, 92, 93, 94].

2.5 Numerical Method

In order to obtain numerical solutions of the nondimensionalized model equation of the nanomechanical resonator, this thesis applies the Euler-Maruyama method [95]. The Euler-Maruyama method integrates first order differential equation and is well suited to solve stochastic differential equation. This section discusses the basics of Euler-Maruyama method and how to use this method to solve a stochastic differential equation.

2.5.1 Euler-Maruyama method

Euler-Maruyama method is a modified version of Euler method of numerical integration where we also need to convert higher order differential equations into first order differential equations. When no stochastic terms are considered, the Euler-Maruyama method yields the Euler method of numerical integration.

A generic stochastic differential in its scalar form can be written as follows:

$$X(t) = X_0 + \int_0^t f(X(s))ds + \int_0^t g(X(s))dWs \tag{2.35}$$

where, X_0 is the initial value, f and g are the scalar functions. The left integration is the numerical integration based on the deterministic part and the right integral is based on the stochastic part of the model. Considering both, X(t) is the stochastic process (understood as a sequence of random variables realized in each point in time) that is the solution of the SDE. This integral representation is not conventional when compared with the deterministic case. The regular way to write equation in terms of a differential form which is:

$$dX(t) = f(X(t))dt + g(X(t))dW(t) \tag{2.36}$$

where, $X(0) = X_0$ is the initial value, t is defined as $0 \leq t \leq T$. Then, X(t) will be the solution of Eqn. 2.35 at each point in time. Here, we note that, there is no mathematical meaning of $dW(t)/t$ since the derivative of stochastic motion does not exist; however, the differential exists [95]. If g is zero, the equation is a deterministic ODE which can be written as $dX(t)/dt = f(X(t)); X(0) = X_0$.

After writing the equation in the differential form as in Eqn. 2.36, next step is to discretize the interval [0,T] in which the integral has to be computed. If L is a number of increment, discretized time interval,$\Delta t = T/L$. and $t_j = j\Delta t$. If the approximate numerical value of $X(t_j)$ is written as X_j, the E-M model can be written as:

$$X(t_{j+1}) = X(t_j) + f(X(t_j))\Delta t + g(X(t_j))dW(t_j) \tag{2.37}$$

where j=1,2,3...,L. Looking at the Eqn. 2.37, it is obvious that if we want to calculate the value of $X(t_{j+1})$ we need the value from previous step that is the value of $X(t_j)$. For the first step we need to define the initial value and after that the $X(t_{j+1})$ values are calculated by loop until the stability of the solution is achieved. Here, it is important to note that, the convergence of solution depends on the values of simulation time, T and step size ΔT. Tweaking these values will take us to the converged correct solution. Like in the case of Brownian noise where dW(t) is determined using a random number generator based on the normal distribution [95], differential noise of Lévy distribution can be determined using a corresponding random number generator available in the literature [96].

2.5.2 Formulation of Model Equation for Numerical Solution

The focus of our simulation is to numerically solve the model equation of a nanomechanical resonator given in Eqn.2.25 and Eqn. 2.27.These two equations can written using the vector formulation of Ito stochastic differential equations as follows:

$$d\bar{x} = \bar{A}dt + \tilde{B}d\bar{W} \tag{2.38}$$

where $\bar{x}$ is the vector valued state variable, $\bar{W}$ is the Lévy stochastic process vector, and $\bar{A}$ and $\tilde{B}$ may take the following form:

$$\bar{A} = \begin{bmatrix} x_2 \\ -x_1 - x_1^3 - \delta x_2 - \eta x_1^2 x_2 + F_D cos(\Omega t) \end{bmatrix} \tag{2.39}$$

$$\tilde{B} = \sigma \begin{bmatrix} 0 \\ 1 \end{bmatrix} \tag{2.40}$$

Eqn. 2.38 is solved numerically based on the Euler method ($\sigma = 0$) in case of the deterministic model (Eqn. 2.25), and the Euler-Maruyama method [95] for stochastic model (Eqn. 2.27) ($\sigma \neq 0$). In both cases, step rate of 3000 Hz is used with a simulation time of 2000 seconds. Lévy noise profiles were randomly generated following methods available in the literature [96, 97]. Since the noise profiles are random, 50 Euler-Maruyama simulations are performed in the case of stochastic model and an average is calculated to ensure the consistency of the results.

2.5.3 Quality Factor

Quality factor of a resonator refers to the amount of energy stored per oscillation with respect to the amount of energy dissipated per oscillation period. Lower quality factor indicates higher amount of damping is present in the system and amount of energy lost is higher. The following equation (Eqn. 2.41) can be used for the standard definition of quality factor:

$$Q = 2\pi \frac{\text{Energy stored}}{\text{Energy dissipated per cycle}} \tag{2.41}$$

If the system response and resonance are dominated by nonlinearity of the system, the quality factor can be expressed as follows [66]:

$$Q = \omega_0 \frac{\tilde{E}}{\langle \frac{d\tilde{E}}{d\tilde{t}} \rangle} = 1.09 \frac{\Omega_{res}}{\Delta\Omega} \tag{2.42}$$

where $\tilde{E}$ is the energy of the resonator at any time and $\langle ... \rangle$ indicates time averaging in such a time period which is longer than the oscillation time period and shorter in the sense that lower amount of energy lost is marked. Ω_{res} is the resonance frequency and $\Delta\Omega$ represents resonance width which can be calculated by $\Delta\Omega = 2\pi[FWHM]$ where, "FWHM is the width at which the profile curve reaches half of its maximum value, measured from the positive minima value it reaches"[66].

Eichler *et al.* experimentally showed that the formula $Q = 1.09\frac{\Omega_{res}}{\Delta\Omega}$ works correctly in the case of higher quality factor when the oscillation is found in the high frequency regime. Since there has not been any experimental evidence found to support this factor of 1.09 for the lower quality factor, to avoid confusion, the thesis will use the following relation which serves to characterize the quality factor in any frequency regime:

$$Q \propto \frac{\Omega_{res}}{\Delta\Omega} \tag{2.43}$$

Hence, calculating the ratio of the resonance frequency to the resonance width ($\frac{\Omega_{res}}{\Delta\Omega}$) aids the discussion of enhancement of the Q-factor. We note that Ros *et al.* [66] also used Eqn.2.43 to discuss the Q factor.

Chapter 3

Deterministic Results

3.1 Introduction

In this chapter, the nondimensional model equation (Eqn. 2.25) for the deterministic regime. derived in the previous section, will be solved both analytically and numerically which will give us a good understanding of the dynamics of a nanomechanical resonator. Firstly, analytical solution to the model will be sought using the method of harmonic balance. Then, accuracy of the analytical solution will be investigated using numerical simulation. Since the understanding of the dynamics of a nanomechanical resonator greatly relies upon its frequency response characteristics, the analytical solution and numerical methods will be used to analyze the same. The hysteresis analysis is added considering the effects of nonlinear damping and external drive on the hysteresis regime. Finally, the deterministic model with parametric excitation is studied where the excitation is regarded as of the harmonic type. The analysis of this chapter will be used as a basis to study the stochastic model in the next chapter.

3.2 Analytical Frequency-Amplitude Relation

Classical perturbation methods yield impressively accurate results within a range of frequencies which are closer to the frequencies of the undamped system [90]. However, systems with strong nonlinearity are not well understood with these methods. On the contrary, the harmonic balance method can be reliably applied to the systems with

strong nonlinearity [90] showing remarkable similarity between analytical and numerical solution. Considering this fact, we use the harmonic balance method to analytically solve Eqn.2.25.

Considering only one term in the expansion as stated in Section 2.4,it can assumed that:

$$x = X\cos(\Omega t + \phi) \tag{3.1}$$

where, X is the maximum response displacement of the resonator under harmonic forcing. Taking the first and second derivative of the assumed solution:

$$\begin{aligned} \dot{x} &= -\Omega X \sin(\Omega t + \phi) \\ \ddot{x} &= -\Omega^2 X \cos(\Omega t + \phi) \end{aligned} \tag{3.2}$$

Substituting the values of x, $\dot{x}$ and $\ddot{x}$ into the Eqn. 2.25:

$$\begin{aligned} &-\Omega^2 X\cos(\Omega t+\phi) + X\cos(\Omega t+\phi) + \delta[-\Omega X\sin(\Omega t+\phi)] + \\ &\Big(X\cos(\Omega t+\phi)\Big)^3 + \eta[X\cos(\Omega t+\phi)]^2[-\Omega X\sin(\Omega t+\phi)] = F_D\cos(\Omega t) \\ \implies &\cos(\Omega t+\phi)[(1-\Omega^2)X] - \delta\Omega X[\sin(\Omega t+\phi)] + \frac{1}{4}X^3[4\cos^3(\Omega t+\phi)] \\ &-\eta\Omega X^3[\cos^2(\Omega t+\phi)]\, sin(\Omega t+\phi) = F_D\cos(\Omega t) \\ \implies &\cos(\Omega t+\phi)[(1-\Omega^2)X] - \delta\Omega X[\sin(\Omega t+\phi)] + \frac{1}{4}X^3\Big[3\cos(\Omega t+\phi) + \\ &cos\Big(3(\Omega t+\phi)\Big)\Big] - \eta\Omega X^3[\cos^2(\Omega t+\phi)]\, sin(\Omega t+\phi) = F_D\cos(\Omega t) \\ \implies &\cos(\Omega t+\phi)[(1-\Omega^2)X] - \delta\Omega X[\sin(\Omega t+\phi)] + \frac{1}{4}X^3\Big[3\cos(\Omega t+\phi) + \\ &cos\Big(3\Omega t+3\phi\Big)\Big] - \eta\Omega X^3[1-\sin^2(\Omega t+\phi)]\, sin(\Omega t+\phi) = F_D\cos(\Omega t) \end{aligned} \tag{3.3}$$

Since it is assumed that the solution contains the first harmonics only, neglecting the $3\Omega t$ term:

$$\begin{aligned}
\cos(\Omega t+\phi)[(1-\Omega^2)X]-(\delta\Omega X)[\sin(\Omega t+\phi)]+\frac{1}{4}X^3\Big[3\cos(\Omega t+\phi)\Big]+\\
-\eta\Omega X^3[sin(\Omega t+\phi)-\sin^3(\Omega t+\phi)] &= F_D\cos(\Omega t)\\
\\
\implies \cos(\Omega t+\phi)[(1-\Omega^2)X]-(\delta\Omega X)[\sin(\Omega t+\phi)]+\frac{3}{4}X^3\cos(\Omega t+\phi)+\\
-\eta\Omega X^3[sin(\Omega t+\phi)]+\eta\Omega X^3[\sin^3(\Omega t+\phi)] &= F_D\cos(\Omega t)\\
\\
\implies \cos(\Omega t+\phi)[(1-\Omega^2)X]-(\delta\Omega X)[\sin(\Omega t+\phi)]+\frac{3}{4}X^3\cos(\Omega t+\phi)+\\
-\eta\Omega X^3[sin(\Omega t+\phi)]+\frac{1}{4}\eta\Omega X^3[4\sin^3(\Omega t+\phi)] &= F_D\cos(\Omega t)\\
\\
\implies \cos(\Omega t+\phi)[(1-\Omega^2)X]-(\delta\Omega X)[\sin(\Omega t+\phi)]+\frac{3}{4}X^3\cos(\Omega t+\phi)+\\
-\eta\Omega X^3[sin(\Omega t+\phi)]+\frac{1}{4}\eta\Omega X^3[3\sin(\Omega t+\phi)-\sin 3(\Omega t+\phi)] &= F_D\cos(\Omega t)\\
\\
\implies \cos(\Omega t+\phi)[(1-\Omega^2)X]-(\delta\Omega X)[\sin(\Omega t+\phi)]+\frac{3}{4}X^3\cos(\Omega t+\phi)+\\
-\eta\Omega X^3[sin(\Omega t+\phi)]+\frac{1}{4}\eta\Omega X^3[3\sin(\Omega t+\phi)-\sin(3\Omega t+3\phi)] &= F_D\cos(\Omega t)
\end{aligned} \tag{3.4}$$

Again, neglecting the $3\Omega t$ term:

$$\begin{aligned}
\implies \cos(\Omega t+\phi)[(1-\Omega^2)X]-(\delta\Omega X)[\sin(\Omega t+\phi)]+\frac{3}{4}X^3\cos(\Omega t+\phi)+\\
-\eta\Omega X^3[sin(\Omega t+\phi)]+\frac{1}{4}\eta\Omega X^3[3\sin(\Omega t+\phi)] &= F_D\cos(\Omega t)\\
\\
\implies \cos(\Omega t+\phi)[(1-\Omega^2)X+\frac{3}{4}X^3]-\sin(\Omega t+\phi)[\delta\Omega X+\eta\Omega X^3-\frac{3}{4}\eta\Omega X^3]\\
= F_D\cos(\Omega t)
\end{aligned} \tag{3.5}$$

For the simplification of the algebraic calculation, let us assume:

$$(1-\Omega^2)X + \frac{3}{4}X^3 = A$$

and

$$\delta\Omega X + \eta\Omega X^3 - \frac{3}{4}\eta\Omega X^3 = B \tag{3.6}$$

So, Eqn. 3.5 will be converted into:

$$\cos(\Omega t+\phi)A - \sin(\Omega t+\phi)B = F_D\cos(\Omega t)$$

$$\implies [\cos(\Omega t)\cos\phi - \sin(\Omega t)\sin\phi]\,A - [\sin(\Omega t)\cos\phi + \cos(\Omega t)\sin\phi]\,B = F_D\cos(\Omega t)$$

$$\implies \cos(\Omega t)[A\cos\phi - B\sin\phi] + \sin(\Omega t)[-A\sin\phi - B\cos\phi] = F_D\cos(\Omega t) \tag{3.7}$$

Equating the coefficients of $\cos(\Omega t)$ from Eqn. 3.7:

$$A\cos\phi - B\sin\phi = F_D \tag{3.8}$$

and equating the coefficients of $\sin(\Omega t)$ from Eqn. 3.7:

$$-A\sin\phi - B\cos\phi = 0 \tag{3.9}$$

Taking square in Eqn. 3.8 and Eqn. 3.9 :

$$A^2\cos^2\phi - 2AB\sin\phi\cos\phi + B^2\sin^2\phi = F_D^2 \tag{3.10}$$

$$A^2\sin^2\phi + 2AB\sin\phi\cos\phi + B^2\cos^2\phi = 0 \tag{3.11}$$

Summing up the squared equations (Eqn. 3.10 and Eqn. 3.11):

$$A^2(\cos^2\phi+\sin^2\phi) + B^2(\cos^2\phi+\sin^2\phi) = F_D^2$$

$$\implies A^2 + B^2 = F_D^2 \tag{3.12}$$

Substituting the values of A and B from Eqn. 3.6 into the Eqn. 3.12:

$$
\begin{aligned}
[\frac{3}{4}X^3 + (1-\Omega^2)X]^2 + \Omega^2X^2[\delta + \frac{1}{4}\eta X^2]^2 &= F_D^2 \\
\implies [\frac{3}{4}X^3 + (1-\Omega^2)X]^2 + \Omega^2X^2(\delta + \frac{1}{4}\eta X^2)^2 &= F_D^2 \\
\implies \frac{9}{16}X^6 + (1-\Omega^2)^2X^2 + \frac{3}{2}X^4(1-\Omega^2) + \Omega^2X^2\Big[\delta^2 + \frac{1}{2}\delta\eta X^2 + \frac{1}{16}\eta^2X^4\Big] &= F_D^2 \\
\implies \frac{9}{16}X^6 + (1-2\Omega^2+\Omega^4)X^2 + \frac{3}{2}X^4(1-\Omega^2) + \Omega^2\Big[\delta^2X^2 + \frac{1}{2}\delta\eta X^4 + \\
\frac{1}{16}\eta^2X^6\Big] &= F_D^2 \\
\implies \Omega^4X^2 + \Omega^2\Big[\frac{1}{16}\eta^2X^6 + \frac{1}{2}\delta\eta X^4 - \frac{3}{2}X^4 + \delta^2X^2 - 2X^2\Big] &= F_D^2
\end{aligned}
\tag{3.13}
$$

Eqn. 3.13 is quadratic in Ω^2 and now, solving for Ω^2:

$$
\begin{aligned}
\Omega^2 = (-\frac{1}{32}\eta^2X^4 + \frac{3}{4}X^2 - \frac{1}{4}\eta X^2\delta - \frac{1}{2}\delta^2 + 1)\pm \\
\Big[\Big(\frac{1}{32}\eta^2X^4 - \frac{3}{4}X^2 + \frac{1}{4}\eta X^2\delta + \frac{1}{2}\delta^2 - 1\Big)^2 - (\frac{9}{16}X^4 + \frac{3}{2}X^2 - \frac{F_D^2}{X^2} + 1)\Big]^{\frac{1}{2}}
\end{aligned}
\tag{3.14}
$$

Neglecting negative values of Ω:

$$
\begin{aligned}
\Omega_{1,2} = \Bigg[(-\frac{1}{32}\eta^2X^4 + \frac{3}{4}X^2 - \frac{1}{4}\eta X^2\delta - \frac{1}{2}\delta^2 + 1)\pm \\
\Big[\Big(\frac{1}{32}\eta^2X^4 - \frac{3}{4}X^2 + \frac{1}{4}\eta X^2\delta + \frac{1}{2}\delta^2 - 1\Big)^2 - \\
(\frac{9}{16}X^4 + \frac{3}{2}X^2 - \frac{F_D^2}{X^2} + 1)\Big]^{\frac{1}{2}}\Bigg]^{\frac{1}{2}}
\end{aligned}
\tag{3.15}
$$

Eqn. 3.15 establishes the relation between frequency (Ω) and amplitude. In this thesis it is assumed that linear damping to be very low ($\delta << 1$) unless stated otherwise. Hence, after applying $\delta << 1$, Eqn. 3.15 can be written as follows:

$$
\begin{aligned}
\Omega_{1,2} = \Bigg[(-\frac{1}{32}\eta^2X^4 + \frac{3}{4}X^2 + 1) \pm \Big((\frac{1}{32}\eta^2X^4 - \frac{3}{4}X^2 - 1)^2 - \\
(\frac{9}{16}X^4 + \frac{3}{2}X^2 - \frac{F_D^2}{X^2} + 1)\Big)^{\frac{1}{2}}\Bigg]^{\frac{1}{2}}
\end{aligned}
\tag{3.16}
$$

Here we also note that up sweep frequency response is represented by the following equation taking the negative (-) sign from the ± sign of Eqn.3.16:

$$\Omega_{upsweep} = \Bigg[(-\frac{1}{32}\eta^2 X^4 + \frac{3}{4}X^2 + 1) - \Big((\frac{1}{32}\eta^2 X^4 - \frac{3}{4}X^2 - 1)^2 - (\frac{9}{16}X^4 + \frac{3}{2}X^2 - \frac{F_D^2}{X^2} + 1)\Big)^{\frac{1}{2}}\Bigg]^{\frac{1}{2}} \tag{3.17}$$

and down sweep of the frequency response is denoted by the following equation taking the positive (+) sign of the ± sign from Eqn.(3.16):

$$\Omega_{downsweep} = \Bigg[(-\frac{1}{32}\eta^2 X^4 + \frac{3}{4}X^2 + 1) + \Big((\frac{1}{32}\eta^2 X^4 - \frac{3}{4}X^2 - 1)^2 - (\frac{9}{16}X^4 + \frac{3}{2}X^2 - \frac{F_D^2}{X^2} + 1)\Big)^{\frac{1}{2}}\Bigg]^{\frac{1}{2}} \tag{3.18}$$

Using the analytical solution found above, some of the frequency response plots (Fig. 3.1) of a nanomechanical resonator based on the analytic solution are given here which will be used next to determine the accuracy of the solution.

Fig. 3.1 depicts frequency response plot with varying nonlinear damping. It shows that with the increase of nonlinear damping, the amplitude of the resonator goes down. This is reasonable since additional damping will cause greater energy loss in the oscillation and hence amplitudes will be smaller. It is also noted that with increase of nonlinear damping, resonance frequency goes down as well. The figure also clearly tells us that the resonator is in the hardening regime and hence the resonance frequency is greater than unity.

Using numerical solution posted next and the analytical solutions shown here, the next sections will be discussing about the important characteristics of the dynamics of a nanomechanical resonator.

3.3 Numerical Frequency-Amplitude Relation

In this section, numerical solution of the governing deterministic differential equation of a nanomechanical resonator (Eqn. 2.25) is solved using Euler method discussed in

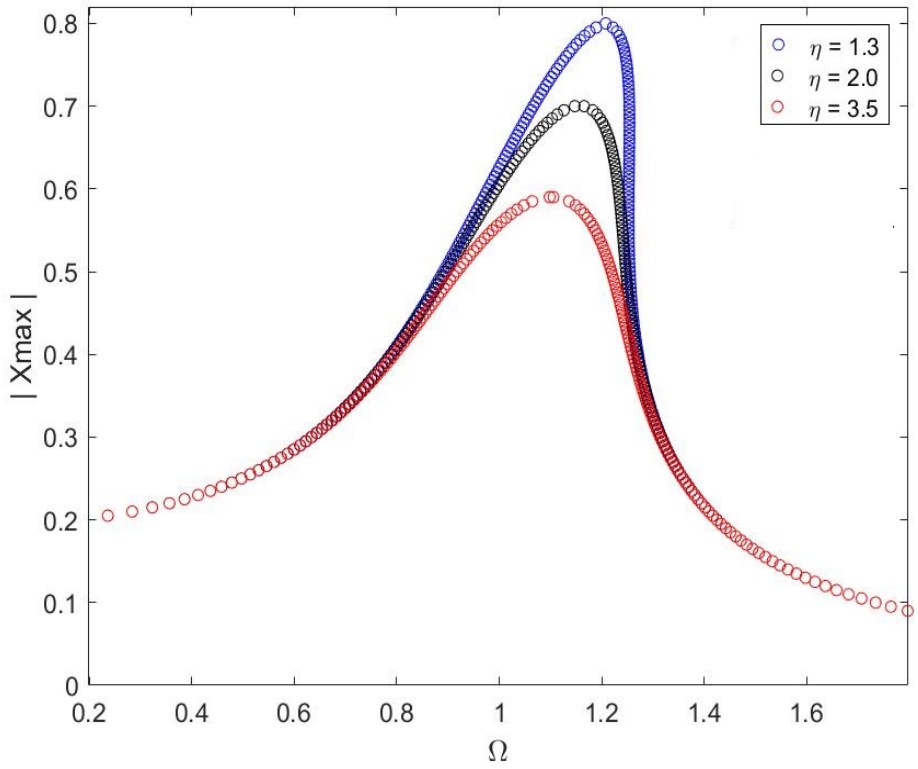

Figure 3.1: Frequency response plot of a nanomechanical resonator based on the analytic solution. From top to bottom $\eta = 1.3, 2.0$ and 3.5 respectively. Here, $F_D = 0.2, \delta = 0.001$.

the Sec. 2.5. The initial values of the two state variables were taken to be zero. Some of the frequency response plots (Fig. 3.2) of a nanomechanical resonator based on the numerical solution are given at this point. With the same parameter values of η, F_D, δ, the plot shows same qualitative relation with the analytical solution. That is, with the increase of nonlinear damping, resonance frequency and amplitude both go down and the resonator is operating in the hardening regime as well.

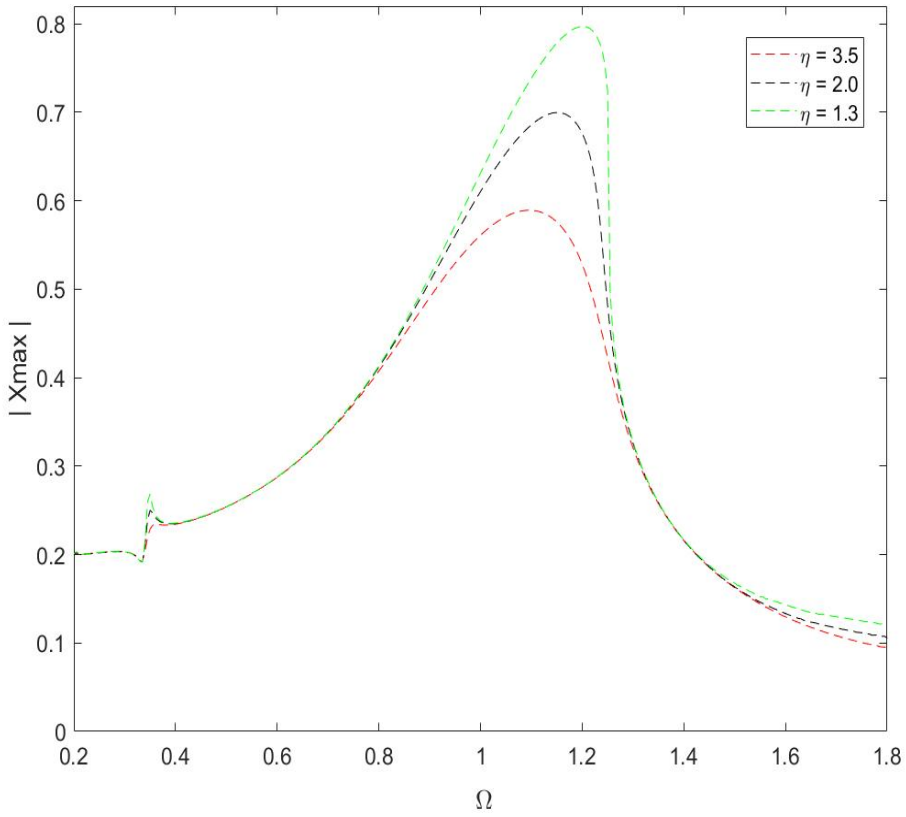

Figure 3.2: Frequency response plot of a nanomechanical resonator based on the numerical solution. From top to bottom $\eta = 1.3, 2.0$ and 3.5 respectively. Here, $F_D = 0.2, \delta = 0.001$.

3.4 Comparison of Analytical and Numerical Frequency-Amplitude Relation

The accuracy of the analytical solution (Eqn. 3.16) based on the Harmonic balance method will be determined here with the help of numerical solution using Euler method. To do that, both of solutions posted earlier in Fig. 3.1 and Fig. 3.2 are superimposed in a single figure below having the same parameter values ($F_D = 0.2, \delta = 0.001$ and $\eta = 1.3, 2.0$ and 3.5).

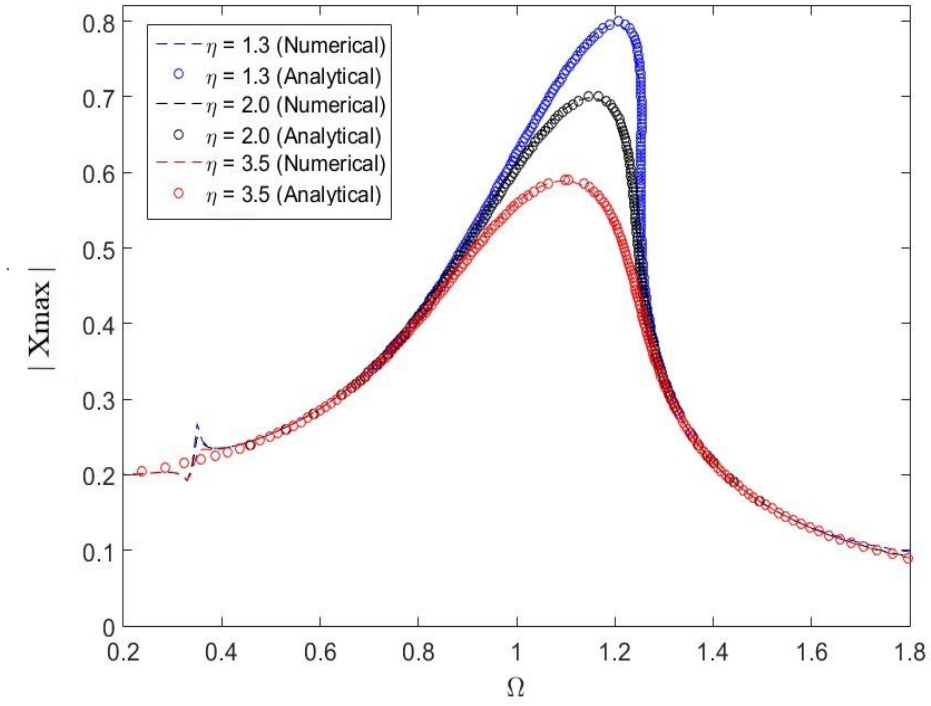

Figure 3.3: Superposition of frequency response plots of a nanomechanical resonator based on the numerical and analytical solution. From top to bottom $\eta = 1.3, 2.0$ and 3.5 respectively. Here, $F_D = 0.2, \delta = 0.001$.

Looking at the combined plot of numerical and analytical solution in Fig. 3.3, it can be clearly said that the solution obtained using the method of harmonic balance (Eqn. 3.16 shows excellent agreement with the numerical solution in each of the frequency response curve which establishes that the harmonic balance solution is accurate.

Additionally, it asserts the validity of the harmonic balance method in case of strong nonlinearity as well.

The only discrepancy between the numerical and analytical solutions is found in the neighbourhood of $\Omega \sim \frac{1}{3}$. It will be easier to address this point by looking closely at the time response plot of the numerical solution of Eqn.2.25 at that frequency.

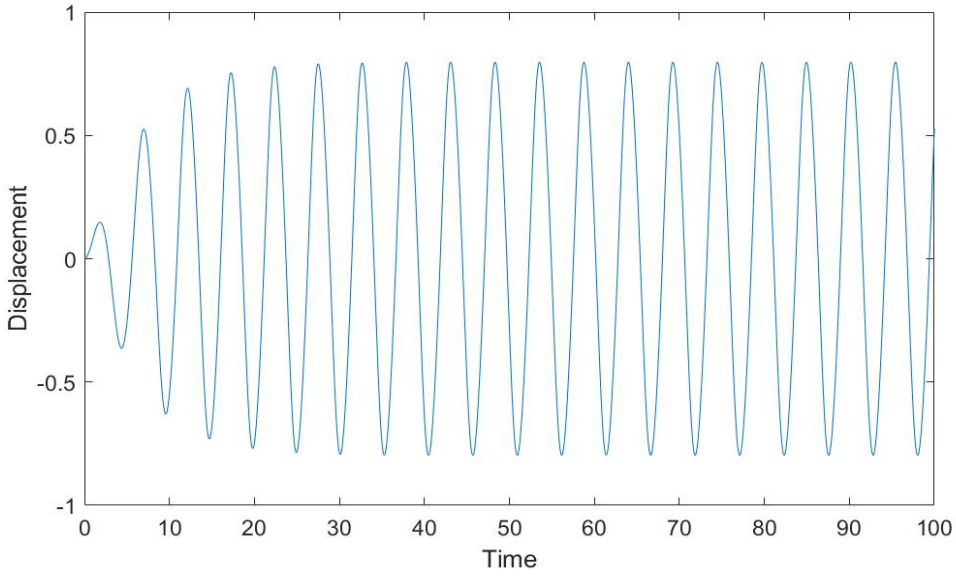

Figure 3.4: Time-Displacement plot of a resonator's response in some limited time frame. Initial value is zero. Here, $F_D = 0.2, \delta = 0.001, \Omega = 1.2, \eta = 1.3$.

Fig.3.4 shows the time response plot at a frequency of $\Omega = 1.2$ with a nonlinear damping coefficient of $\eta = 1.3$. At this frequency the maximum displacement value matches with the analytical one (Xmax=0.795) in Fig.3.3. In the same way, the time response plot of Fig.3.5 using the same numerical parameters at the frequency of $\Omega = 0.34$ indicates that the maximum displacement value (Xmax) with numerical solution is around 0.214. However, Fig.3.3 gives us this value to be around 0.219. So,there is an error of around 2.33%. The reason behind this mismatch lies in the assumption underlying the harmonic balance method. In the harmonic balance method, it is assumed that the solution is harmonic. Whereas, looking at the time response plot it is clear that at $\Omega = 0.34$, the response is sub-harmonic and at $\Omega = 1.2$, the response is harmonic. Since, the analytical solution explicitly assumed that the solution is harmonic in

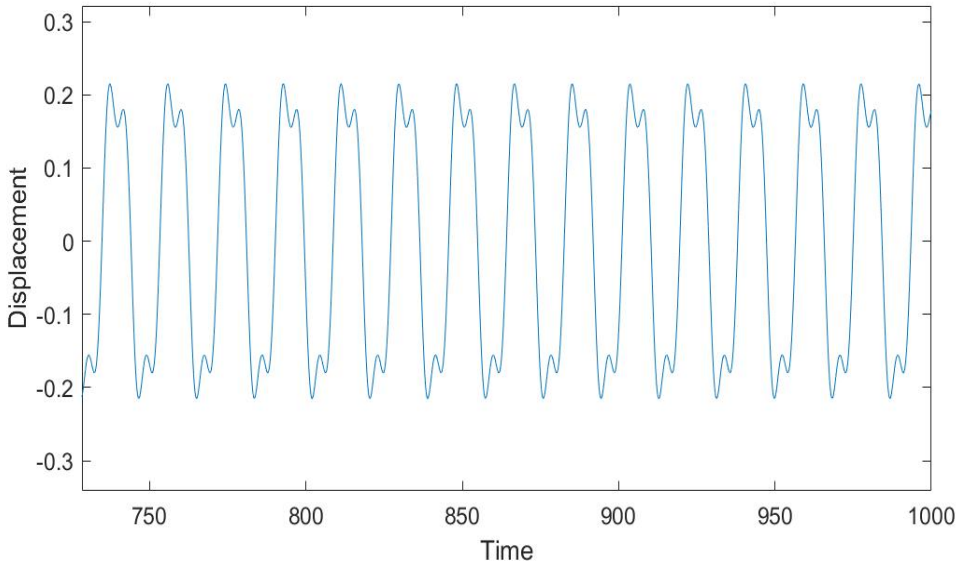

Figure 3.5: Time-Displacement plot of a resonator's response in some limited time frame. Initial value is zero. Here, $F_D = 0.2, \delta = 0.001, \Omega = 0.34, \eta = 1.3$.

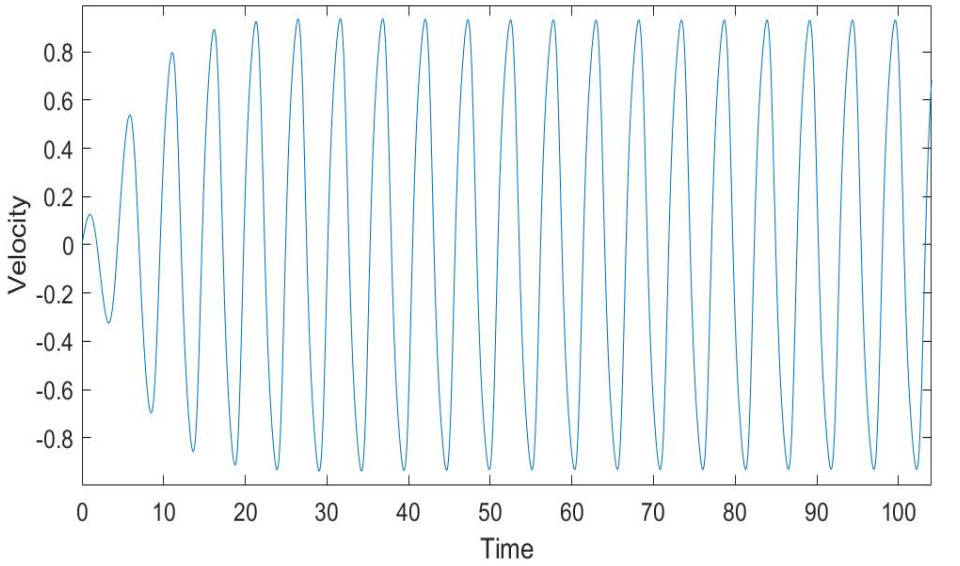

Figure 3.6: Time-Velocity plot of a resonator's response in some limited time frame. Initial value is zero. Here, $F_D = 0.2, \delta = 0.001, \Omega = 1.2, \eta = 1.3$.

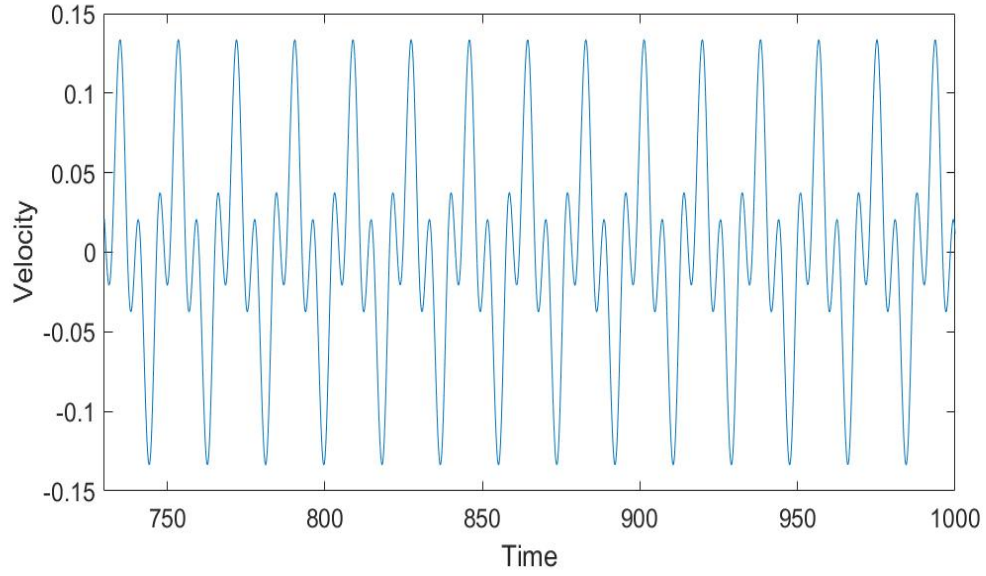

Figure 3.7: Time-Velocity plot of a resonator's response in some limited time frame. Initial value is zero. Here, $F_D = 0.2, \delta = 0.001, \Omega = 0.34, \eta = 1.3$.

all frequencies which is not entirely true, the mismatch occurs. However, the fact that the dynamics is not entirely sub-harmonic is the redeeming feature here. Otherwise, the method of harmonic balance would have provided insufficiently accurate results for the other parameter values considered in this model. To support this reasoning, time-velocity plots are also added in Fig.3.6 with $\Omega = 1.2$ and Fig.3.7 with $\Omega = 0.34$. These plots also show full harmonic time-velocity for $\Omega = 1.2$ and sub-harmonic time-velocity for $\Omega = 0.34$.

3.5 Comparison with Perturbation Method Solution

Previously, secular perturbation theory ([98, 99]) was applied [26] to get the analytic solution of Eqn. 2.25. That solution is given here in terms of notations followed in this thesis. The full derivation can be found in [26].

$$\Omega_{1,2} = \epsilon \left[\frac{3}{8}\sqrt{X\epsilon} \pm \frac{1}{8}\Big[\frac{1}{\sqrt{X\epsilon}} \Big(16 \Big(\frac{F_D}{\epsilon^{\frac{3}{2}}} \Big)^2 - \sqrt{X\epsilon}(4 + \eta\sqrt{X\epsilon})^2 \Big) \Big]^{\frac{1}{2}} \right] + 1 \tag{3.19}$$

where, ϵ is the small expansion parameter known as the perturbation parameter and $\epsilon << 1$. This does not accurately match with the numerical results for different cases. Particularly, under the effect of higher driving force F_D when the oscillation amplitude is larger, the mismatch is quite pronounced. Considering this discrepancy, we chose to use the harmonic balance method which ended up showing excellent agreement with the numerical solution even under higher external drive amplitudes.

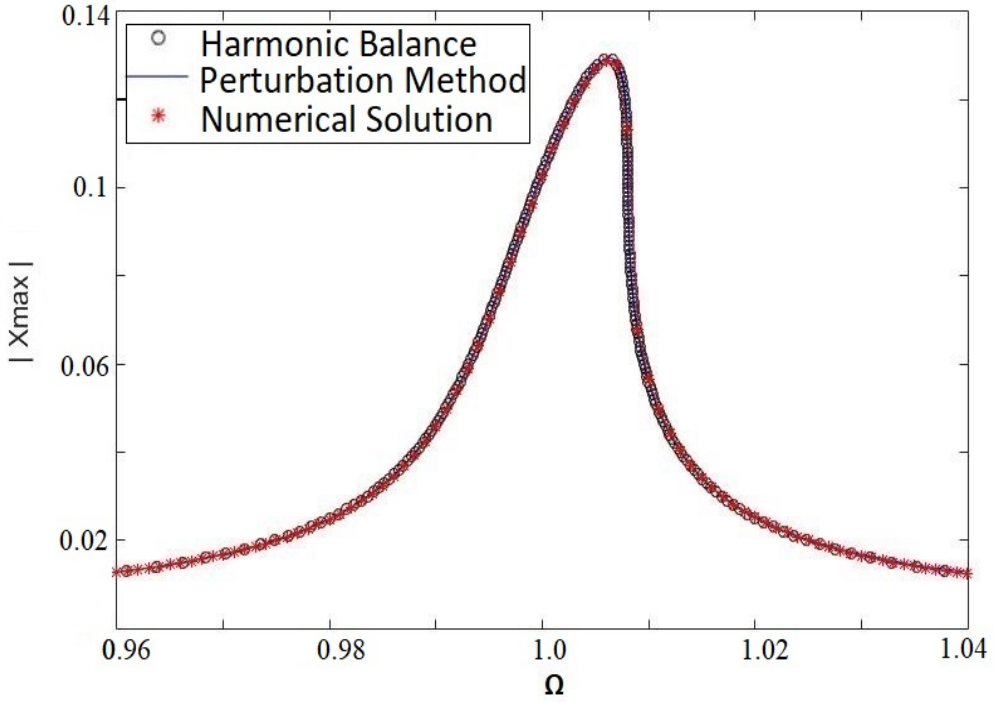

Figure 3.8: Comparison of Numerical and harmonic balance and Perturbation solution of maximum oscillation amplitude vs Ω in case of small external drive amplitude ($F_D = 0.001$). Here, $\epsilon = 0.001, \eta = 1.6, \delta = 0.001$

Fig. 3.8 shows that there is a noteworthy match among numerical, harmonic balance and perturbation method solution when the oscillation amplitude is small under lower driving amplitude whereas Fig. 3.9 shows the dissimilarity of perturbation solution with harmonic balance and numerical solution under higher driving force.

Another limitation with the perturbation solution found here is that, as is to be expected, the solution depends on the perturbation parameter (ϵ). It is also noted that,

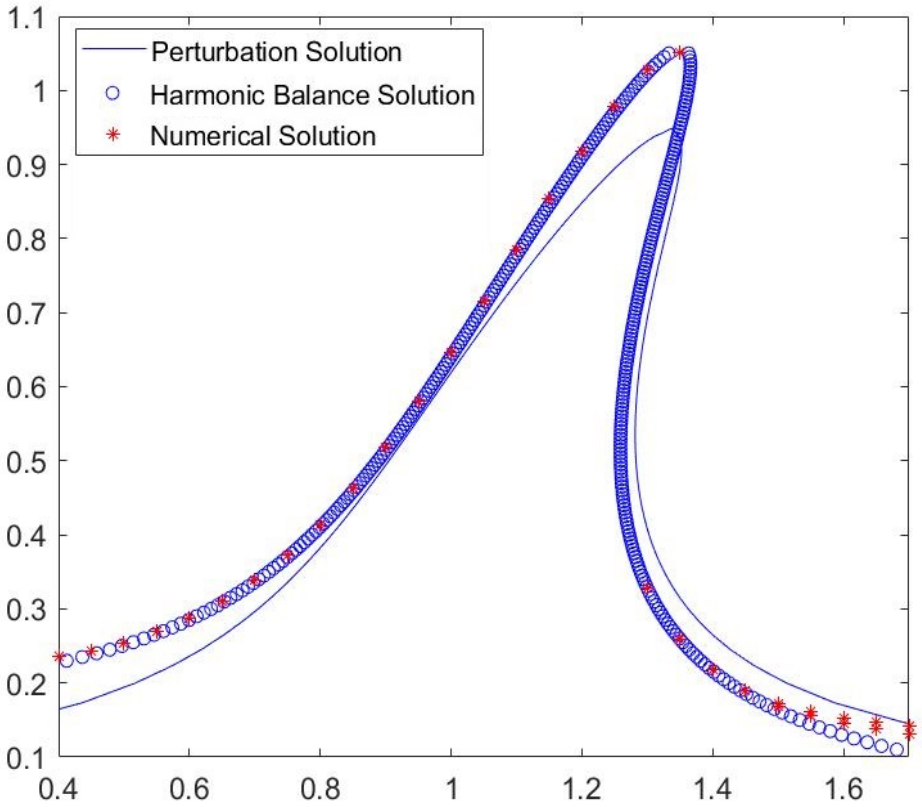

Figure 3.9: Comparison of Numerical, harmonic balance and perturbation solution of maximum oscillation amplitude vs Ω in case of large external drive amplitude ($F_D = 0.2$).Here, $\epsilon = 0.1, \eta = 0.5, \delta = 0.001$

the sub-harmonic resonance near $\Omega \sim 1/3$ is also not found using this method jusy like in the case of the harmonic balance method. In summary, the method of harmonic balance is an excellent choice to study the dynamics of a nanomechanical resonator.

3.6 Additional Analytical Relations

The method of harmonic balance not only gives us the frequency-amplitude relation but also yields some other relations which contribute to an in-depth understanding of the dynamics of a nanomechanical resonator.

From the previously assumed solution of equation Eqn. 2.25 $x = Xcos(\Omega t + \phi)$, and going a little back from Eqn. 3.16 using Eqn. 3.9 (equating the coefficients of $sin(\Omega t)$), it can be shown that phase angle is related to the nonlinear damping coefficient η by following relation. Here we note that the relationship is obtained imposing the condition of linear damping being very small ($\delta << 1$). Plot for phase angle is given in Fig.3.10

$$tan\phi = -\frac{\eta\Omega X^2}{4 + 3X^2 - 4\Omega^2} \tag{3.20}$$

The phase angle can used to characterize the resonance frequency (Ω_{res}) of a nanoresonator. In the presence of a smaller external forcing frequency ($\Omega << \Omega_{res}$), the phases of the resonator and driving force are the same. In contrast, the phase response of the resonator shows disagreement with the external drive when the frequency is larger. The higher the driving frequency, the more the resonator is out of of phase with the external drive. When the driving frequency is same as the resonance frequency, the phase response is $-\pi/2$ and the phase response reaches $-\pi$ when the frequency is very high ($\Omega >> \Omega_{res}$). Here we also note that in both high and low frequency regions, the phase response of the resonator is nearly identical for different nonlinear damping coefficients. Alternatively stated, the variation of the phase response under different conditions is marked only when the driving frequency is close to the resonance frequency ($\Omega \approx \Omega res$).

Fig.3.10 also illustrates the relation between nonlinear damping and resonance frequency. Under higher nonlinear damping, the phase angle reaches $-\pi/2$ earlier than in the case of lower nonlinear damping. Hence, the resonance frequency gets smaller with increasing nonlinear damping coefficient (η). This statement is also found to be true in the frequency response plot shown earlier (Fig. 3.1).

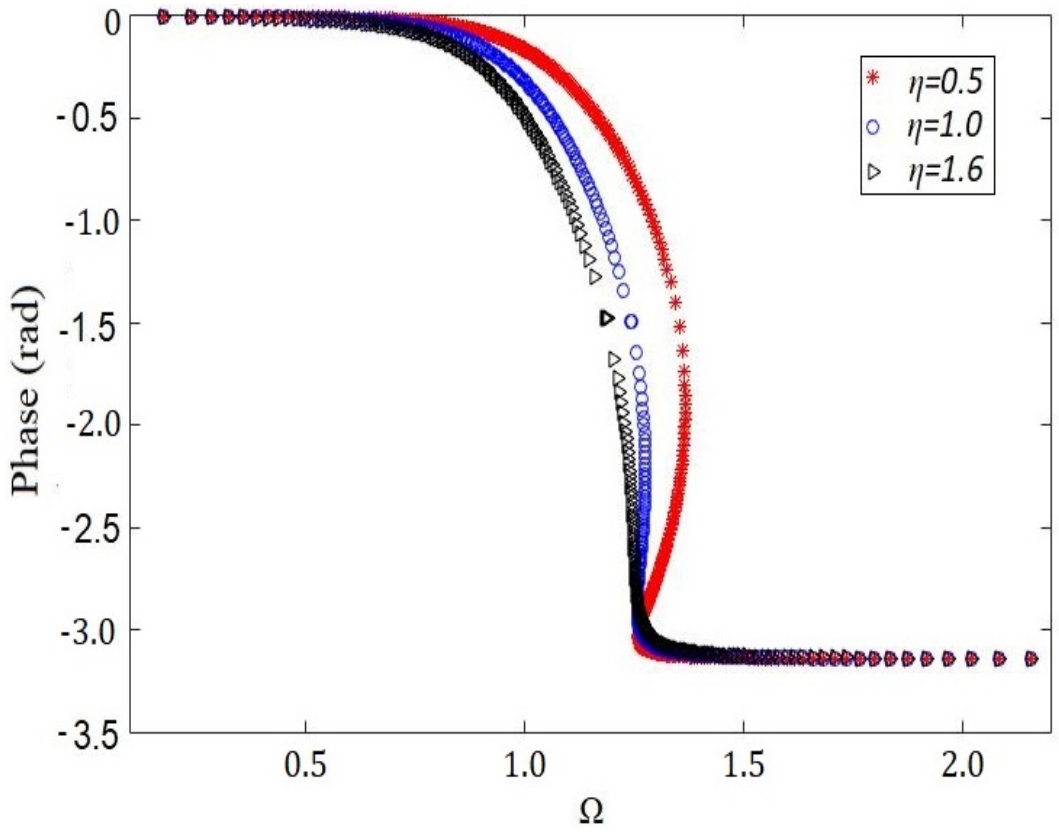

Figure 3.10: Variation of phase angle with frequency. Here, $F_D = 0.2$, δ =0.001. η= 0.5 (red star), 1.0 (blue circle), 1.6 (black triangle).

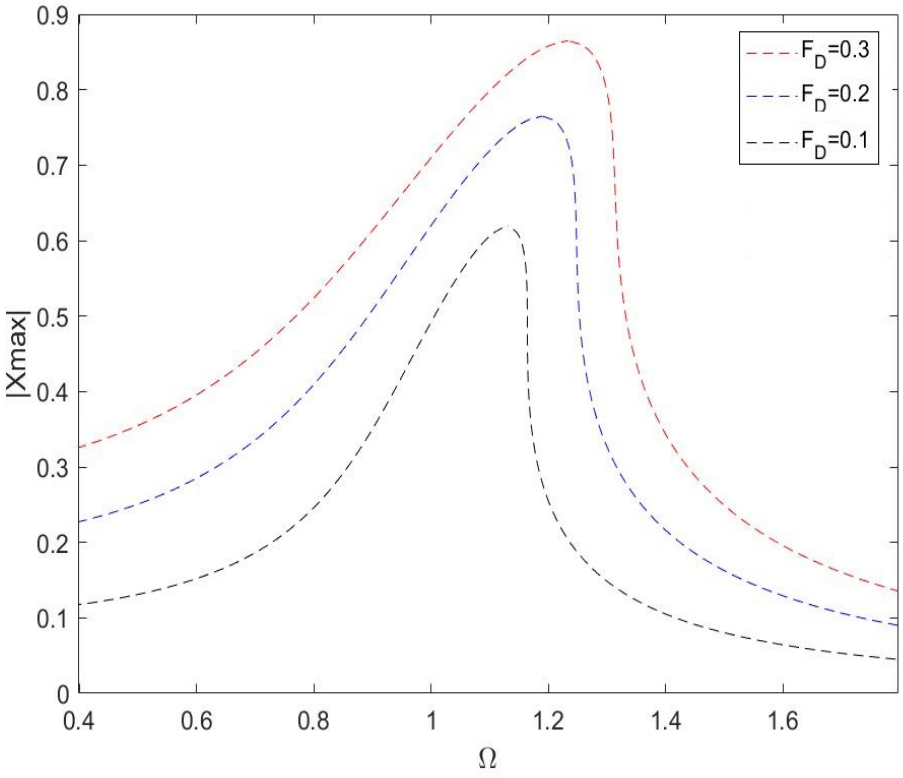

Figure 3.11: Frequency response under different driving forces,F_D. Here, $\eta = 1.5$, δ =0.001. F_D varies from top to bottom as $F_D = 0.3, 0.2, 0.1$ respectively.

Turning to a related question, here a relation between resonance amplitude (X_{res}) and resonance frequency (Ω_{res}) is derived. As stated earlier, Fig. 3.1 shows frequency response curves of a nanoresonator varying the nonlinear damping coefficient. Another set of frequency response curves are plotted in Fig.3.11 varying the driving force while keeping the nonlinear damping constant. In both cases, Fig.3.1 and Fig. 3.11 show that the curves are differentiable at every point of Ω-Xmax plane (C^1 continuity exists). Moreover, maximum amplitude occurs at the resonance frequency. So, imposing the condition of $\frac{dX}{d\Omega} = 0$ at maximum where the amplitude refers to the resonance amplitude (X_{res}) and frequency refers to the resonance frequency (Ω_{res}) should give us a relation between maximum amplitude and resonance frequency. The condition will be imposed on Eqn. 3.13. Under very weak linear damping ($\delta << 1$) the Eqn.3.13 will be turned into:

$$\Omega^4 X^2 + \Omega^2 \Big[\frac{1}{16}\eta^2 X^6 - \frac{3}{2}X^4 - 2X^2 \Big] = F_D^2 \tag{3.21}$$

Taking derivative both sides of Eqn.3.21 with respect to Ω and putting $\frac{dX}{d\Omega} = 0$:

$$\begin{aligned}
X^2(-4\Omega + 4\Omega^3) + \frac{3}{2}X^4(-2\Omega) + \frac{1}{16}\eta^2 X^6(2\Omega) &= 0 \\
\implies X^2(4\Omega^3 - 4\Omega) - 3\Omega X^4 + \frac{1}{8}\eta^2 X^6 \Omega &= 0 \\
\implies (4\Omega^3 - 4\Omega) - 3\Omega X^2 + \frac{1}{8}\eta^2 X^4 \Omega &= 0 \\
\implies (4\Omega^2 - 4) - 3X^2 + \frac{1}{8}\eta^2 X^4 &= 0 \\
\implies 4(\Omega^2 - 1) = 3X^2 - \frac{1}{8}\eta^2 X^4 & \\
\implies \Omega^2 - 1 = \frac{3}{4}X^2 - \frac{1}{32}\eta^2 X^4 & \\
\implies \Omega^2 = 1 + \frac{3}{4}X^2 - \frac{1}{32}\eta^2 X^4 & \\
\implies \Omega = \pm\sqrt{1 + \frac{3}{4}X^2 - \frac{1}{32}\eta^2 X^4} &
\end{aligned} \tag{3.22}$$

Neglecting negative sign:

$$\Omega_{res} = \sqrt{1 + \frac{3}{4}X_{res}^2 - \frac{1}{32}\eta^2 X_{res}^4} \tag{3.23}$$

Eqn.3.23 provides resonance amplitude, X_{res} if the corresponding resonance frequency, Ω_{res} is known and vice versa. Fig.3.12 shows the plot of resonance amplitude (X_{res}) and resonance frequency (Ω_{res}) using Eqn.3.23 and numerical solution under different nonlinear damping conditions keeping the driving force fixed. The plot shows remarkable agreement in between numerical and analytical solution (Eqn.3.23).

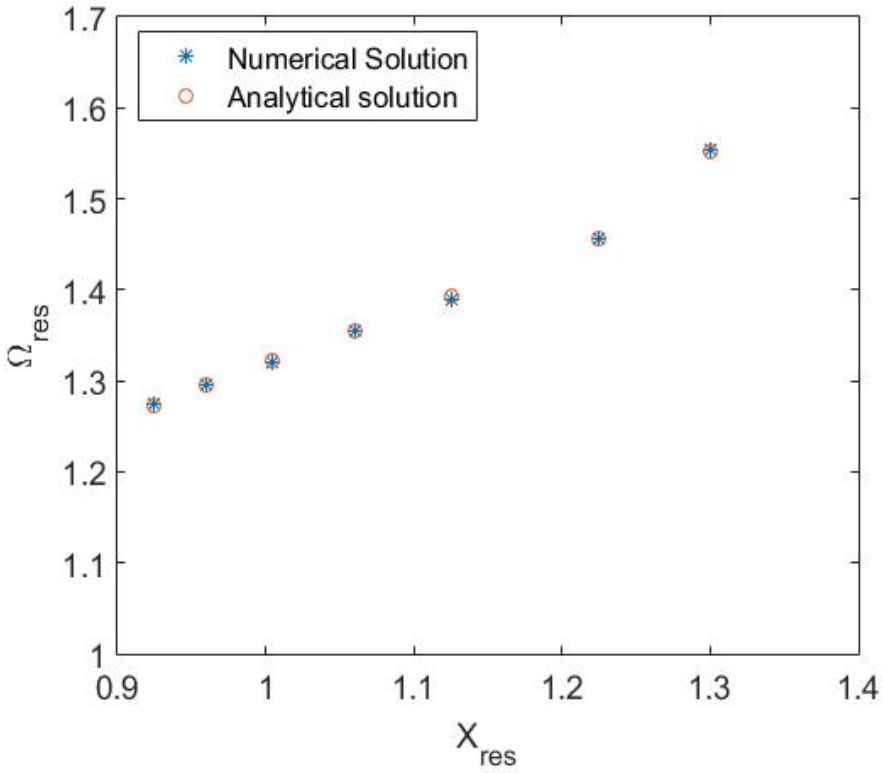

Figure 3.12: Validation of Eqn.3.23 by plotting X_{res} vs Ω_{res}. From left to right η =0.8, 0.7, 0.6, 0.5, 0.4, 0.3 and 0.2 respectively. $F_D = 0.2$, δ=0.001.

3.7 Hysteresis Study in Deterministic Regime

It is well known that the Duffing oscillator shows frequency dependent hysteresis behavior. Since the dynamics of a nanoresonator is modeled based on the Duffing equation,

hysteresis phenomenon of a nanoresonator is a natural topic to study. Here, firstly hysteresis is studied based on the nonlinear damping and then the effect of external drive on the hysteresis region is analyzed.

3.7.1 Hysteresis due to Nonlinear Damping

To study the effect of nonlinear damping on the hysteresis regime, nonlinear damping coefficient (η) is tweaked to observe hysteresis at a certain driving force. Using this procedure, several frequency response curves were plotted. Fig. 3.13 shows frequency response graph where nonlinear damping is varied keeping the external drive fixed. The result shows that with an increase in nonlinear damping (from $\eta = 0.2$ to $\eta = 0.5$) the hysteresis region shrinks and at one point the hysteresis region vanishes ($\eta = 1.6$). It is also noted that the hysteresis region shrinks in such a way that the lower frequency of the hysteresis width is fixed and higher frequency gets lower with the increase of nonlinear damping. In other words, the hysteresis window moves towards the lower frequency region with increasing nonlinear damping.

In the Fig.3.13, double arrow line represents the width of hysteresis region. For $\eta = 1.6$ and $F_D = 0.2$, there exists no hysteresis. Hence, no double arrow line is visible. It is noted that, the frequency response curves plotted here are based on the numerical solutions and not using analytical solutions.

A set of frequency response curves are plotted in Fig. 3.14 below in the hysteresis regime both numerically and analytically with varying nonlinear damping. It offers a little more insight into the analytical solution using the harmonic balance method and the numerical solution using Euler method.

From Fig. 3.14 it is clear that in the hysteresis regime, two solutions emerge from the numerical method whereas there exist three possible solutions per the analytical method. The reason behind this apparent discrepancy is that the dotted analytical solutions of hysteresis width presented in Fig.3.14 represent the unstable solutions and the unstable solutions cannot be found in reality [66]. The unstable branches of the frequency response curves are only visible where hysteresis is found (see Fig.3.14, Fig.3.2 and Fig.3.2).

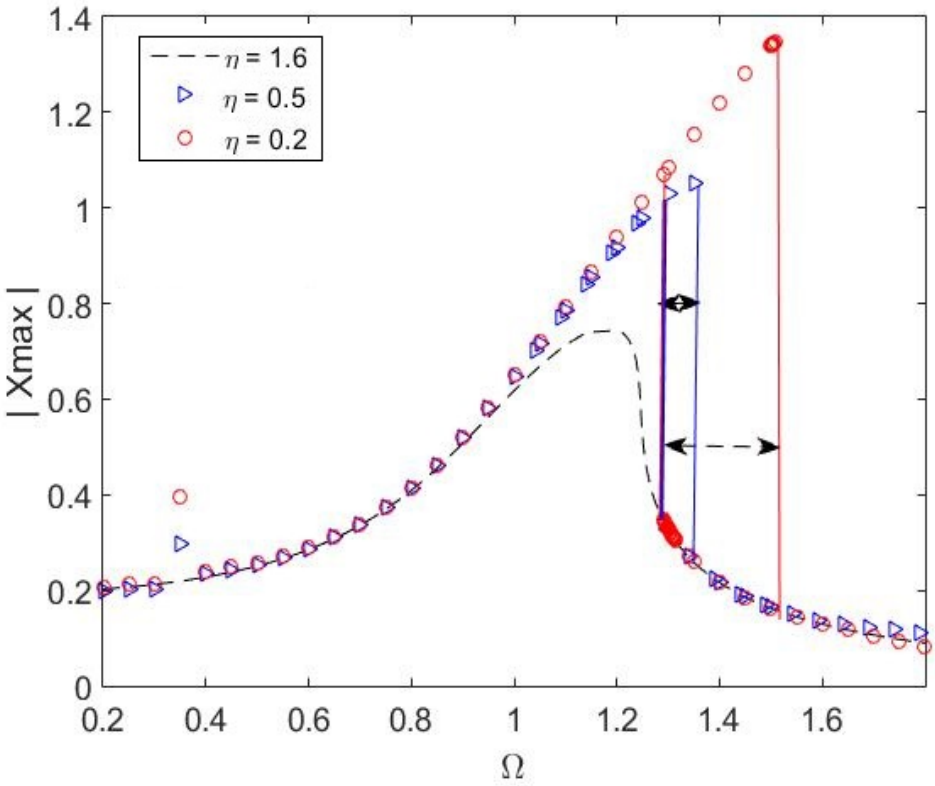

Figure 3.13: Hysteresis width affected by nonlinear damping. Maximum oscillation amplitude vs Ω From top to bottom η=0.2, 0.5 and 1.6. Here, $F_D = 0.2$,$\delta = 0.001$.

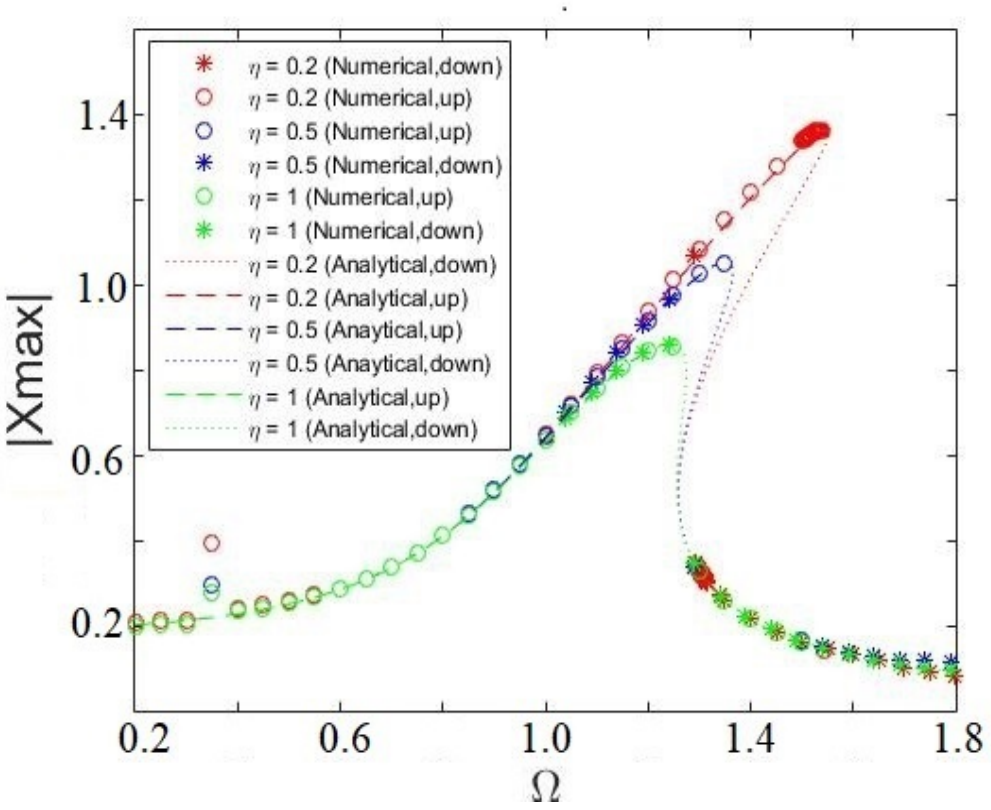

Figure 3.14: Hysteresis width affected by nonlinear damping. Maximum oscillation amplitude vs Ω From top to bottom η=0.2, 0.5 and 1.0. Here, $F_D = 0.2$,$\delta = 0.001$.

Features of the Numerical Solution

The solution in hysteresis regime is easier to obtain if one follows the analytical relation for upsweep and downsweep using Eqn.3.17, Eqn.3.18 or Eqn.3.16. However, one has to be careful when obtaining the numerical solution as highlighted below:

- If the initial value is kept fixed at zero for each frequency in the loop of the numerical solution, one will end up getting the same amplitude. Hence, bistability will be invisible if exists. Fig.3.17 is plotted with zero initial value which represents a time response in the downsweep regime of the hysteresis area.

- The initial value has to be changed for each frequency in such a way that the amplitude and velocity of the previous frequency should be used as the initial value of the next frequency. Fig.3.15 shows this time response plot at $\Omega = 1.54$. The final value of displacement and velocity of $\Omega = 1.535$ are used as initial values time response plot at $\Omega = 1.54$.

- In some cases, step size and simulation time might require a change. So, in the hysteresis regime, to avoid confusion, it is recommended to tweak step size and simulation time to let the solution develop completely. Fig.3.15 is generated using a step size of 1/6000 and simulation time of 6000 sec. Whereas, Fig.3.17 is generated using a step size of 1/1000 and simulation time of 1000 sec. Using a lower simulation time here, one would see a wrong time response curve which will make the frequency response curve wrong as well at this frequency. Fig. shows this incorrect plot.

3.7.2 Hysteresis due to External Drive

To study the effect of harmonically driven external forcing (F_D) on the hysteresis region, the driving force is tweaked to see the existence of hysteresis at a fixed value of the nonlinear damping coefficient. Using this procedure, several frequency response curves are plotted (Fig. 3.18. The results show that the hysteresis window gets smaller with decreasing driving force (from $F_D = 0.25$ to $F_D = 0.05$). However, the amount of this shrinkage with lowering driving force is not as much as it is in the case of increasing

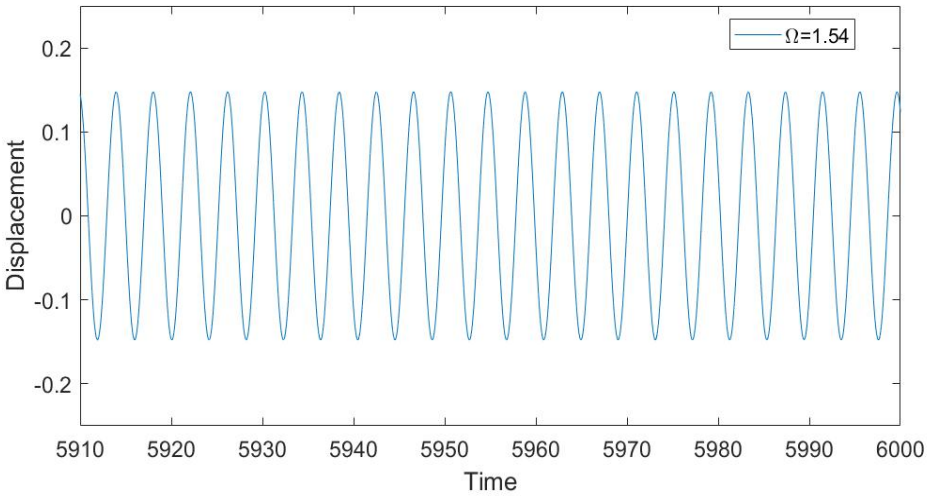

Figure 3.15: Time response at zero initial value. Here, $\eta = 0.2, F_D = 0.2$,$\delta = 0.001, \Omega = 1.54$.Step size=1/6000 and simulation time=6000 sec.

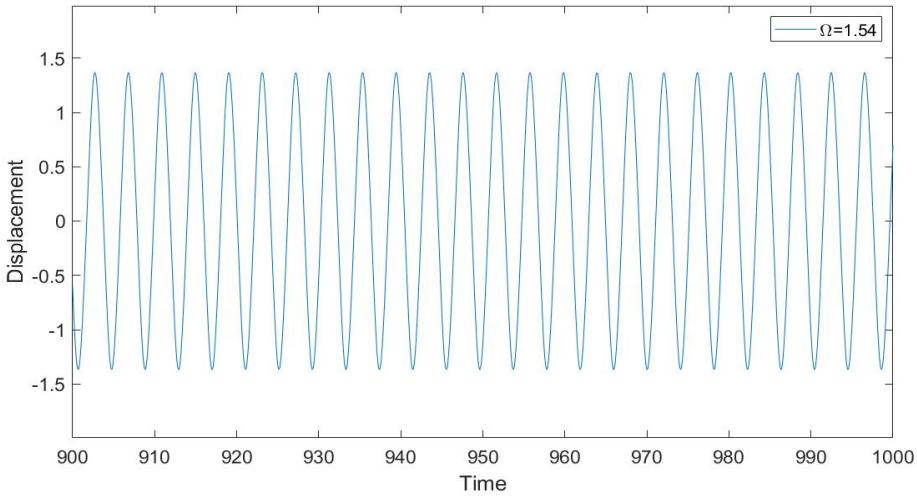

Figure 3.16: Time response at initial value of displacement=1.3674 and velocity=1.9088. Here, $\eta = 0.2, F_D = 0.2$,$\delta = 0.001, \Omega = 1.54$.

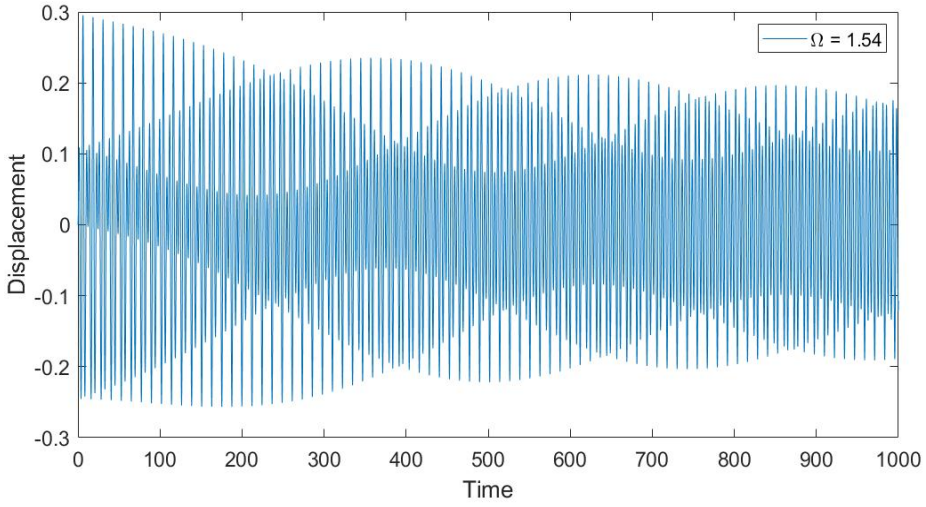

Figure 3.17: Time response at zero initial value. Here, $\eta = 0.2, F_D = 0.2$,$\delta = 0.001, \Omega = 1.54$. Step size=1/1000 and simulation time=1000 sec.

nonlinear damping. It is also noted that with a decrease in external drive, resonance frequency and resonance amplitude are both reduced.

To support this numerical simulation, both analytical and numerical plots are given in Fig.3.19 which exhibit remarkable match between the analytical and numerical solutions. It is clear that there exists a subharmonic resonance near $\Omega \sim 1/3$ and this resonance dies out with decreasing the amplitude of the harmonic external forcing.

3.8 Linear Damping

Study of the frequency response characteristics of a nanoresonator based on the analytical solution of Eqn. 3.15 is presented here. Increasing the linear damping coefficient δ, keeping the nonlinear damping fixed, here we varied the linear damping coefficient (δ). The result shows that with the increase of linear damping, it dominates over the nonlinear damping and hence it makes the curves flatter by reducing the oscillation amplitude. Fig. 3.20 shows this phenomenon where linear damping coefficients are varied from top to bottom as follows: $\delta = 1 \times 10^{-3}, 8 \times 10^{-2}, 2.5 \times 10^{-1}, 8 \times 10^{-1}$.

Moreover, since the frequency response gets flatter, it can be undoubtedly concluded

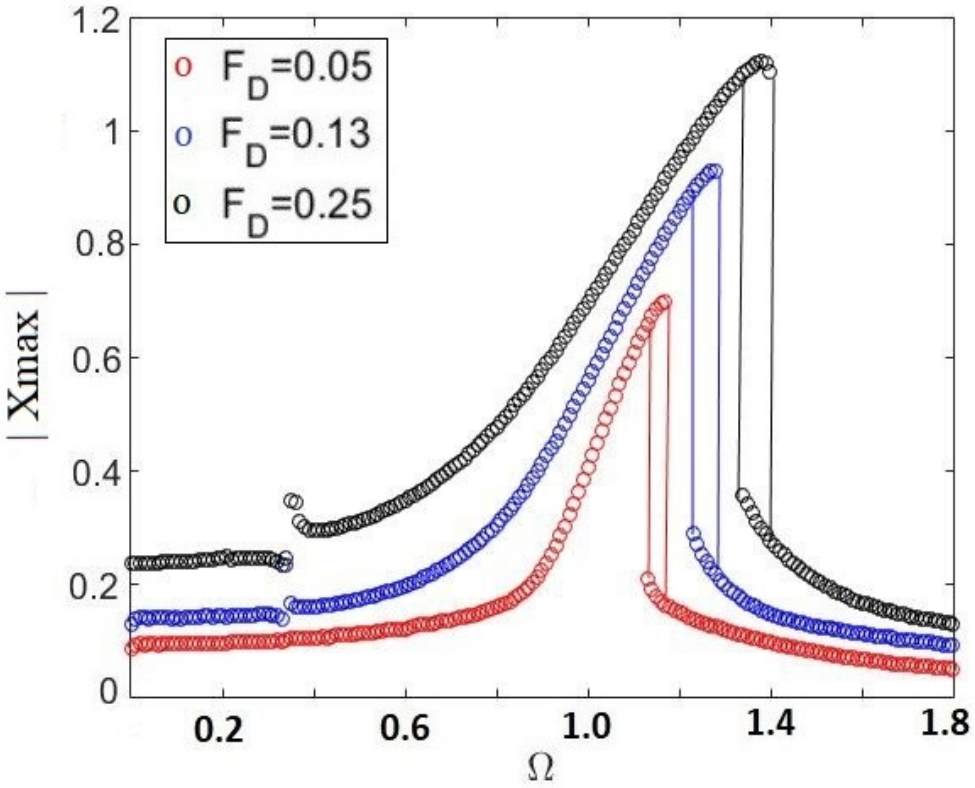

Figure 3.18: Hysteresis region affected by external drive. Maximum oscillation amplitude vs Ω. From top to bottom F_D=0.25, 0.13 and 0.05. Here, $\eta = 0.5, \delta = 0.001$.

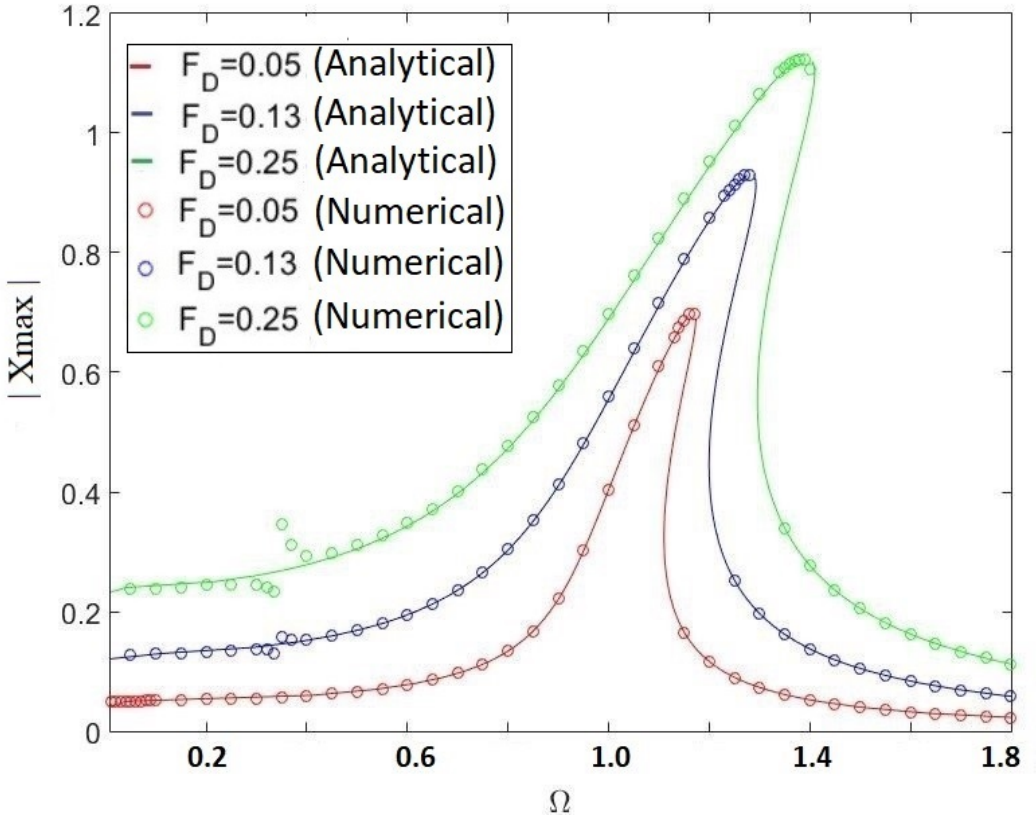

Figure 3.19: Plot of maximum oscillation amplitude vs Ω using numerical solution and HBM method. From top to bottom F_D=0.25, 0.13 and 0.05. Here,$\eta = 0.5, \delta = 0.001$.

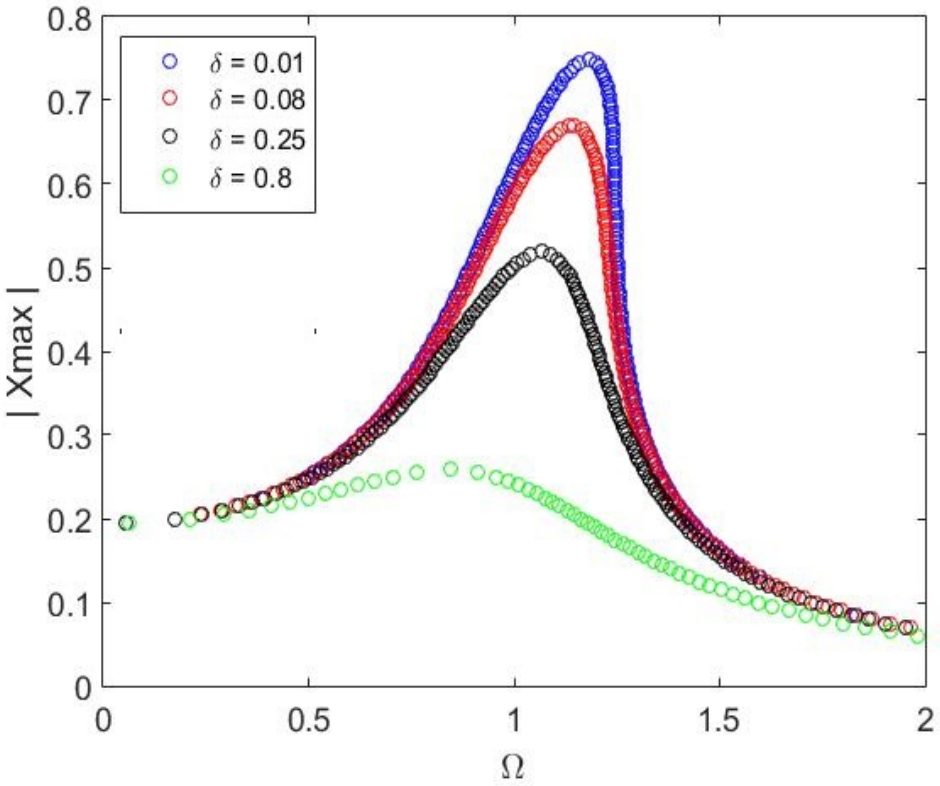

Figure 3.20: Maximum oscillation amplitude vs Ω due to the change in linear damping. From top to bottom, $\delta = 1\times10^{-3}, 8\times10^{-2}, 2.5\times10^{-1}, 8\times10^{-1}$. Here, $F_D = 0.2, \eta = 1.6$.

that in the case of nanoresonators, the Q-factor decreases with the increase of linear damping akin to linear resonators.

3.9 Parametric Excitation

Studying the dynamics of a nanoresonator it is found that in the presence of both external drive and parametric excitation, the frequency response differs from the case of exclusive presence of external drive in such a way that for the combined case, the oscillation amplitude of the resonator is near zero at all places except in the neighbourhood of resonance frequency. In order to understand how parametric forcing affects the quality factor, here it is studied how the ratio of pump frequency and driving frequency (Ω_P/Ω_D) affects the dynamics of a nanoresonator. It is observed that with an increase in the $\frac{\Omega_P}{\Omega_D}$ ratio, the resonance width shrinks and at the same time the resonance frequency decreases as well. This result implies that the $\frac{\Omega_P}{\Omega_D}$ ratio does not have a noteworthy impact on the Q-factor. It also needs to be noted that the resonant shift becomes smaller when the pump frequency ($\Omega_P >> \Omega_D$) becomes very high. Fig.3.21 provides the frequency response curves varying the ratios of pump frequency and driving frequency (Ω_P/Ω_D) and Fig. 3.22 depicts the variation of resonance frequency changing the Ω_P/Ω_D values.

The frequency response curves plotted in Fig.3.21 follows similar trends found in Rhodes *et al.* [100] where they studied the response of a nanoresonator considering parametric excitation based on the the linear Mathieu equation model.

The effect of variation of parametric forcing amplitude on the frequency response curve is studied here at this point. Keeping the ratio of pump frequency and driving frequency fixed at $\frac{\Omega_P}{\Omega_D}$=2, an increase in the harmonic oscillation amplitude resulted in the higher resonance amplitude. At the same time, a slight increase in the resonance frequency is also noted. This phenomenon is plotted in Fig.3.23

3.10 Deterministic Results: Conclusion

The analysis based on the deterministic model of a nanomechanical resonator is presented in this chapter. The results lead to several important conclusions:

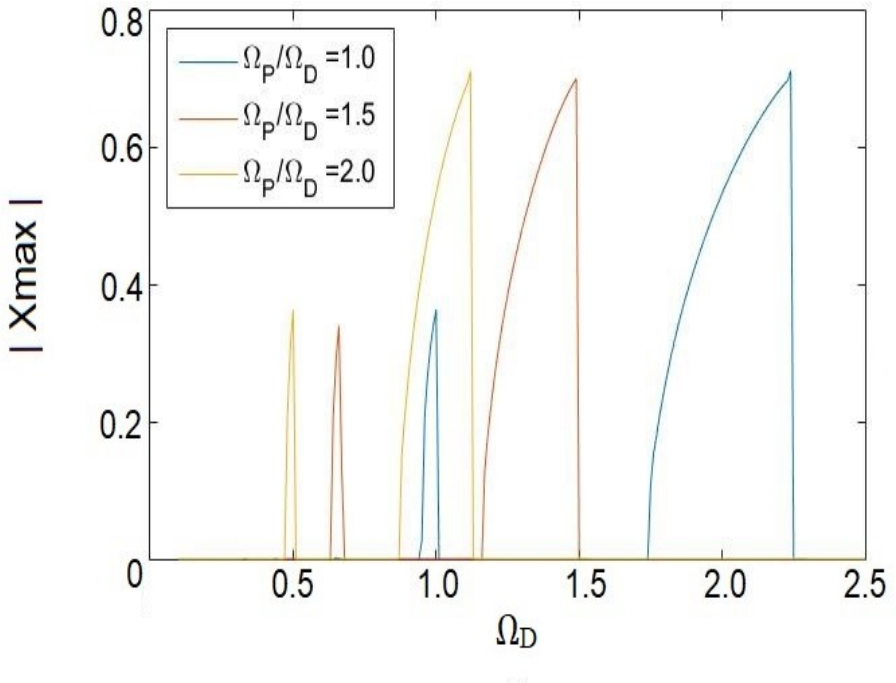

Figure 3.21: Frequency response under parametric excitation. Here, H=0.5, $F_D = 0.1$, $\eta = 1.6$, $\phi_g = 0$, $\delta = 0.001$.

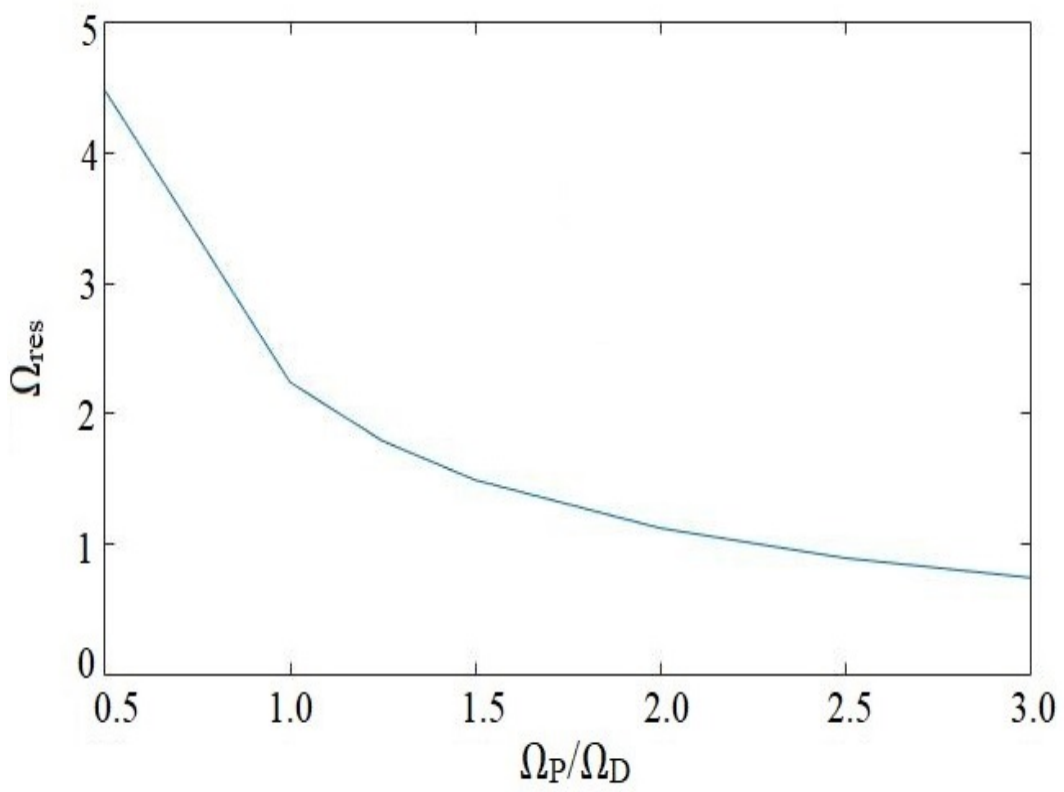

Figure 3.22: Variation of resonant frequency at different external and parametrically driven frequency conditions. Here, H=0.5, $F_D = 0.1$, $\eta = 1.6$, $\phi_g = 0$, $\delta = 0.001$.

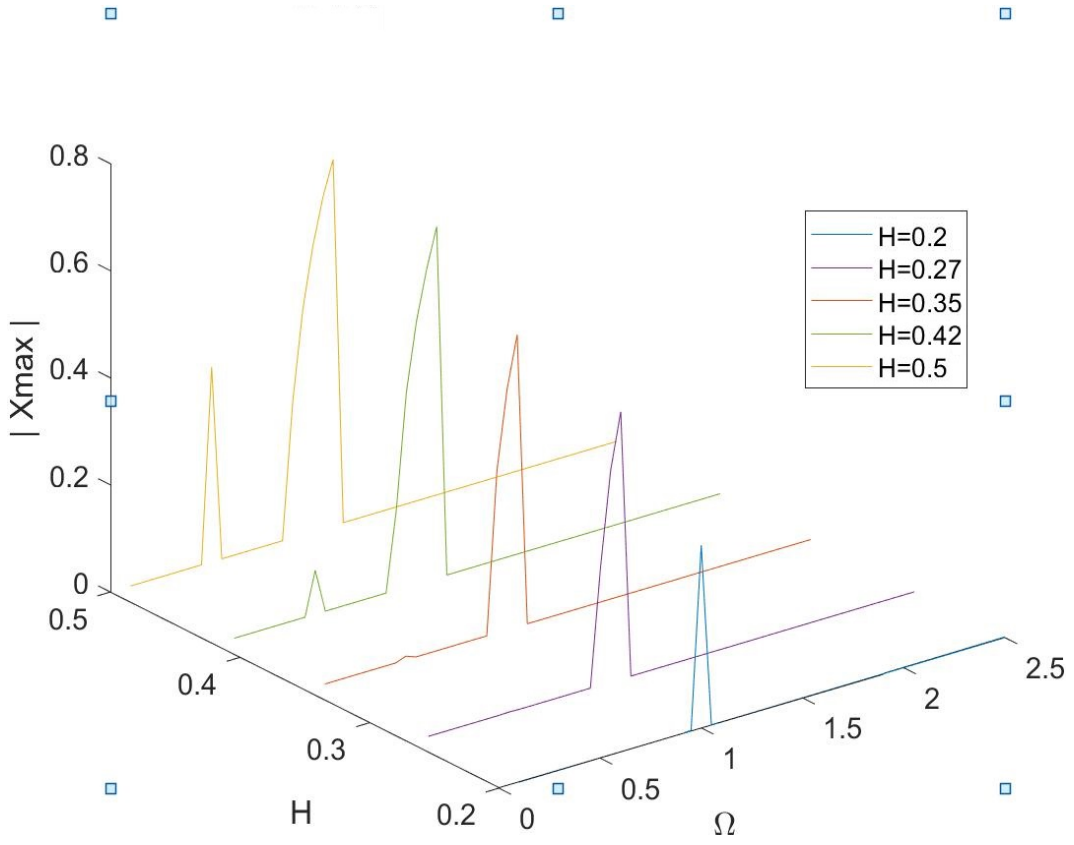

Figure 3.23: Variation of resonance amplitude and resonance frequency at different parametric forcing amplitudes. From right to left, H=0.2,0.27,0.35,0.42 and 0.5 respectively. Here, $F_D = 0.1$, $\eta = 1.6$, $\phi_g = 0$, $\delta = 0.001$.

- The method of Harmonic Balance is a reliable and effective tool to study the dynamics of a nanomechanical resonator. Our results underscore its superiority over the perturbation method.

- Hysteresis in the frequency response curves of a nanomechanical resonator can be controlled by both nonlinear damping and external harmonic forcing. Increasing the magnitude of nonlinear damping coefficient leads to shrinkage in the hysteresis width while an increase in the driving force results in the expansion of the hysteresis region.

- Interesting phenomena like subharmonic resonance are only visible in the numerical simulation. On the other hand, unstable branches of frequency response curves are visible only in the analytic solution.

- Resonance frequency and resonance amplitude can be explained elegantly in terms of phase response curves. This can be accomplished deriving a new relation using the analytical frequency-amplitude relation. Resonance is marked in the phase response curve when the phase angle is $-\pi$.

- If the linear damping is not too low, it will dominate the dynamics. An increase in the linear damping flattens out the frequency response curves which is undesirable in sensing applications.

- Effect of parametric harmonic excitation on the deterministic dynamics is also studied here. Increasing the ratio of pump frequency and external driving frequency $\frac{\Omega_P}{\Omega_D}$, resonance width shrinks and at the same time resonance frequency decreases as well. Increasing the harmonic oscillation amplitude results in higher resonance amplitude with a small increase in the resonance frequency.

In summary, these results together provide significant insights into multiple aspects of the nonlinear dynamics of a nanomechancial resonator. The deterministic analysis described in this chapter provides the basis for the study of dynamics in the stochastic regime.

Chapter 4

Q-factor and Stochastic Dynamics

It has already been mentioned in Chapter 1 (Sec. 1.6) that one of the main objectives of this thesis is to study the dynamics of a nanomechanical resonator in stochastic regime. In this chapter, the modelled equation (Eqn. 2.27) outlined in the Sec.2.3.3 will be solved numerically based on the Euler-Maryuma method. The effect of noise on the hysteresis regime of a frequency response curve is also analyzed here. Additionally, this section will discuss how the quality factor of a nanoresonator can be increased both in deterministic and stochastic regime which is crucial in sensing scheme using a nanoresonator.

4.1 Hysteresis Study in Stochastic Regime

Similar to the deterministic study, stochastic effect on the hysteresis region is discussed in this section. Previously, Ros *et al.* [66] studied the effect of stochastic excitation on the hysteresis characteristics of a nanoresonator based on white Gaussian noise excitation. It is restated that in this thesis, the effects of Lévy flight as a form of external forcing on the hysteresis nature of frequency response curve is studied by solving Eqn. 2.27 applying the Euler-Maruyama scheme and Mantegna's algorithm [97]. $\beta = 1.5$ is considered for Lévy flight excitation in a symmetric distribution (See Eqn.2.30. Fig.4.1 shows the numerically generated probability density function for Lévy stable stochastic process used in the simulation.

It is found that hysteresis window shrinks as a result of increasing noise intensity

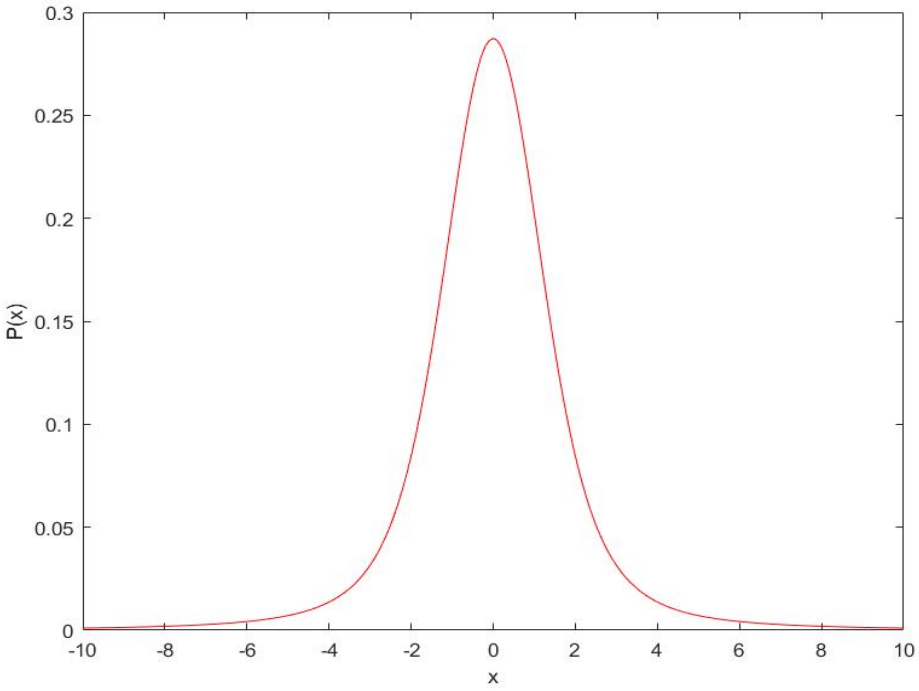

Figure 4.1: Numerically generated probability density function for Lévy stable stochastic process used in the simulation. Here,$\beta = 1.5$.

(σ). Fig.4.2 and Fig.4.3 show this phenomenon where, $\eta = 0.2$, $F_D = 0.2$, $\delta << 1$ and noise intensity was taken as σ=0.002, and σ=0.005. Ros *et al.*[66] observed similar frequency response characteristics studying the system under the influence of white Gaussian noise. The key take way from this study is that the width of hysteresis region shows much more sensitivity in the presence of Lévy excitation. It is also noted that the hysteresis width not only gets smaller due to increase in noise intensity but also the hysteresis window moves toward the higher frequency region.

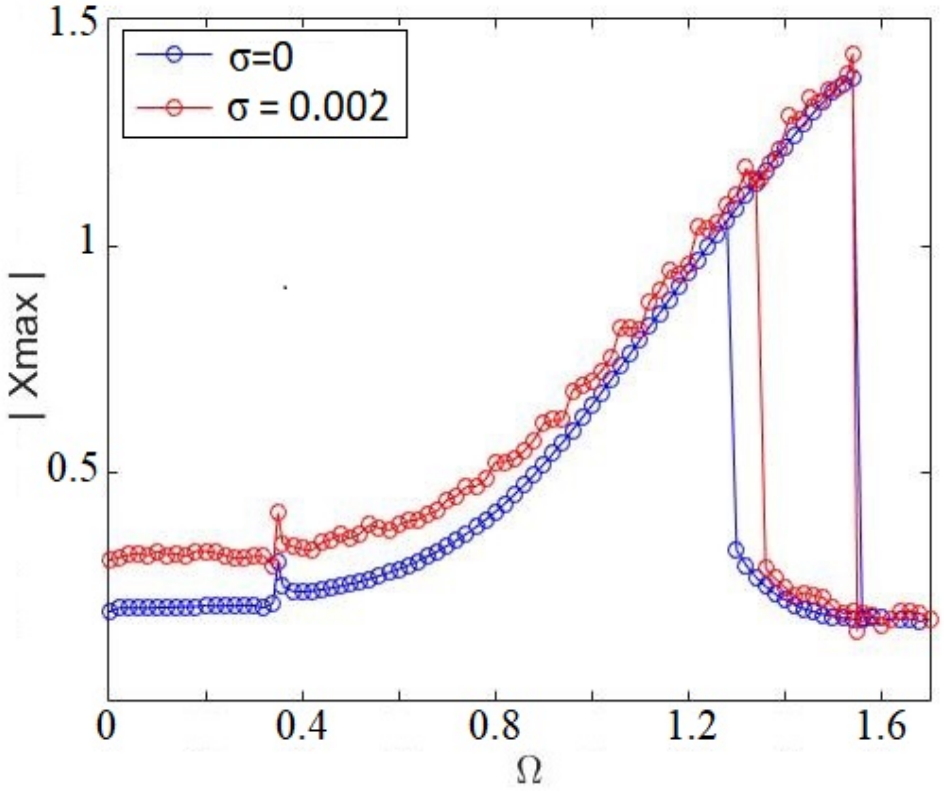

Figure 4.2: Maximum oscillation amplitude vs Ω showing the decrease in hysteresis width due to noise($\sigma = 0.002$). Here, $\delta = 0.001, \eta = 0.2$.

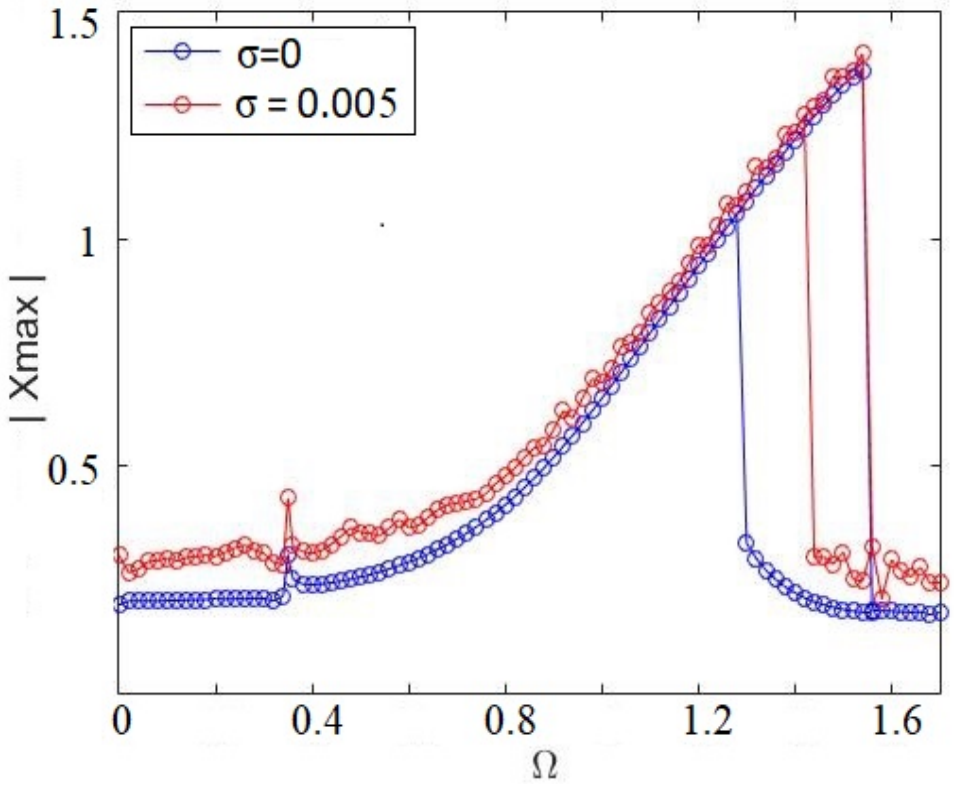

Figure 4.3: Maximum oscillation amplitude vs Ω showing the decrease in hysteresis width due to noise($\sigma = 0.005$). Here, $\delta = 0.001, \eta = 0.2$.

4.2 Q-factor

It is clear from the literature review that Q-factor plays an important role in sensory applications. There exists an inversely proportional relationship in between Q-factor of a nanoresonator and resonance width $\Delta\Omega$ alike linear resonators [66]. Considering experimental feasibility, it is more convenient to think of regulating noise sources rather than changing the external drive or nonlinear damping [66]. Hence, the effects of stochastic excitation on Q-factor is a relevant topic to study. Similar to hysteresis analysis, Lévy stable stochastic process is used here to tune Q-factor. Fig. 4.4 presents the characteristics of frequency response curve influenced by Lévy noise process under various noise intensity,σ. Using the frequency response curves from this plot, variation of resonance width ($\Delta\Omega$) is plotted for different noise intensity (Fig. 4.5). The results show that as the noise strength increases, the window of resonance width decreases while keeping the resonance frequency (Ω_{res}) fixed. As a result, ratio of resonance frequency to the resonance width $\frac{\Omega res}{\Delta\Omega}$ decreases. According to the Eqn. 2.43, the plot clearly provides the evidence that the Q-factor has a proportional relationship with the noise intensity of Lévy flight excitation. In other words, Q-factor increases (or decreases) with increasing (or decreasing) noise intensity. Ros et al. [66] observed similar trend studying the dynamics influenced by white Gaussian noise.

Q-factor has also been studied considering the effect of nonlinear damping on Q-factor. We know that Q-factor has an inversely proportional relationship with linear damping [101]. This relationship also holds true for the nonlinear damping as well that is increasing the nonlinear damping, quality factor decreases. Fig. 4.6 provides the plot based on the same parameter setting used for Fig.3.2.

Later on, effect of driving force on Q-factor is studied. Fig. 4.7 shows the variation in frequency response curves due to the change in driving force. It is found that, increasing the driving force, both resonance frequency and resonance width increase. However, increase in resonance frequency is less than the increase in resonance width which leads to lower the ratio of resonance frequency and resonance width ($\Omega_0/\Delta\Omega$) according to the Equation 2.43. So, quality factor decreases with increasing driving force (see Fig.4.8). So, it is recommended to lower both nonlinear damping and driving force to increase quality factor which will in turn increase the sensitivity of the resonator.

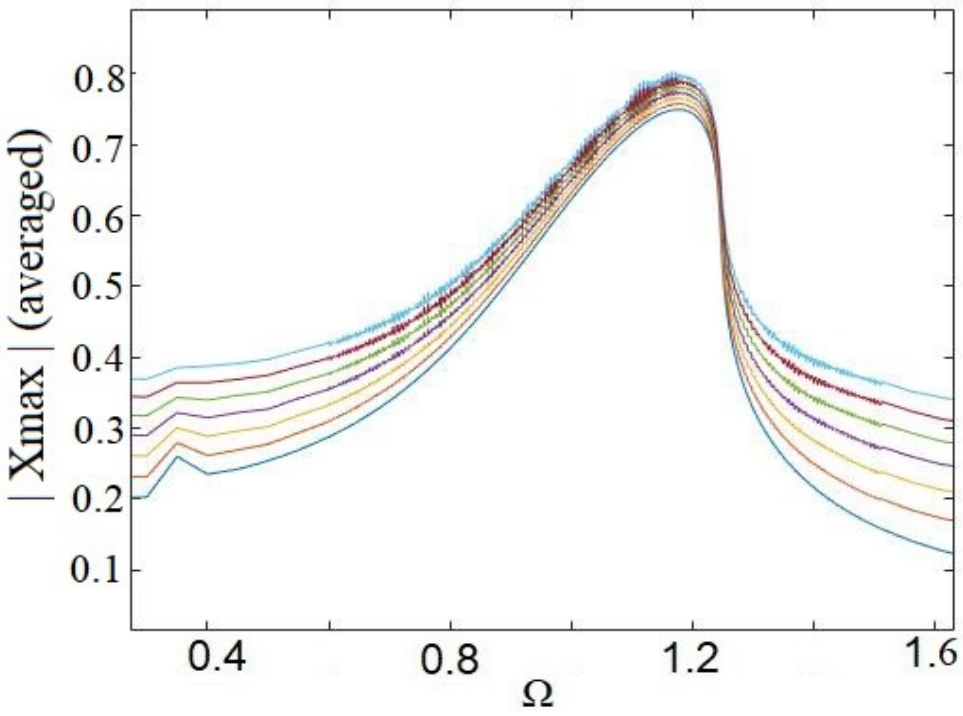

Figure 4.4: Averaged Maximum oscillation amplitude vs Ω for different strength of noise in case of Lévy flight excitation with constant $\eta = 1.6$, $\delta = 0.001$ and $F_D = 0.2$. From bottom to top $\sigma = 0, 5 \times 10^{-4}, 1 \times 10^{-3}$, 1.5×10^{-3},2×10^{-3}, 2.5×10^{-3}, and 3×10^{-3}.

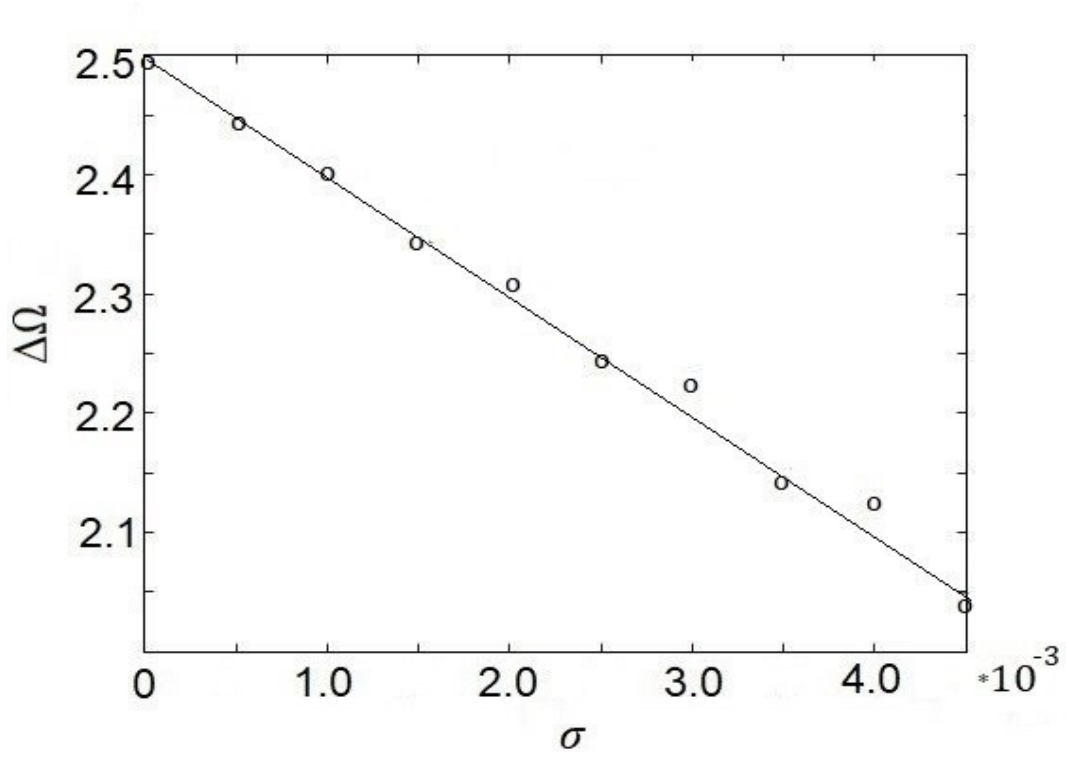

Figure 4.5: Decrease of $\Delta\Omega$ (Increase of quality factor) with increasing noise. Values from simulation are noted by the circles and the solid line shows fitted curve following this equation: $\Delta\Omega = -97.2561\sigma + 2.5456$.

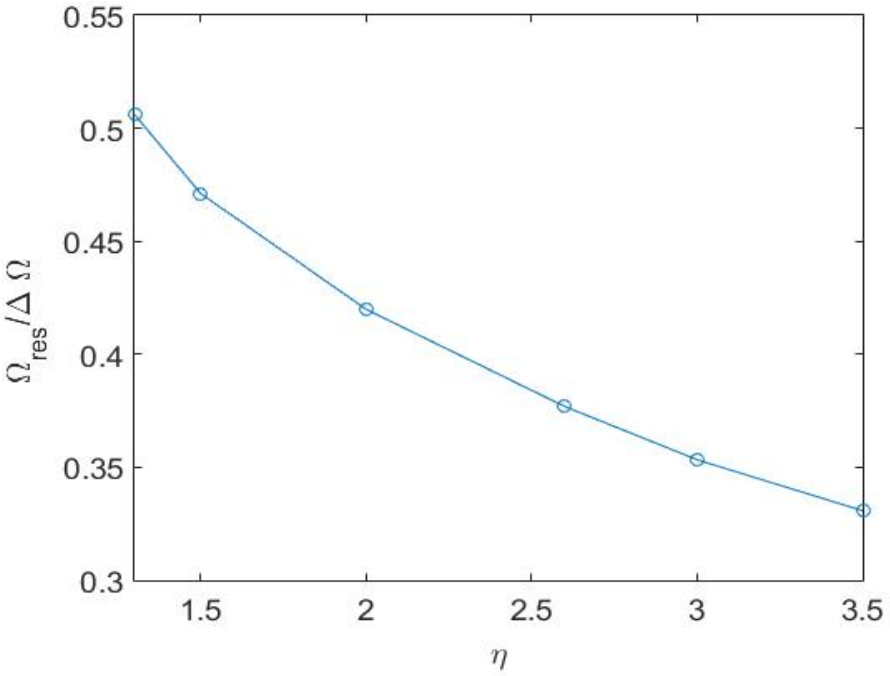

Figure 4.6: Variation of Q-factor with nonlinear damping. Here $F_D = 0.2$ and $\delta = 0.001$.

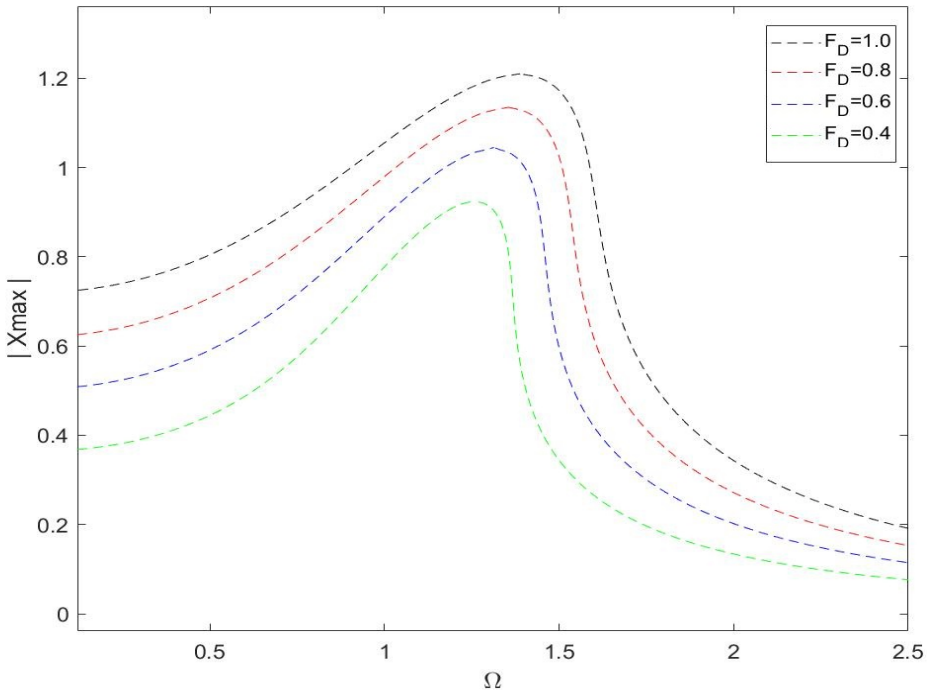

Figure 4.7: Frequency response varying driving force. $\eta = 1.6$ and $\delta = 0.001$.

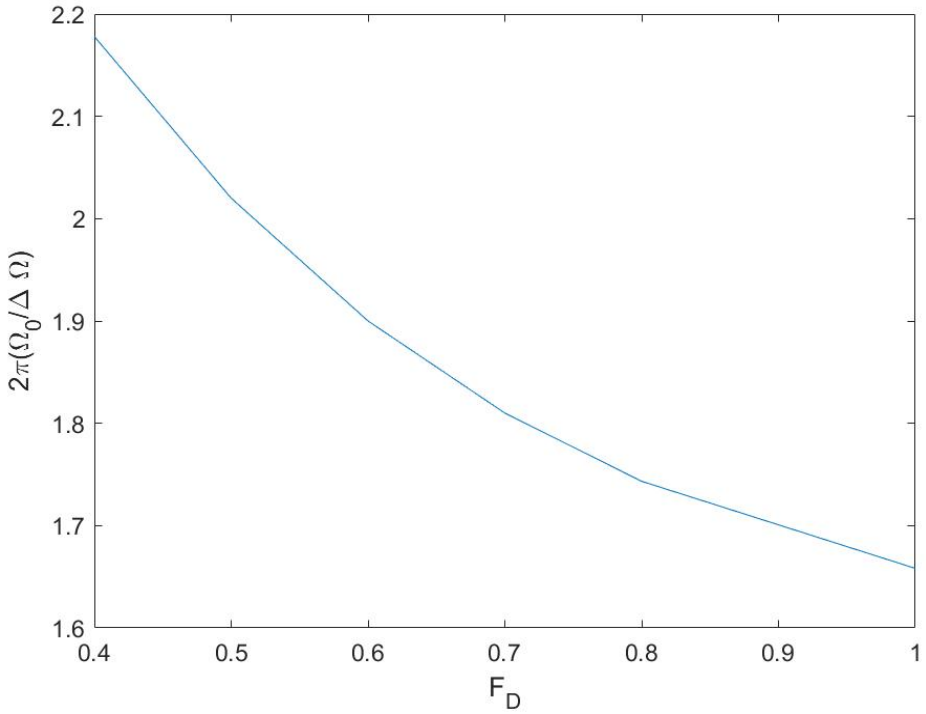

Figure 4.8: Variation of Q-factor with driving force. Here $\eta = 1.6$ and $\delta = 0.001$.

4.3 Conclusion

The analysis based on the stochastic model of a nanomechanical resonator is presented in this chapter. Additionally, ways of enhancing Q-factor are also described. The following core ideas can be taken from this chapter:

- Stochastic model of nanomechanical resonator is solved using Euler-Maruyama method and averaged frequency response curves are plotted. Analyzing the response it is found that increasing the intensity of noise based on Lévy flight excitation can increase the quality factor of a nanoresonator.
- Lévy stable stochastic excitation with increasing intensity can shrink the hysteresis region. Simulation is performed to show this phenomenon increasing the noise intensity from $\sigma = 0$ to $\sigma = 0.002$ and then to $\sigma = 0.005$.
- Decreasing of the nonlinear damping leads to decreasing the energy loss per oscillation. Hence, lowering nonlinear damping increases the quality factor.
- Decreasing the driving force leads to lower the ratio of resonance frequency and resonance width ($\Omega_0/\Delta\Omega$). Hence, lowering driving force increases the quality factor.

Chapter 5

Conclusion and Discussion

In this thesis, different aspects of the dynamics of a nanoresonator are explored. The resonator studied here is modelled considering the effect of nonlinear damping and driven by external harmonic excitation. The dynamical response of the resonator is investigated both in the deterministic and stochastic regime. The results and conclusions obtained here are summarized as follows:

- The method of harmonic balance fits excellently to analyze the dynamics of a nanomechanical resonator based on Duffing equation model. This method has been found superior to the previously used perturbation method to study this dynamics.

- Numerical simulation based on Euler method, remarkably known for solving ordinary differential equation is used to validate the accuracy of the analytical solution from different perspectives (i.e. under different external harmonic driving, different nonlinear damping). The slight mismatch of subharmonic resonance between numerical and analytical solution is well explained with necessary evidence and reasoning.

- The deterministic dynamics is also studied deriving an analytical relation between phase angle and amplitude of the motion of the resonator. It is found that the phase angle can used to characterize the resonance frequency (Ω_{res}) of a nanoresonator. The resonance is found when the phase of the driving frequency is at '$-\pi$'

and the variation of the phase response with frequency is well marked only when driving frequency is close to the resonance frequency ($\Omega \approx \Omega res$).

- Hysteresis is studied both in deterministic and stochastic model. In the deterministic study of hysteresis, it is found that increasing nonlinear damping or decreasing external drive results in decreasing hysteresis region. It is also observed that with increasing external drive or decreasing nonlinear damping, resonance frequency increases. In the stochastic study of hysteresis, it is seen that stochastic excitation with increasing intensity can shrink the hysteresis region.

- When linear damping is not low, it dominates the response of the resonator dynamics. Higher linear damping flattens the frequency response curve leading to lower the quality factor.

- Studying the parametrically driven model, it is observed that in the combined presence of parametric and external excitation, increasing the $\frac{\Omega_P}{\Omega_D}$ ratio results in decreasing the resonance width without affecting Q-factor. It is also found that increasing the harmonic oscillation amplitude of parametric excitation results in the higher resonance amplitude with a small increase in the resonance frequency.

- Analyzing the stochastic model based on Lévy stable stochastic process, we find that increasing the noise intensity, resonance frequency is fixed. However, it decreases the resonance width resulting in an increase in the quality factor. It is restated that quality factor is the key to determine the performance of a sensor; the higher is the quality factor, the better it is.

- In an effort to find other ways to enhance quality factor of the resonator, it is clear that under lower nonlinear damping, energy lost is lower in an oscillation period. Hence, quality factor will be higher and it will show more sensitivity in sensing physical quantities in the case of lower nonlinear damping.

- Higher driving force increases the resonance frequency which is the opposite effect of increasing nonlinear damping. Still, an increase in the driving force decreases the quality factor due to the fact that it increases resonance width much more than increasing resonance frequency. As a result, quality factor decreases. Hence, lower external drive is required for higher quality factor.

Further research direction may include stability analysis as well as analytic characterization of the Q-factor results using the Fokker-Planck formalism. We also expect that being motivated by the analysis and computation, pertinent experiments will be performed to study the dynamics of a nanoresonator under the effect of Lévy flights.

References

[1] Richard Feynman. Theres plenty of room at the bottom. In *Feynman and computation*, pages 63–76. CRC Press, 2018.

[2] Michael Roukes. Nanoelectromechanical systems face the future. *Physics World*, 14(2):25, 2001.

[3] A Eichler, Joel Moser, J Chaste, Mariusz Zdrojek, I Wilson-Rae, and Adrian Bachtold. Nonlinear damping in mechanical resonators made from carbon nanotubes and graphene. *Nature nanotechnology*, 6(6):339, 2011.

[4] Christian A Zorman and Rocco J Parro. Micro-and nanomechanical structures for silicon carbide mems and nems. *physica status solidi (b)*, 245(7):1404–1424, 2008.

[5] A Alvin Barlian, Woo-Tae Park, Joseph R Mallon, Ali J Rastegar, and Beth L Pruitt. Semiconductor piezoresistance for microsystems. *Proceedings of the IEEE*, 97(3):513–552, 2009.

[6] Markku Tilli, Mervi Paulasto-Krockel, Teruaki Motooka, and Veikko Lindroos. *Handbook of silicon based MEMS materials and technologies*. William Andrew, 2015.

[7] Md Sajibul Alam Bhuyan, Md Nizam Uddin, Md Maksudul Islam, Ferdaushi Alam Bipasha, and Sayed Shafayat Hossain. Synthesis of graphene. *International Nano Letters*, 6(2):65–83, 2016.

[8] Kostya S Novoselov, Andre K Geim, Sergei V Morozov, D Jiang, Y_ Zhang, Sergey V Dubonos, Irina V Grigorieva, and Alexandr A Firsov. Electric field effect in atomically thin carbon films. *science*, 306(5696):666–669, 2004.

[9] Changyao Chen. Graphene nems. *Encyclopedia of Nanotechnology*, pages 1–13, 2014.

[10] Xining Zang, Qin Zhou, Jiyoung Chang, Yumeng Liu, and Liwei Lin. Graphene and carbon nanotube (cnt) in mems/nems applications. *Microelectronic Engineering*, 132:192–206, 2015.

[11] Changgu Lee, Xiaoding Wei, Jeffrey W Kysar, and James Hone. Measurement of the elastic properties and intrinsic strength of monolayer graphene. *science*, 321(5887):385–388, 2008.

[12] AH Castro Neto, Francisco Guinea, Nuno MR Peres, Kostya S Novoselov, and Andre K Geim. The electronic properties of graphene. *Reviews of modern physics*, 81(1):109, 2009.

[13] KS Novoselov, SV Morozov, TMG Mohinddin, LA Ponomarenko, DC Elias, R Yang, II Barbolina, P Blake, TJ Booth, D Jiang, et al. Electronic properties of graphene. *physica status solidi (b)*, 244(11):4106–4111, 2007.

[14] Mark P Levendorf, Carlos S Ruiz-Vargas, Shivank Garg, and Jiwoong Park. Transfer-free batch fabrication of single layer graphene transistors. *Nano letters*, 9(12):4479–4483, 2009.

[15] Robert A Barton, Jeevak Parpia, and Harold G Craighead. Fabrication and performance of graphene nanoelectromechanical systems. *Journal of Vacuum Science & Technology B, Nanotechnology and Microelectronics: Materials, Processing, Measurement, and Phenomena*, 29(5):050801, 2011.

[16] John A Pelesko and David H Bernstein. *Modeling Mems and Nems*. CRC press, 2002.

[17] Richard C Dorf. *Sensors, Nanoscience, Biomedical Engineering, and Instruments: Sensors Nanoscience Biomedical Engineering*. CRC press, 2016.

[18] Jim Lewis. Protein design as a pathway to molecular manufacturing. *Proc. Natl. Acad. Sci. USA*, 78(9):5275–5278, 1981.

[19] KL Ekinci, XMH Huang, and ML Roukes. Ultrasensitive nanoelectromechanical mass detection. *Applied Physics Letters*, 84(22):4469–4471, 2004.

[20] Kilho Eom, Harold S Park, Dae Sung Yoon, and Taeyun Kwon. Nanomechanical resonators and their applications in biological/chemical detection: nanomechanics principles. *Physics Reports*, 503(4-5):115–163, 2011.

[21] Thomas Braun, Viola Barwich, Murali Krishna Ghatkesar, Adriaan H Bredekamp, Christoph Gerber, Martin Hegner, and Hans Peter Lang. Micromechanical mass sensors for biomolecular detection in a physiological environment. *Physical Review E*, 72(3):031907, 2005.

[22] K Jensen, Kwanpyo Kim, and A Zettl. An atomic-resolution nanomechanical mass sensor. *Nature nanotechnology*, 3(9):533, 2008.

[23] Ya-Tang Yang, Carlo Callegari, XL Feng, Kamil L Ekinci, and Michael L Roukes. Zeptogram-scale nanomechanical mass sensing. *Nano letters*, 6(4):583–586, 2006.

[24] Hsin-Ying Chiu, Peter Hung, Henk W Ch Postma, and Marc Bockrath. Atomic-scale mass sensing using carbon nanotube resonators. *Nano letters*, 8(12):4342–4346, 2008.

[25] Akshay K Naik, MS Hanay, WK Hiebert, XL Feng, and Michael L Roukes. Towards single-molecule nanomechanical mass spectrometry. *Nature nanotechnology*, 4(7):445, 2009.

[26] Heinz Georg Schuster, Ron Lifshitz, and MC Cross. *Reviews of nonlinear dynamics and complexity*. Wiley-VCH-Verlag.

[27] Mai Duc Dai, Kilho Eom, and Chang-Wan Kim. Nanomechanical mass detection using nonlinear oscillations. *Applied Physics Letters*, 95(20):203104, 2009.

[28] O Basarir, S Bramhavar, and KL Ekinci. Motion transduction in nanoelectromechanical systems (nems) arrays using near-field optomechanical coupling. *Nano letters*, 12(2):534–539, 2012.

[29] KL Ekinci. Electromechanical transducers at the nanoscale: actuation and sensing of motion in nanoelectromechanical systems (nems). *small*, 1(8-9):786–797, 2005.

[30] Xue Ming Henry Huang, Christian A Zorman, Mehran Mehregany, and Michael L Roukes. Nanoelectromechanical systems: Nanodevice motion at microwave frequencies. *Nature*, 421(6922):496, 2003.

[31] L Sekaric, JM Parpia, HG Craighead, T Feygelson, BH Houston, and JE Butler. Nanomechanical resonant structures in nanocrystalline diamond. *Applied Physics Letters*, 81(23):4455–4457, 2002.

[32] Georg Anetsberger, Olivier Arcizet, Quirin P Unterreithmeier, Rémi Rivière, Albert Schliesser, Eva Maria Weig, Jörg P Kotthaus, and Tobias J Kippenberg. Near-field cavity optomechanics with nanomechanical oscillators. *Nature Physics*, 5(12):909, 2009.

[33] DS Greywall, B Yurke, PA Busch, AN Pargellis, and RL Willett. Evading amplifier noise in nonlinear oscillators. *Physical review letters*, 72(19):2992, 1994.

[34] DA Dikin, Xinqi Chen, W Ding, G Wagner, and RS Ruoff. Resonance vibration of amorphous sio 2 nanowires driven by mechanical or electrical field excitation. *Journal of applied physics*, 93(1):226–230, 2003.

[35] AN Cleland, JS Aldridge, DC Driscoll, and AC Gossard. Nanomechanical displacement sensing using a quantum point contact. *Applied Physics Letters*, 81(9):1699–1701, 2002.

[36] Antoine Reserbat-Plantey, Laëtitia Marty, Olivier Arcizet, Nedjma Bendiab, and Vincent Bouchiat. A local optical probe for measuring motion and stress in a nanoelectromechanical system. *Nature nanotechnology*, 7(3):151, 2012.

[37] Andreas Isacsson. Nanomechanical displacement detection using coherent transport in graphene nanoribbon resonators. *Physical Review B*, 84(12):125452, 2011.

[38] Onur Basarir, Suraj Bramhavar, Gilberto Basilio-Sanchez, Theodore Morse, and Kamil L Ekinci. Sensitive micromechanical displacement detection by scattering evanescent optical waves. *Optics letters*, 35(11):1792–1794, 2010.

[39] B Ilic, D Czaplewski, M Zalalutdinov, HG Craighead, P Neuzil, C Campagnolo, and C Batt. Single cell detection with micromechanical oscillators. *Journal of Vacuum Science & Technology B: Microelectronics and Nanometer Structures Processing, Measurement, and Phenomena*, 19(6):2825–2828, 2001.

[40] Bojan Ilic, D Czaplewski, Harold G Craighead, Pavel Neuzil, Christine Campagnolo, and Carl Batt. Mechanical resonant immunospecific biological detector. *Applied physics letters*, 77(3):450–452, 2000.

[41] Gossett A Campbell and Raj Mutharasan. Detection of pathogen escherichia coli o157: H7 using self-excited pzt-glass microcantilevers. *Biosensors and Bioelectronics*, 21(3):462–473, 2005.

[42] B Ilic, Y Yang, and HG Craighead. Virus detection using nanoelectromechanical devices. *Applied physics letters*, 85(13):2604–2606, 2004.

[43] A Gupta, D Akin, and Rashid Bashir. Single virus particle mass detection using microresonators with nanoscale thickness. *Applied Physics Letters*, 84(11):1976–1978, 2004.

[44] Jeong Hoon Lee, Ki Hyun Yoon, Kyo Seon Hwang, Jaebum Park, Saeyoung Ahn, and Tae Song Kim. Label free novel electrical detection using micromachined pzt monolithic thin film cantilever for the detection of c-reactive protein. *Biosensors and Bioelectronics*, 20(2):269–275, 2004.

[45] Amit K Gupta, Pradeep R Nair, Demir Akin, Michael R Ladisch, Steve Broyles, Muhammad A Alam, and Rashid Bashir. Anomalous resonance in a nanomechanical biosensor. *Proceedings of the National Academy of Sciences*, 103(36):13362–13367, 2006.

[46] J Fritz, MK Baller, HP Lang, H Rothuizen, P Vettiger, E Meyer, H-J Güntherodt, Ch Gerber, and JK Gimzewski. Translating biomolecular recognition into nanomechanics. *Science*, 288(5464):316–318, 2000.

[47] Rachel McKendry, Jiayun Zhang, Youri Arntz, Torsten Strunz, Martin Hegner, Hans Peter Lang, Marko K Baller, Ulrich Certa, Ernst Meyer, Hans-Joachim

Güntherodt, et al. Multiple label-free biodetection and quantitative dna-binding assays on a nanomechanical cantilever array. *Proceedings of the National Academy of Sciences*, 99(15):9783–9788, 2002.

[48] Ming Su, Shuyou Li, and Vinayak P Dravid. Microcantilever resonance-based dna detection with nanoparticle probes. *Applied Physics Letters*, 82(20):3562–3564, 2003.

[49] Thomas Kodadek. Biochemistry: Molecular cloaking devices. *Nature*, 453(7197):861, 2008.

[50] Robert G Smock and Lila M Gierasch. Sending signals dynamically. *Science*, 324(5924):198–203, 2009.

[51] B Ilic, Y Yang, K Aubin, R Reichenbach, S Krylov, and HG Craighead. Enumeration of dna molecules bound to a nanomechanical oscillator. *Nano Letters*, 5(5):925–929, 2005.

[52] Madhukar Varshney, Philip S Waggoner, Christine P Tan, Keith Aubin, Richard A Montagna, and Harold G Craighead. Prion protein detection using nanomechanical resonator arrays and secondary mass labeling. *Analytical chemistry*, 80(6):2141–2148, 2008.

[53] Keith C Schwab and Michael L Roukes. Putting mechanics into quantum mechanics. *Physics Today*, 58(7):36–42, 2005.

[54] Daniel Rugar, R Budakian, HJ Mamin, and BW Chui. Single spin detection by magnetic resonance force microscopy. *Nature*, 430(6997):329, 2004.

[55] MD LaHaye, Olivier Buu, Benedetta Camarota, and KC Schwab. Approaching the quantum limit of a nanomechanical resonator. *Science*, 304(5667):74–77, 2004.

[56] Aaron D OConnell, Max Hofheinz, Markus Ansmann, Radoslaw C Bialczak, Mike Lenander, Erik Lucero, Matthew Neeley, Daniel Sank, H Wang, Ms Weides, et al. Quantum ground state and single-phonon control of a mechanical resonator. *Nature*, 464(7289):697, 2010.

[57] Kiran E Khosla, Michael R Vanner, Natalia Ares, and Edward Alexander Laird. Displacemon electromechanics: how to detect quantum interference in a nanomechanical resonator. *Physical Review X*, 8(2):021052, 2018.

[58] Ali Husain, J Hone, Henk W Ch Postma, XMH Huang, T Drake, Mladen Barbic, Axel Scherer, and ML Roukes. Nanowire-based very-high-frequency electromechanical resonator. *Applied Physics Letters*, 83(6):1240–1242, 2003.

[59] Najib Kacem and Sebastien Hentz. Bifurcation topology tuning of a mixed behavior in nonlinear micromechanical resonators. *Applied Physics Letters*, 95(18):183104, 2009.

[60] Najib Kacem, Sébastien Baguet, Sébastien Hentz, and Régis Dufour. Nonlinear phenomena in nanomechanical resonators: mechanical behaviors and physical limitations. *Mechanics & Industry*, 11(6):521–529, 2010.

[61] Trey A Roessig, Roger T Howe, and Albert P Pisano. Nonlinear mixing in surface-micromachined tuning fork oscillators. In *Proceedings of International Frequency Control Symposium*, pages 778–782. IEEE, 1997.

[62] Vincent Gouttenoire, Thomas Barois, Sorin Perisanu, Jean-Louis Leclercq, Stephen T Purcell, Pascal Vincent, and Anthony Ayari. Digital and fm demodulation of a doubly clamped single-walled carbon-nanotube oscillator: towards a nanotube cell phone. *Small*, 6(9):1060–1065, 2010.

[63] J Scott Bunch, Arend M Van Der Zande, Scott S Verbridge, Ian W Frank, David M Tanenbaum, Jeevak M Parpia, Harold G Craighead, and Paul L McEuen. Electromechanical resonators from graphene sheets. *Science*, 315(5811):490–493, 2007.

[64] Robert L Badzey and Pritiraj Mohanty. Coherent signal amplification in bistable nanomechanical oscillators by stochastic resonance. *Nature*, 437(7061):995, 2005.

[65] Bayram Deviren and Mustafa Keskin. Thermal behavior of dynamic magnetizations, hysteresis loop areas and correlations of a cylindrical ising nanotube in an oscillating magnetic field within the effective-field theory and the glauber-type stochastic dynamics approach. *Physics Letters A*, 376(10-11):1011–1019, 2012.

[66] OG Cantu Ros, Gloria Platero, and Luis L Bonilla. Effects of noise on hysteresis and resonance width in graphene and nanotubes resonators. *Physical Review B*, 87(23):235424, 2013.

[67] SA Beznosyuk. Modern quantum theory and computer simulation in nanotechnologies: quantum topology approaches to kinematic and dynamic structures of self-assembling processes. *Materials Science and Engineering: C*, 19(1-2):369–372, 2002.

[68] Subramanian Ramakrishnan, Md Raf E Ul Shougat, and Prasanth Sukumar. Effects of white noise excitation on tristable piezoelectric energy harvesters with asymmetric potential wells. In *2018 IEEE 13th Nanotechnology Materials and Devices Conference (NMDC)*, pages 1–4. IEEE, 2018.

[69] K Nakada, S Yakata, and Takashi Kimura. Noise-induced transition of mutual phase synchronization in coupled spin torque nano oscillators. *IEEE Transactions on Magnetics*, 48(11):4558–4561, 2012.

[70] Leon Glass and Joel S Pasternack. Stable oscillations in mathematical models of biological control systems. *Journal of Mathematical Biology*, 6(3):207, 1978.

[71] Ronald T Hartlen and Iain G Currie. Lift-oscillator model of vortex-induced vibration. *Journal of the Engineering Mechanics Division*, 96(5):577–591, 1970.

[72] Jonathan L Helm, David Sbarra, and Emilio Ferrer. Assessing cross-partner associations in physiological responses via coupled oscillator models. *Emotion*, 12(4):748, 2012.

[73] Stanley Pau, Gunnar Björk, Joseph Jacobson, Hui Cao, and Yoshihisa Yamamoto. Microcavity exciton-polariton splitting in the linear regime. *Physical Review B*, 51(20):14437, 1995.

[74] Piotr J Franaszczuk and Katarzyna J Blinowska. Linear model of brain electrical activityeeg as a superposition of damped oscillatory modes. *Biological cybernetics*, 53(1):19–25, 1985.

[75] Gerrit Burgers, Fei-Fei Jin, and Geert Jan Van Oldenborgh. The simplest enso recharge oscillator. *Geophysical research letters*, 32(13), 2005.

[76] MdRaf E UI Shougat and Subramanian Ramakrishnan. The hysteresis phenomenon and q factor enhancement in nonlinear nems resonators driven by lévy stable stochastic processes. In *2018 IEEE 13th Nanotechnology Materials and Devices Conference (NMDC)*, pages 1–4. IEEE, 2018.

[77] Guanyu Wang, Dajun Chen, Jianya Lin, and Xing Chen. The application of chaotic oscillators to weak signal detection. *IEEE Transactions on industrial electronics*, 46(2):440–444, 1999.

[78] K Murali and M Lakshmanan. Transmission of signals by synchronization in a chaotic van der pol–duffing oscillator. *Physical Review E*, 48(3):R1624, 1993.

[79] P Bhowmik, S Das, D Nandi, A Chakraborty, A Konar, and AK Nagar. Electroencephalographic signal based clustering of stimulated emotion using duffing oscillator. In *The 3rd International Multi-Conference on Engineering and Technological Innovation, IMETI*, 2010.

[80] Pavel Bhowmik, Sauvik Das, Amit Konar, Dolphia Nandi, and Aruna Chakraborty. Emotion clustering from stimulated electroencephalographic signals using a duffing oscillator. *International Journal of Computers in Healthcare*, 1(1):66–85, 2010.

[81] Takahiro Murakami, Yasumi Ukida, Masami Fujii, Michiyasu Suzuki, and Takashi Saito. Study on detection of epileptic discharges based on a duffing oscillator model. In *ASME 2014 International Mechanical Engineering Congress and Exposition*, pages V003T03A083–V003T03A083. American Society of Mechanical Engineers, 2014.

[82] GJ Fodjouong, HB Fotsin, and P Woafo. Synchronizing modified van der pol–duffing oscillators with offset terms using observer design: application to secure communications. *Physica Scripta*, 75(5):638, 2007.

[83] Barry E DeMartini, Jeffrey F Rhoads, Kimberly L Turner, Steven W Shaw, and Jeff Moehlis. Linear and nonlinear tuning of parametrically excited mems oscillators. *Journal of Microelectromechanical Systems*, 16(2):310–318, 2007.

[84] Wenhua Zhang, Rajashree Baskaran, and Kimberly L Turner. Effect of cubic nonlinearity on auto-parametrically amplified resonant mems mass sensor. *Sensors and Actuators A: Physical*, 102(1-2):139–150, 2002.

[85] Kimberly L Turner, Scott A Miller, Peter G Hartwell, Noel C MacDonald, Steven H Strogatz, and Scott G Adams. Five parametric resonances in a microelectromechanical system. *Nature*, 396(6707):149, 1998.

[86] Ron Lifshitz and MC Cross. Nonlinear dynamics of nanomechanical and micromechanical resonators. *Review of nonlinear dynamics and complexity*, 1:1–52, 2008.

[87] Xin-She Yang. *Engineering optimization: an introduction with metaheuristic applications*. John Wiley & Sons, 2010.

[88] Alexei V Chechkin, Ralf Metzler, Joseph Klafter, Vsevolod Yu Gonchar, et al. Introduction to the theory of lévy flights. *Anomalous transport: Foundations and applications*, 49(2):431–451, 2008.

[89] Hüseyin Haklı and Harun Uğuz. A novel particle swarm optimization algorithm with levy flight. *Applied Soft Computing*, 23:333–345, 2014.

[90] MJ Brennan, I Kovacic, A Carrella, and TP Waters. On the jump-up and jump-down frequencies of the duffing oscillator. *Journal of Sound and Vibration*, 318(4-5):1250–1261, 2008.

[91] RE Mickens. A generalization of the method of harmonic balance. 1986.

[92] Koncay Huseyin and Rui Lin. An intrinsic multiple-scale harmonic balance method for non-linear vibration and bifurcation problems. *International journal of non-linear mechanics*, 26(5):727–740, 1991.

[93] S Bravo Yuste. Comments on the method of harmonic balance in which jacobi elliptic functions are used. *Journal of sound and vibration*, 145(3):381–390, 1991.

[94] JL Summers and MD Savage. Two timescale harmonic balance. i. application to autonomous one-dimensional nonlinear oscillators. *Philosophical Transactions of the Royal Society of London. Series A: Physical and Engineering Sciences*, 340(1659):473–501, 1992.

[95] Desmond J Higham. An algorithmic introduction to numerical simulation of stochastic differential equations. *SIAM review*, 43(3):525–546, 2001.

[96] Yingjie Liang and Wen Chen. A survey on computing lévy stable distributions and a new matlab toolbox. *Signal Processing*, 93(1):242–251, 2013.

[97] Xin-She Yang and Suash Deb. Multiobjective cuckoo search for design optimization. *Computers OR*, 40:1616–1624, 2013.

[98] Louis N Hand and Janet D Finch. *Analytical mechanics*. Cambridge University Press, 1998.

[99] Steven H Strogatz. *Nonlinear Dynamics and Chaos with Student Solutions Manual: With Applications to Physics, Biology, Chemistry, and Engineering*. CRC Press, 2018.

[100] Jeffrey F Rhoads, Steven W Shaw, and Kimberly L Turner. Nonlinear dynamics and its applications in micro-and nanoresonators. *Journal of Dynamic Systems, Measurement, and Control*, 132(3):034001, 2010.

[101] James M Lehto Miller, Azadeh Ansari, David B Heinz, Yunhan Chen, Ian B Flader, Dongsuk D Shin, L Guillermo Villanueva, and Thomas W Kenny. Effective quality factor tuning mechanisms in micromechanical resonators. *Applied Physics Reviews*, 5(4):041307, 2018.

Appendix A

MATLAB Scripts

A.1 Deterministic Code for Numerical Simulation

The script below is used to perform deterministic simulation using Euler method which generates the frequency response curves:

```
clc
clear all
format long
N=3000; dt=1/N;T=3000;
%%%% Upsweep frequecny response curve
X1(1)=0;
X2(1)=0;i=0;k=0;
C1=1;C2=0.001; n=1.6; Fd=0.2;j=2;
%n=nonlin. damp. coeff.,Fd=drive amplitude,C2=lin. damp. coeff.
S2 = zeros(1,N*T+1);
Absolute2= zeros(1,N*T+1);
%%%% Loop for Upsweep frequecny response curve
for w2=0:0.05:2.0
    k=k+1
    for j=2:N*T+1
        X2(j)=X2(j-1)+dt*(-C1)*X1(j-1)-C2*X2(j-1)
        -(C1^3)*X1(j-1)^3-n*X1(j-1)^2*X2(j-1)
```

```
        +Fd*cos(w2*(j-1)*dt);
        X1(j)=X1(j-1)+dt*(X2(j-1));
        if (((j-1)*dt) > T-100)
        S2(j)=X1(j); %save the final 100 sec displacement value
        S2_p(j)=X2(j); %save the final 100 sec velocity value
    end
    Absolute2(j)=abs(S2(j));%disp. values into absolute
    Absolute2_p(j)=abs(S2_p(j));%velocity values into absolute
    end
    Xmax2(k)= max(Absolute2)
    %taking the maximum value of the displacement
    Xmax2_p(i)= max(Absolute2_p)
    %taking the maximum value of the velocity
    X1(1)=max(Absolute2);
    %using the final value of
    displacement as the initial in next loop
    X2(1)=max(Absolute2_p);
    %using the final value of
    velocity as the initial in next loop
end
plot(0:0.05:2.0,Xmax2,'bo') %plotting the upsweep curve
hold on
%%%% Downsweep frequecny response curve
S1 = zeros(1,N*T+1);
Absolute1= zeros(1,N*T+1);
%%%% Loop for Downsweep frequecny response curve
for w1=2.0:-0.05:0
    i=i+1;
    for j=2:N*T+1
    X2(j)=X2(j-1)+dt*(-C1)*X1(j-1)-C2*X2(j-1)
    -(C1^3)*X1(j-1)^3-n*X1(j-1)^2*X2(j-1)
    +Fd*cos(w1*(j-1)*dt);
```

```
    X1(j)=X1(j-1)+dt*(X2(j-1));
        if (((j-1)*dt) > T-100)
        S1(j)=X1(j); %save the final 100 sec displacement value
        S1_p=X2(j); %save the final 100 sec velocity value
    end
    Absolute1(j)=abs(S1(j)); %disp. values into absolute
    Absolute1_p(j)=abs(S1_p(j));% velocity values into absolute
end
    Xmax1(i)= max(Absolute1) %maxm value of the displacement
    Xmax1_p(i)= max(Absolute1_p) %maxm value of the velocity
    X1(1)=max(Absolute1); %initializing values for next loop
    X2(1)=max(Absolute1_p); %initializing values for next loop
end
   plot(2.0:-0.05:0,Xmax1,'bo') %plotting the downsweep curve
```

A.2 Deterministic Code for Analytical Solution Plot

The script below is used to plot deterministic analytical solution using the HBM method which generates the frequency response curves:

```
clear all
clc
%fixing values for non.lin.damp.co-eff, drive amplitude
n=1.6; Fd=0.2;i=0;
P=0:0.005:1.09; %range of amplitude want to plot
%Loop for the plot
for X=P
    i=i+1;
    B2=(1/16)*n^2*X^6-(3/2)*X^4-2*X^2
    A=X^2
    C=(9/16)*X^6+(3/2)*X^4+X^2-Fd^2
    Char=B2^2-4*A*C
    Omegasquare3=(-B2+sqrt(B2^2-4*A*C))/(2*A); %for downsweep
```

```
    Omegasquare4=(-B2-sqrt(B2^2-4*A*C))/(2*A); %for upsweep
    Omega3(i)=sqrt(Omegasquare3);
    Omega4(i)=sqrt(Omegasquare4);

    if (Omegasquare3<0)
        Omega3(i)=nan  %ignoring complex soln.
    end
    if (Omegasquare4<0)
        Omega4(i)=nan %ignoring complex soln.
    end
end
plot(Omega3,P,'g--');
xlim([0.1  5]) %axes limit
ylim([0  0.82]) %axes limit
hold on
plot(Omega4,P,'g--'); %plotting
```

A.3 Code for Numerical Simulation in Stochastic Regime

The script below is used to perform stochastic simulation using Euler-Maruyama method which generates the frequency response curve for a specific noise intensity:

```
clc
clear all
format long
N=3000; dt=1/N;T=3000;
Numofruns=50; %no of runs for average
dL= sqrt(dt)*levy(Numofruns,N*T+1,1.5);
C1=1; Fd=0.2;j=2;
n=1.6;k=0;m=0;x=0;noise=0;sigma=0.001;
%%% Loop for upsweep frequency response curve
for C2=[0.0001];
    i=0
```

```
X1(1)=0;%initial value
X2(1)=0;%initial value
S1 = zeros(1,N*T+1);
Absolute1= zeros(1,N*T+1);
for w1 = 0:0.01:2;
     i=i+1;
     Xmax1(i)=0;
    for y=1:Numofruns;%averaging loop
    for j=2:N*T+1
    X2(j)=X2(j-1)+dt*(-C1*X1(j-1)-C2*X2(j-1)-
    (C1^3)*X1(j-1)^3-n*X1(j-1)^2*X2(j-1)...
        +Fd*cos(w1*(j-1)*dt))+sigma*dL(y,j-1);
    X1(j)=X1(j-1)+dt*(X2(j-1));
    if (((j-1)*dt) > T-100)
        S1(j)=X1(j);% saving final 100 s values
    end
    Absolute1(j)=abs(S1(j));%turning saved values into absolute
    end
    Xmax1(i)= Xmax1(i)+max(Absolute1);
    %summing up the max values
    X1(1)=0;
    X2(1)=0;
    end
    Xmax1(i)=Xmax1(i)/Numofruns;
    %averaging the max displacement values
end
   plot(0:0.01:2,Xmax1,'-o')%plotting downsweep curve
   hold on;%hold the curve for next curve in the same figure
end
%%%% Loop for downsweep frequency response curve
for C2=[0.0001];
    i=0;
```

```
X1(1)=0;
X2(1)=0;
S1 = zeros(1,N*T+1);
Absolute1= zeros(1,N*T+1);
for w2 = 2:-0.01:0;
      i=i+1;
      Xmax2(i)=0;
     for y=1:Numofruns;
     for j=2:N*T+1
     X2(j)=X2(j-1)+dt*(-C1*X1(j-1)-C2*X2(j-1)-
     (C1^3)*X1(j-1)^3-n*X1(j-1)^2*X2(j-1)...
          +Fd*cos(w2*(j-1)*dt))+sigma*dL(y,j-1);
     X1(j)=X1(j-1)+dt*(X2(j-1));
            if (((j-1)*dt) > T-100)
                S1(j)=X1(j);% saving final 100 s values
            end
     Absolute1(j)=abs(S1(j));%turning saved values into absolute
     end
     Xmax2(i)= Xmax2(i)+max(Absolute1);
     %summing up the max values
     X1(1)=0;
     X2(1)=0;
     end
     Xmax2(i)=Xmax2(i)/Numofruns;
     %averaging the max displacement values
end
    plot(2:-0.01:0,Xmax2,'-o')%plotting downsweep curve
end
```

A.3.1 m file for Lévy function calling

Levy.m function script used in the stochastic simulation:

```
function [z] = levy(n,m,beta)
%'Multiobjective cuckoo search for
design optimization Xin-She Yang, Suash Deb'.

% Input
% n = Number of steps
% m = Number of Dimensions
% beta = Power law index, Note: 1 < beta < 2
% Output
% z     -> 'n' levy steps in 'm' dimension

    num = gamma(1+beta)*sin(pi*beta/2);
    % used for Numerator
    den = gamma((1+beta)/2)*beta*2^((beta-1)/2);
    % used for Denominator

    sigma_u = (num/den)^(1/beta);% Standard deviation

    u = random('Normal',0,sigma_u^2,n,m);

    v = random('Normal',0,1,n,m);

    z = u./(abs(v).^(1/beta));

end
```

A.4 Probability Density Function

Using MATLAB 2019a, code for probability density function plot is given here:

```
clear all
%generating the distributions
```

```
pd1 = makedist('Stable','alpha',2,
'beta',0,'gam',1,'delta',0);
pd2 = makedist('Stable','alpha',1.5,
'beta',0,'gam',1,'delta',0);
pd3 = makedist('Stable','alpha',0.5,
'beta',0,'gam',1,'delta',0);

%Calculate the pdf for each distribution.

x = -10:.1:10;
pdf1 = pdf(pd1,x);
pdf2 = pdf(pd2,x);
pdf3 = pdf(pd3,x);


%Plot all three pdf functions on
the same figure for visual comparison.

figure
 plot(x,pdf1,'b-');
 plot(x,pdf2,'r-');
 hold on
 plot(x,pdf3,'b-');
hold off
```